Mesosphere-Lower Thermosphere Planetary and Tidal waves structure over the Southern Hemisphere using SANAE and Halley SuperDARN HF RADAR

By

Perfect Privilege Chifoto

Submitted in partial fulfilment of the academic requirements for the Degree of Master of Science in the School of Physics, University of KwaZulu-Natal (Westville).

Supervisor: Prof. Sivakumar Venkataraman

Co-supervisor: Dr. Nkanyiso B. Mbatha

October 2015

Abstract

The study focuses on planetary and tidal wave structure in the Mesosphere-Lower Thermosphere (MLT) region at high latitude using SuperDARN High Frequency (HF) radar observations over the South African National Antarctic Expedition (SANAE), (72°S, 3°W) and Halley (76°S, 27°W). Hourly continuous zonal and meridional wind measurements in the MLT (~94 km) region for the year 2007 were used for the present analysis. Fast Fourier Transform (FFT) and wavelet analysis methods were implemented for wave filtering and to reveal dominant wave periods and their time of occurrence.

Planetary waves were investigated for their origin and propagation upwards as they distribute energy and momentum. Wavelet analysis revealed tidal variability at planetary wave scale, with dominant periods below 30 days. This made it possible to investigate the day-to-day, seasonal and inter-annual variability of tidal waves with planetary waves, at major dynamical events like Sudden Stratospheric Warming (SSW). From the analysis of results, seasonal variations of the mean wind and planetary wave interaction with tidal waves was investigated and proved a wave-wave interaction in the MLT. Minor Sudden stratospheric Warming events for the years 2007 and 2010 were investigated using NCEP reanalysis data from the United Kingdom Meteorological Office (UKMO) data assimilation.

Declaration

The work described in this thesis was carried by the author at the University of KwaZulu-Natal, School of Chemistry and Physics, Discipline of Physics, Westville Campus, Durban, from February 2013 to October 2015 under supervision of Prof. Sivakumar Venkataraman and Dr. Nkanyiso Bongumusa Mbatha.

This work represents original work by the author and has not been submitted in any form to any university. The work of others has been duly acknowledged where used in the text.

Author: Perfect Privilege Chifoto

Signature: .....Date: .....

As the candidate's supervisor I hereby certify that the above statement is correct

Signed: ..... Name: ..... Date: .....

As the candidate's co-supervisor I hereby certify that the above statement is correct

Signed: ..... Name: ..... Date: .....

Acknowledgements

I would like to acknowledge and give great thanks to the following people, whom I am much indebted to for their generous contribution they rendered to the success of this thesis:

- Prof. Sivakumar Venkataraman, supervisor, for guidance and support throughout the duration of this project.
- Dr. Nkanyiso B. Mbatha, co-supervisor, for guidance and support throughout the duration of this project and for always accommodating me on his very limited time.
- University of KwaZulu-Natal, for good facilities and suitable resources for research.
- Mr. J. Nadesia, for always supporting and giving me useful ideas throughout the study period.
- My family and friends for their great support in every aspect.
- Nyarugo family, for accommodation, financial and moral support.

Dedication

- My wife and son (Sithandazile & Carel Chifoto)

Contents

List of Figures

List of Tables

Chapter 1: Introduction

Understanding the structure and dynamics of the Mesosphere-Lower thermosphere (MLT) and the whole middle atmosphere is important as this region is known to be a sensitive indicator of the health of the middle atmosphere as a whole (e.g. Charne and Drazin 1961, Andrews et al., 2007 and Anne, 2012). In particular, the middle atmosphere is an important region which is used to study global climate change and its accompanying processes. Specifically, the polar upper middle atmosphere and upper atmosphere provides a unique natural laboratory for studying the complex physical, dynamical and chemical processes in the earth's atmosphere and space environment. However, the MLT region still remains the most difficult region to observe due to the limitation of the relevant instruments.

When the fluid parcels are displaced from their equilibrium latitudes or altitudes, the balance between inertia and restoring forces results in wave motions namely planetary waves, tidal waves and gravity waves (Andrews et al., 1987). These wave motions have a fundamental impact on the lower-upper atmosphere coupling and are measured as fluctuations in wind, density, temperature and pressure. Atmospheric waves may propagate horizontally and vertically from their sources in the troposphere to the upper atmosphere carrying momentum and energy. Due to the intensely decreased air density in the upper atmosphere and the conservation of the wave energy, the wave amplitude becomes large enough to induce nonlinear wave breaking and turbulence (Matsuno, 1971; Holton, 1976; Andrews et al., 1987 and Shepherd et al., 2000). Consequently, the energy and momentum of the waves are transferred by the mean flow. This wave breaking process determines the global circulation and temperature distribution of the upper atmosphere. The middle atmospheric dynamics also involves daily, seasonal to long-lasting wind variations. The dynamics of the middle atmosphere is well outlined in the work of Bremer et al., (1997), where they concluded that the zonal component of the prevailing wind as well as the semidiurnal tidal amplitude were weakly negatively correlated with solar activity during most months. The cause of such variation in the amplitude of the zonal wind and tides is the major concern for this study to investigate all the activities and consequences in cases where Sudden Stratospheric Warming events are simulated.

1.1 The Atmospheric Structure

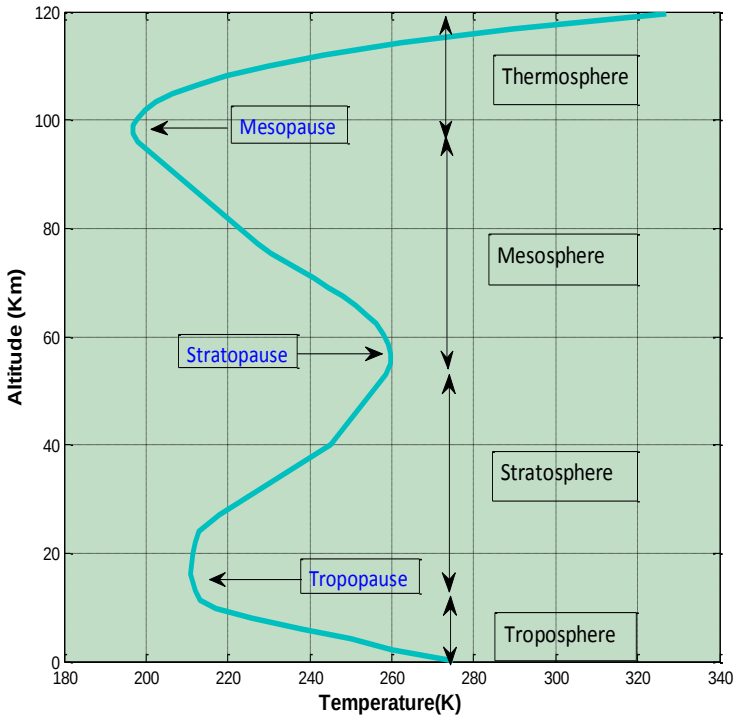

Figure 1.1: The MSISE (Mass Spectrometer Incoherent Scatter Extended) 90 Model vertical structure of atmospheric temperature year: 2007.

Observations show that the vertical variations of pressure and temperature in the atmosphere follow an entirely different pattern. The basic vertical structure of the temperature distribution in the neutral atmosphere can be understood on radiative-convective grounds (e.g. Houghton, 1986 and Andrews et al., 1987). It shows that the temperature varies differently in different atmospheric layers. The four principal layers of the atmosphere defined in Figure 1.1 are: the troposphere, the stratosphere, the mesosphere and the thermosphere. These are discussed in more detail in the following section.

1.1.1 Troposphere

The troposphere is the lowest layer which extends to a height varying between about 8 km at the poles to 16 km over the equator depending upon both the season and latitude. In this layer, the

temperature drops steadily with height at the rate of about 6.5 $K.km^{-1}$ until a minimum value of between 207 K and 209 K is reached at a level called the tropopause. This layer is denser than all the layers of the atmosphere above and it constitutes up to 75% of the mass of the atmosphere. It is primarily composed of nitrogen (78%) and oxygen (21%) with only small concentrations of other trace gases. Nearly all atmospheric water vapour or moisture is found in the troposphere. The temperature distribution in the troposphere is maintained by the convective and turbulent transfer of heat due to absorption of solar radiation at the surface of the atmosphere. Sometimes in the troposphere, the temperature does not decrease with height but rather it increases. Such a situation is known as a temperature inversion. Temperature inversions limit or prevent the vertical mixing of air. Such atmospheric stability can lead to air pollution episodes, with air pollutants emitted at ground level, becoming trapped underneath the temperature inversion.

1.1.2 Stratosphere

Above the troposphere lies the stratosphere where the temperature increases gradually with height to reach a maximum of about 260 K at a height of about 50 km above the earth's surface. This is based on figure 1.1 using similar method of analysis to the one employed by Saha, (2008), on U.S. standard atmosphere. The increase of temperature in this layer is due to the presence of ozone, which absorbs ultraviolet (UV) radiation from the sun and acts as a source of heat for the atmosphere. Since ozone controls the thermal structure of this layer, it is also sometimes called the ozonosphere and consequently, the stratosphere is almost completely free of clouds or other forms of weather. The top of the stratosphere is called the stratopause marking the beginning of the next layer called the mesosphere.

1.1.3 Mesosphere

The mesosphere or middle sphere is the third layer in the atmosphere, occupying the region between 50 km to 90 km above the Earth's surface. Above the stratopause, the temperature drops again to reach a minimum of about 194 K to 196 K at about 96 km. The mesosphere is the coldest of all the atmospheric layers such that it is cold enough to freeze water vapor into ice clouds called noctilucent clouds which were well explained by Von Zahn et al., (2004). The level of this minimum temperature is called the mesopause which marks the beginning of the next

layer called the thermosphere. Chemical heating influences greatly the mesosphere region in a variety of ways, including increases in electrical conductivity and heating rates, as well as upward expansion. Large amounts of energy in the form of chemical potential energy are deposited in the MLT through the dissociation of molecular oxygen and ozone. The mesosphere is also a layer in which a number of meteors burn up while entering the earth's atmosphere.From the earth's surface, they are seen as shooting stars.

1.1.4 Thermosphere

The mesopause marks the level from where the temperature starts rising again, this time almost monotonously to large values at a greater height of the atmosphere and this layer is called the thermosphere. The importance of this layer lies in the fact that it intercepts the highly charged solar rays from space and the high energy ultra-violet radiation from the sun which are both harmful to life on the earth's surface. The atoms and molecules of gases such as oxygen and nitrogen present in this layer absorb the high energy short-wave radiation from the sun and get ionized. The ionized layer helps in global telecommunication by reflecting radio waves. For this reason, this layer is also sometimes called the ionosphere. The temperature of the thermosphere varies greatly with solar activity, with a value of about 2000 K at the time of 'active sun' and 500 K at the time of 'quiet sun' at 500 km altitude (Banks and Kockarts 1973). Because of the large variation in the thermal structure of the thermosphere with active and quiet sun, this part of the thermosphere is often called the heterosphere.

Above the heterosphere lies the exosphere. Absorption of solar ultraviolet radiation occurs principally in three regions which are: at the surface of the earth due to near-blackbody absorption (apart from albedo effects), in a broad layer centered at about 50 km altitude due primarily to ozone and above about 85 km altitude due primarily to molecular oxygen. The lower part of the thermosphere from 80 km to 550 km above the earth's surface contains the ionosphere. Beyond the ionosphere extending out to perhaps 10,000 km is the exosphere or outer thermosphere, which gradually merges into space.

The atmosphere can be treated like system which can attain a baroclinic state that is towards a radiative equilibrium due to the sun's radiation. It is the propagation of thermal waves created by pressure difference that will re-establish a barotropic state. Generally, the dynamics of the atmosphere are catered to by the conservation of mass, momentum and thermodynamic energy. As such the atmospheric movements can in general be modeled by the laws of fluid dynamics that is when considering the atmosphere as a fluid. There are so many assumptions and approximations to be put into consideration when dealing with the middle atmosphere. The atmosphere is considered to be a classical, continuous Newtonian fluid that is acted upon by gravitational force. In some cases the horizontal component of the Coriolis force is neglected. In this study, the basic equations based on Forbes, (1995); Andrews, (2000); Holton, (2004) and Baumgaertner, (2007) which were further explained in the studies done by Mbatha, (2012) and Kleinknecht, (2010), were considered.

1.2 Main Objectives

The main objectives of this thesis are as follows;

- Investigating the contribution of Planetary waves in MLT dynamics.
- Verifying if there is a wave – wave interaction between planetary waves and tidal waves with the mean flow.
- Extracting the type of waves and wave periods dominant during the occurrence of minor Sudden Stratospheric Warming.
- Calculating the wavenumbers found in more dominant waves in the MLT.

1.3 Thesis Outline

Chapter one focuses on the atmosphere's temperature profile background. In Chapter two atmospheric waves are discussed in detail (i.e. their origin, propagation and dissipation as they distribute momentum and energy). Instrumentation and Data analysis techniques are presented in Chapter 3. This includes the methodology of data capturing by Super DARN HF radar instruments and its subsequent processing. Data analysis techniques for further analysis was also presented in this chapter. Chapter 4 presents the investigation of planetary wave activity and tides using SANAE and Halley HF radar data. This involves the calculation of zonal

wavenumbers and noting dominant wave periods present. Chapter 5 presents the analysis of minor SSW during the year 2007 and 2010 using NCEP reanalysis data and UKMO assimilation data. For the specific year of this study year 2007, the data from SANAE and Halley HF radar was used to calculate zonal wavenumbers and the interaction of planetary waves with tides during the occurrence of minor SSW events. The Summary and Conclusion of all the results in this thesis are presented in chapter 6 and thereafter, future work and references are provided.

Chapter 2: Atmospheric Waves and Sudden Stratospheric Warming (SSW)

2.1 Introduction

All atmospheric waves are periodic disturbances in the field of atmospheric variables such as wind, temperature, geo-potential height, etc. This chapter focuses on planetary waves which are atmospheric waves with periods from 2 to about 30 days (sometimes called Rossby waves). Figure 2.1 shows that planetary waves are forced modes generated in the troposphere by wind flow over continental scale topography, continent-ocean heating contrasts, nonlinear interactions among transient tropospheric wave disturbances, cyclones and thunderstorms. They are known to propagate both horizontally and vertically carrying momentum in the middle and upper atmosphere. Most importantly, these waves are responsible for setting up the polar stratosphere to conditions which favour the occurrence of Sudden Stratospheric Warming (SSW).

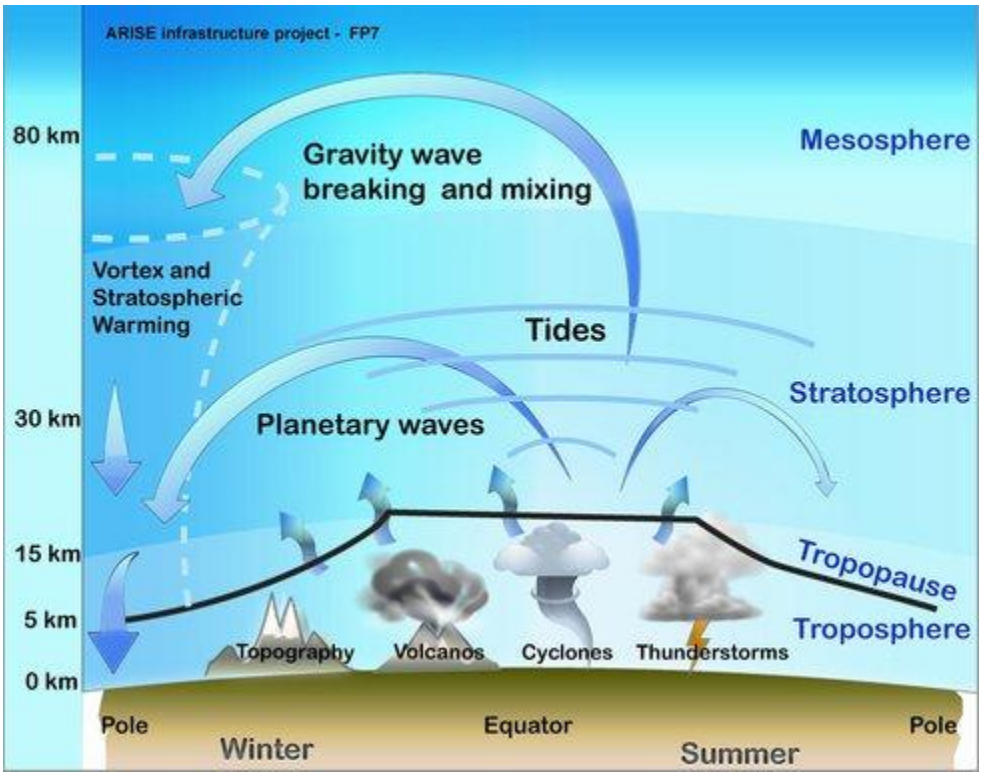

Figure 2.1: Dynamics of the troposphere-stratosphere-mesosphere exchanges including the contribution of gravity waves and planetary waves (source: http://arise-project.eu/atmospheric-dynamics.php).

This leads to the displacement or breakdown of the polar vortex and the split of the ozone hole as shown in Figure 2.1. The interaction of gravity waves, planetary waves and tides contribute to the dynamics of the troposphere-stratosphere-mesosphere wave activities which are more dominant during the winter season as shown.

2.1.1 Planetary Waves

Planetary waves (or Rossby waves) are excited due to the meridional gradient of potential vorticity. They have periods of two to several days and have one or more longitudinal peaks around the globe. Planetary wave propagation is variable since the Coriolis effect varies with latitude and is dependent upon the rotation and spherical geometry of the earth. The Coriolis effect is due to the earth's rotation and deflects a portion of air to move to the right of its motion in the Northern Hemisphere and to the left in the Southern Hemisphere. Planetary waves are also forced modes generated in the troposphere by flow over continental scale topography, by continent-ocean heating contrasts, and by nonlinear interactions among transient tropospheric wave disturbances as studied in the work of Holton, (1975); Volland, (1988); Forbes, (1995) and Mbatha, (2012).

Planetary waves are mostly generated in the troposphere around the equator and propagate upward into the stratosphere and towards the poles. In the stratosphere they break and deposit momentum, driving the stratospheric Brewer-Dobson circulation (Shepherd, 2000). The interaction between planetary waves and the zonal mean flow is known to be the major driver of winter stratospheric dynamics (Andrews, 1987). Classical studies showed that the zonal mean flow affects planetary wave propagation by changing the refractive index (Charney et al., 1961). The dissipating planetary waves interacting with the zonal mean flow are responsible for setting up the polar stratosphere to conditions which favour the occurrence of the SSW.

2.1.2 Tidal Waves

Atmospheric tidal waves (or commonly referred as tides) are generated because the atmosphere is periodically heated by the Sun. These solar tides profoundly affect the large-scale dynamics of

the mesosphere and lower thermosphere where they attain large amplitudes and dominate the large-scale wind and temperature fields. Like other waves the tidal components grow in amplitude with increasing altitude since atmospheric density decreases and energy must be conserved. Tidal waves are separated into three types, namely (diurnal ~24 h, semidiurnal ~12 h tides and terdiurnal ~8 h) however, this study focuses only on diurnal tides (DT) and semidiurnal tides (SDT). A diurnal tide has a single high tide and a single low tide per tidal day whilst a semidiurnal tide has two high tides and two low tides of approximately equal height each tidal day. The earth rotates at a diurnal cycle hence any point in the atmosphere is therefore subject to a diurnal cycled solar radiation force. If the radiation is absorbed and then released as heat, the solar heating may have the same cycle as the forcing. Solar thermal heating and the tidal response can be expressed periodically as follows (Zhang et al., 2010);

$$\sum_{s=-L}^{s=+L}\sum_{n=1}^{N} A_{n,s}(\theta,h)\cos\left(n\Omega t + s\lambda - \phi_{n,s}(\theta,h)\right), \qquad \textbf{(2.1)}$$

where $A_{n,s}$ is the amplitude of the tidal component specified by n and s, t is the universal time, λ is the longitude, θ the latitude, h the altitude, $\phi_{n,s}$ is the phase and $\Omega = 2\pi/24$ per hour. The positive integers, $n = 1,2,3,\ldots$ denotes diurnal, semidiurnal, terdiurnal and so on. The radiation can either be absorbed by ozone in the stratosphere or by water vapour in the troposphere. Tides play an important role in the mesosphere and lower thermosphere in transporting momentum and wave energy upward which then dissipate through various instabilities and nonlinear wave interactions.

2.2 Sudden Stratospheric Warming (SSW)

The first explanation of the Sudden Stratospheric Warming was put forward by Matsuno (1971), who introduced a simple model of wave mean-flow interaction induced by dissipating planetary waves. There are four different types of SSW namely, minor SSW, major SSW, Canadian warming, and final Warming. Most of them come under the label of World Meteorological Organization (WMO), though there is no documented WMO definition.

2.2.1 Major Sudden Stratospheric Warming

Major SSW is common in the Northern Hemisphere and this is due to high topographic features such as high mountains which excite planetary waves when the wind flows over continental scale topography. In this study a principle which states that a stratospheric warming can be said to be major, if at 10 hPa or below the latitudinal mean temperature increases abruptly pole ward from 60° latitude with an associated wind circulation reversal (World Meteorological Organisation, WMO,(1985)). The details of the year 2002 unprecedented Southern Hemisphere major stratospheric warming has been studied by others (e.g. Baldwin et al., 2003; Dowdy et al., 2004; Dowdy, 2005 and Mbatha et al., 2010b).

2.2.2: Final Warming

Final warming is a SSW which occurs in late winter mainly because the radiative cycle in the stratosphere is such that the mean flow is easterly and during summer it takes a westward direction of propagation in the Southern Hemisphere. A final warming occurs on this transition so that the polar vortex winds change direction for the warming; however it does not change back until the following winter. This is because the stratosphere has entered the summer westerly phase. It is referred to as final as there is no other warming expected to occur over the summer.

2.2.3 Canadian Warming

Canadian warming occurs in early winter and it is only common in the Northern Hemisphere and generally in Canada, because they have no counterpart in the Southern Hemisphere. Canadian warming can reverse the temperature gradients or partly change the wind direction, but they do not lead to the breakdown of the cyclonic polar vortex (Butler et al., 2015).

2.2.4 Minor Sudden Stratospheric Warming

A stratospheric warming is labeled as minor if there is a significant increase of temperature at any stratospheric level in any area of the winter time hemisphere, which does not lead to a reversal of zonal wind flow. This means that a SSW is classified as a minor warming if the criteria and conditions for determining a major warming mentioned above are not met. A study by Labitzke et al., (2000) classified the SSW as a minor warming if there is a significant increase

of temperature at least by 25 K per week below 10 hPa level in any area of the winter hemisphere.

Stratospheric warming involves interactions between the zonal flow of the polar stratosphere and upward propagating planetary waves consisting primarily of zonal wavenumbers 1 and 2. Normally, the zonal flow is very strong in the wintertime lower polar stratosphere and vertically propagating waves tend to be deflected towards the equator. If the lower stratosphere is pre-conditioned by the earlier wave activity, the zonal flow is weakened or moved pole ward and vertically propagating waves tend to be deflected pole ward (e.g. Matsuno, 1971; Holton, 1976; Andrews et al., 1987 and Mbatha et al., 2010b). The area above the heat flux maximum (divergence of wave forcing) acts to decelerate the eastward zonal flow. A residual circulation then induces sinking motion below and pole ward of this forcing region. The sinking motion causes the temperatures to increase due to adiabatic warming. This reduces the thermal gradient which in turn reduces the zonal wind speed. These large temperature and wind anomalies then propagate downward into the lower stratosphere (Baldwin et al., 1999 and Limpasuvan et al., 2004).

Chapter 3: Instrumentation and Data Analysis Techniques

3.1 Introduction

This chapter focuses on a brief description of the instruments used and also data analysis techniques such as Fourier analysis, and wavelet analysis. Fourier transformation is a very good technique which is used to determine the frequency content of the signal but unfortunately it is unable to provide the time of occurrence and the time evolution of individual spectral components. Wavelet analysis has been chosen to study the time evolution of tidal variability because Fourier transforms cannot resolve transient frequencies.

3.2.1 Operation of the SuperDARN HF Radars

The SANAE (72°S, 3°W) and Halley (76°S, 27°W) High Frequency (HF) radar systems are part of the Super Dual Auroral Radar Network (SuperDARN) HF Radar network, which are located in Antarctica. SuperDARN is a network of coherent ground based HF Doppler radars (Greenwald et al., 1995). SuperDARN HF Radars were initially meant to monitor the backscatter from decameter-scale ionospheric irregularities (Hall et al., 1997). A study by Hall et al., (1997) confirmed that echoes at ranges close to the SuperDARN radars are actually due to scatter from meteor trails near approximately 94 km altitude, except when there is high geomagnetic disturbance. The near range scatter can be used to study and monitor neutral winds at meteor heights hence for this study, SuperDARN HF Radars are utilized.

The network orientation allows the radars to work in pairs with a common area of view. This allows maps of two dimension high latitude plasma circulation to be obtained from the line of sight Doppler shifts observed by both radars (Greenwald et al., 1995). The coordination of SuperDARN radars is achieved by operating them in a common mode of operation (Greenwald et al., 1995). The SuperDARN radar network for the year 2014 consisted of a total of about 21 radars in the Northern Hemisphere and about 11 in the Southern Hemisphere. Most SuperDARN radars are monitored by several institutions together with various funding agencies. The SANAE HF radar located in the Antarctic is monitored by the University of KwaZulu-Natal and it is one of the radars used in this study. SuperDARN radars are operated at very high frequencies of

between 8 and 20 MHz, which allows the radar signal to be refracted by ionospheric irregularities which results in either direct back scatter if the radar wavelength is twice that of the scattering ionospheric irregularity. At times the radar signal is scattered in the forward and backward motion along the direction of the signal path creating a field of view, (Lester, 2013). The field of view of radars (Figure 3.2) is a result of a 16 antenna array connected to a phasing matrix which permits the single beam to scan over 16 directions separated by 3.25° creating an azimuthal width of 52°. The azimuthal resolution ranges from about 2.5° at 20 MHz to 6° at 8 MHz and the peak power is about 10 kW. A multi-pulse sequence with individual pulse lengths of 200 to 300 μs is operated and such a pulse length gives a range resolution of between 30 to 45 km. SuperDARN radars have another array of 4 antennas which are used to determine the angle of arrival of the backscattered signal.

According to Lester, (2013), the Doppler velocity and spectral widths can be derived from an autocorrelation function (ACF) which can be computed from integrating the returned signal. By using multi-pulse sequence the SuperDARN radars calculate the back scatter power, mean Doppler velocity and the spectral width of the Doppler power for each range considering a certain percentage of return signal as significant. The returning pulses are sampled and processed to yield the complex ACF for various time delays among the pulses. After every 7 seconds the measurements are taken at each of the 16 beam positions. The pulse sequence is about 40 milliseconds and successive pulses have a duration of 60 milliseconds which results in 60 ACFs in each of the 7 transmitting seconds to be averaged for each measurement. The measurements can be taken for up to 75 range gates along the beam where each range gate is equal to 45 km resulting in an approximate maximum range of 3600 km. The acquisition of the zonal and meridional winds in the meteor region is achieved by using the data from the first several range gates of the radar. This is mainly because the meteor trail echoes occur predominantly in and below the lower *E* region (~95 km) according to Hussey et al., (2000). The backscatter at this distance of approximately (90-95 km) is primarily due to meteors hence, hourly wind averages are calculated for each beam direction giving a line of sight wind velocity which is crucial in this study.

The ACFs are averaged over the integration time and then this data is stored in files. These files usually store all complex ACF data for a 2 hour block. Concurrently, the ACFs are analysed in

real time by a program called FITACF and stored in files. These files can be used to create summary plots which typically display the power (dB), Doppler velocity ($m.s^{-1}$) and spectral width ($m.s^{-1}$). This process is repeated during the integrations performed on each of the 16 radar beams. The results saved in files can be presented in the form of summary plots as shown in Figure 3.1.

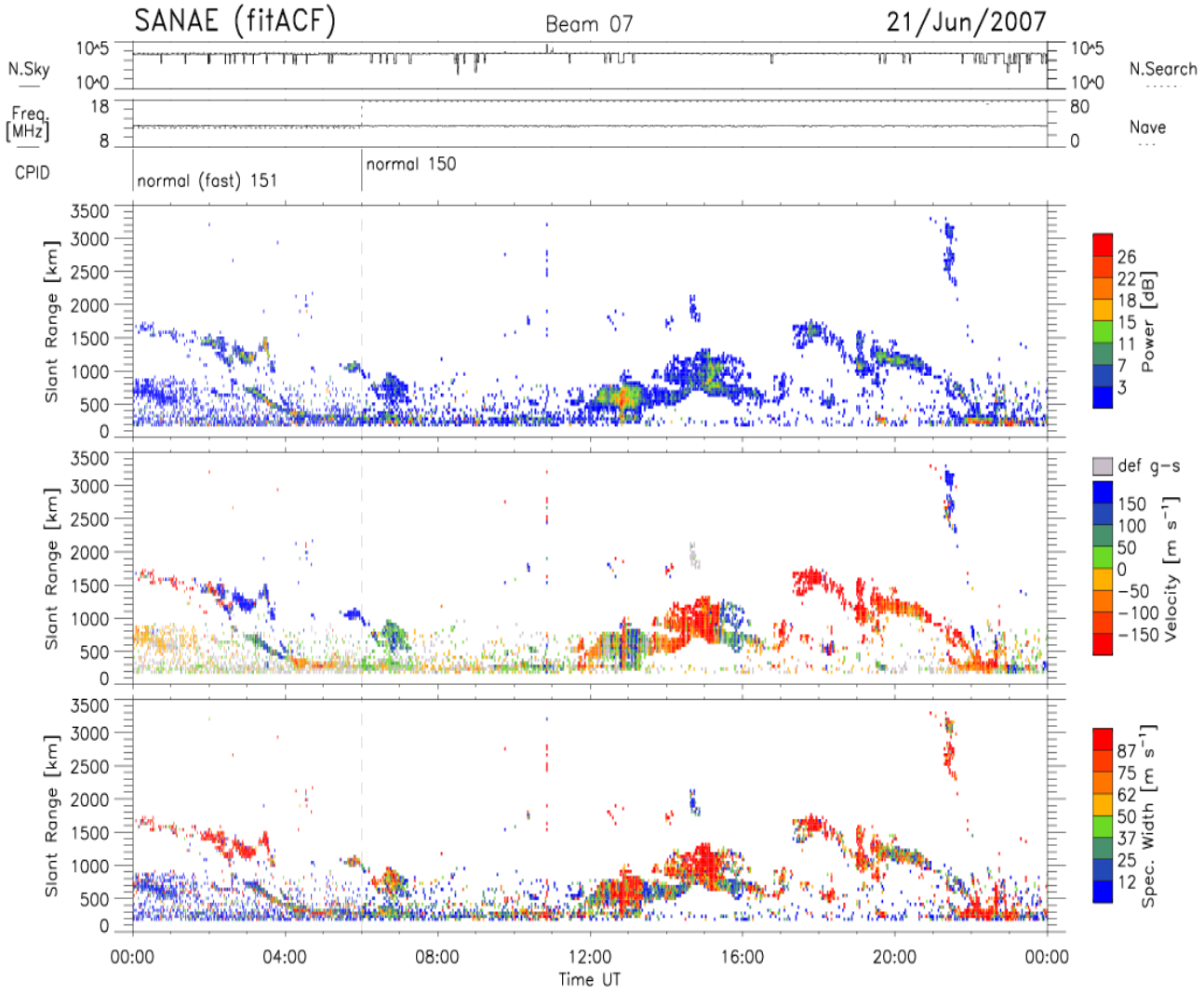

Figure 3.1: Summary plot of power (dB) (top panel), velocity ($m.s^{-1}$) (middle panel), and Lorentzian spectral width ($m.s^{-1}$) (bottom panel) for Halley beam for May 2007.

There are so many studies in which SuperDARN radar data was utilized and hence, has become a stepping stone for further studies. Lima et al., (2012) investigated the sudden stratospheric warming effects on the mesospheric tides and 2 day wave dynamics using meteor HF radar at meteor radar measurements obtained at São João do Cariri, Brazil (7.4°S, 36.5°W). They concluded that from the year 2005 to 2006 there was some unusual MLT dynamics which was characterised by increased amplitude of the quasi-2-day and tidal oscillations. During this time interval a major SSW event was observed in the NH polar stratosphere. Pancheva et al., (2004) investigated the planetary waves and variability of the semidiurnal tide in the mesosphere and lower thermosphere over Esrange (68°N, 21°E) during winter. They found a 16-day wave from global wavelet spectrum analysis of data ranging from October 1999 to December 2002. (Hussey et al., 2000) compared horizontal wind data from near co-located medium frequency (MF) radar and SuperDARN radars at Saskatoon, Canada (52°N, 107°W). In their work they observed good agreement between the SuperDARN radar wind and those recorded by the MF radar at around ~95 km. They have concluded that the two systems complement each other effectively.

Kumar et al., (2006) investigated the meteor radar observations of solar tides and planetary wave interaction in the MLT region over Trivandrum (8.5°N, 77°E). From continuous meteor radar observations of the MLT region during August 2004 to August 2005 they discovered that there was evidence of wave-wave interaction in the MLT region. Espy et al., (2005) combined simultaneous data recorded by SuperDARN and MF radars over Antarctica and studied the periods, wavenumber, and propagation direction of the planetary waves in the MLT. A study by Hibbins and Jarvis (2008) compared wind and tidal measurements in the upper mesosphere recorded with an imaging Doppler interferometer (IDI) and SuperDARN radar at Halley, Antarctica, and observed a correlation of approximately 0.2 between the SuperDARN meridional wind and tides with the IDI, at a height between 90 and 95 km above the earth's surface. Mbatha et al., (2010b) studied the impact of sudden stratosphere warming in the upper mesosphere-lower thermosphere regions using satellite and HF radar measurements. They managed to show that the mean zonal wind from SANAE HF radar displayed an enhancement due to a series of large planetary wave amplifications in the stratosphere throughout the winter season of the year 2002 at ~94 km. In this thesis, data from SANAE and Halley radar stations was used. The geographical locations of SANAE and Halley high frequency radars are shown in Figure 3.2 and

their longitudinal difference of 24 degrees made them suitable for this study in estimating reliable wavenumbers.

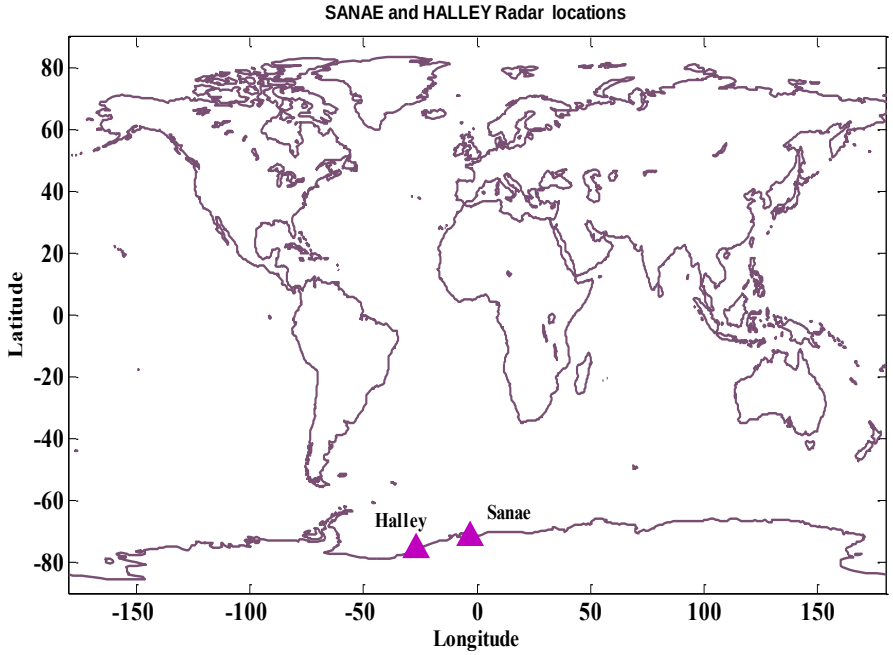

Figure 3.2: Geographical locations of SANAE and Halley high frequency radars.

A list showing all Southern Hemisphere SuperDARN radars and their locations is tabulated in the following Table 3.1. Apart from the close proximity of the SANAE and Halley HF radars, the two radars were also chosen because of the availability of data during the period when the interaction between planetary waves and tides is investigated.

Table 3.1: List of Southern Hemisphere SuperDARN radars and their geo-locations.

Southern Hemisphere SuperDARN Radars			
Radar name	**Latitude**	**Longitude**	**Code**
Falwand Island	-51.83	-58.98	Fir
TIGER Unwin	-46.51	168.38	Unw
Kerguelen	-49.22	70.14	Ker
McMurdo	-77.88	166.73	Mcm
Halley	**-75.52**	**-26.63**	**Hal**

SANAE	**-71.68**	**-2.85**	**San**
Syowa East	-69.00	39.58	Sye
Syowa South	-69.00	39.58	Sys
Zhongshan	-69.38	76.38	Zho
Tiger	-43.40	147.20	Tig
Unwin	-46.51	168.38	Unw

The SuperDARN network has been designed so that the fields of view of at least two radars overlap each other. In this study data from SANAE and Halley radar was used and these radars' field of views overlaps as illustrated in figure 3.3 right panel, highlighted in blue.

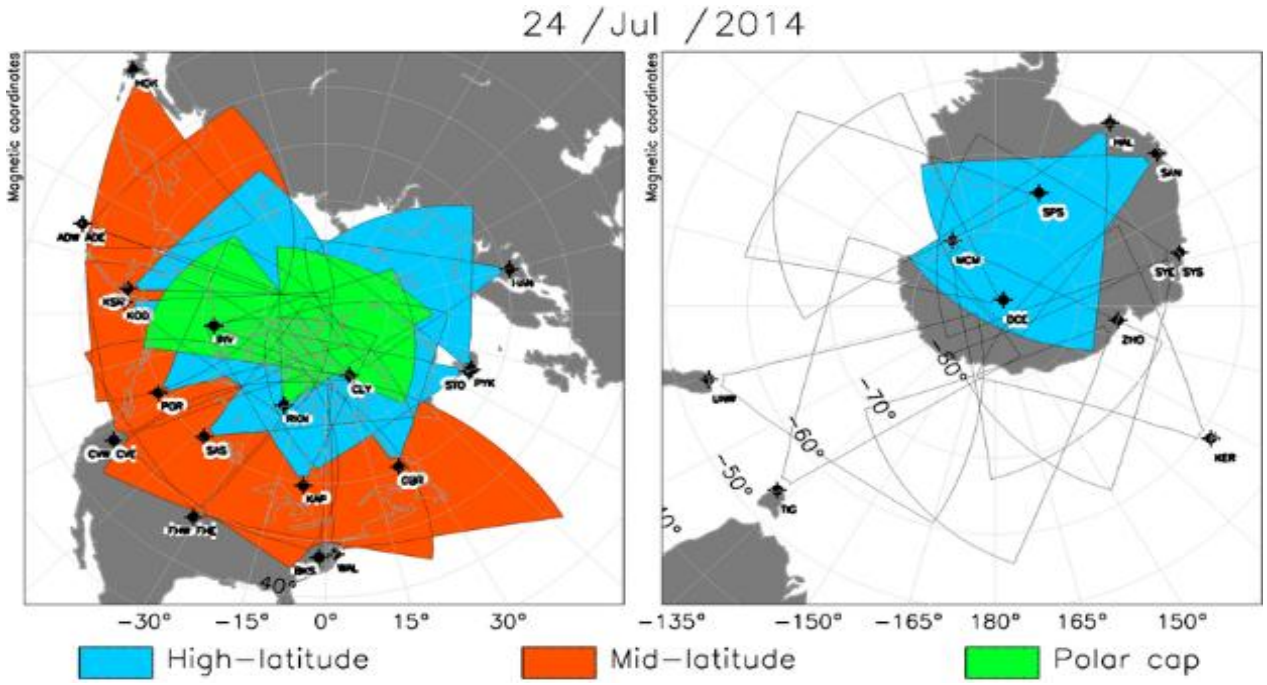

Figure 3.3: Schematic diagram showing SuperDARN radar geo-locations and their field of view. On the left panel is the Northern Hemisphere whilst right panel represents the Southern Hemisphere radar locations and their field-of-views. (Source: Virginia Tech, http://vt.superdarn.org/tiki-index.php).

Figure 3.4 shows the SANAE radar antenna consisting of 16 transmitting antennas in the main array at the Southern Hemisphere Antarctica, which are capable of about 600 Watts output each, for a maximum peak power of 9.6 kW. The 16 T-shaped towers stood 15 m high in an east-west line more than 200 m long, supporting a grid of aluminum antenna elements which collectively transmit and receive signals allowing scientists to study the upper atmosphere over the South Pole.

Figure 3.4: The SANAE 16 antenna array.

The returned backscattered signal from the Radar comprises of the power, or signal to noise ratio, on a logarithmic scale (dB), which is a measure of the magnitude of the high frequency power is backscattered to the radar. The second parameter is known as the light of sight velocity, which is a measure of the motion of the irregularities in the atmosphere either towards or away from the radar. An irregularity (meteor or small particle) moving transverse to the beam may have a velocity of zero. The last parameter is the spectral width (Lorentzian), which is a measure of the full width at half maximum of the peak in a corresponding single-peaked Doppler spectrum.

3.3.1 NCEP/NCAR Re-analysis Data

Zonal wind and temperature data used in this work were obtained from the National Centre for

Environmental Prediction and National Centre for Atmospheric Research (NCEP/NCAR) reanalysis project from 2002-2013. The NCEP, formerly known as the National Meteorological Center (NMC)/NCAR, reanalysis project began in 1991 as an outgrowth of the NMC Climate Data Assimilation System (CDAS) project. From the collaboration of NCEP and NCAR for global analysis of atmospheric fields in support of the needs of the research and climate monitoring communities, daily meteorological values on 2.5 latitude by 2.5 longitude resolution for 17 pressure levels. NCEP/NCAR re-analysis data is a combination of assimilated data from globally scattered meteorological instruments. These instruments focus on land surface, ocean surface, upper air such as global radiosonde data, Comprehensive Ocean Atmosphere Data Set (COADS) marine surface data, aircraft data, surface landscape synoptic data and satellite sounder. NCEP/NCAR reanalysis data is used for data analysis as well as data assimilation, (Kalnay et al., 1996).

3.3.2 UKMO Data Assimilation

The technique of data assimilation was implemented since October 1991 by United Kingdom Meteorological Office (UKMO) to produce a global meteorological analysis of the troposphere and stratosphere. As described by Lorenc et al., (1991), the UKMO data assimilation system is advancement from the system previously used to analyse observations for operational weather forecasting. The data assimilation system is well described in the work of Swinbank et al., (1994). The UKMO data assimilation system produces the following elements among others on a daily basis, zonal wind, meridional wind and temperature from various pressure levels ranging from 1000 to 0.1 hPa. A global numerical model with a horizontal resolution of 2.5° and 3.75° steps in the latitude and longitude respectively is implemented. All recordings are subjected to a quality control system before they can be recommended for a numerical model. UKMO data was used for Comparison of U.K. Meteorological Office and U.S. National Meteorological Centre stratospheric analyses during the Northern and Southern winter (Manney et al., 1996). Using UKMO and medium frequency data it was observed that mesospheric cooling and stratospheric warming in the tropical regions is correlated with stratospheric warming events at middle and high latitudes (Shepherd et al., 2007).

Table 3.2: Pressure levels in (hPa) and their relevant altitudes in (km).

Pressure (hPa)	Altitude (km)
1000	0.0
700	3.0
500	5.5
300	9.5
200	12.0
150	14.0
100	16.5
70	19.0
50	21.0
30	24.5
20	27.0
10	32.0
7	34.5
5	37.0
3	41.0
2	44.0
1	49.5
0.5	55.0
0.3	59.0

3.4 Data Analysis Techniques

3.4.1 Fourier Transform

The transformation from the time domain to the frequency domain is based on forward Fourier Transform (FT). Every signal can be written as a sum of sinusoids with different amplitudes and frequencies. Fourier Transform is a technique that is used to investigate the frequency content of

a signal. Using FT you can decompose a signal into sinusoids of different frequencies which add to the original signal. Brook et al., (1998) defined the Fourier Transform of a signal $x(t)$ as

$$X(\omega) = \int_{-\infty}^{\infty} x(t)e^{-i\omega t}dt \quad \textbf{(3.1)}$$

The inverse Fourier Transform is defined as

$$x(t) = \frac{1}{2\pi}\int_{-\infty}^{\infty} X(\omega)\, e^{i\omega t}d\omega \quad \textbf{(3.2)}$$

Where $\omega = 2\pi f$

Equation 3.1 gives the Fourier Transform of a signal (i.e. presenting the frequency components in a signal) without actually providing the exact time of occurrence of each frequency. Such a technique will be of importance for a stationary signal. For this reason, Fourier Transform is not a good method for signals whose spectral components vary with time, hence other methods like Short Time Fourier Transform (STFT) or Wavelet analysis can be implemented.

3.4.2 Short-Time Fourier Transform (STFT)

Fourier Transform is not a good method for signals whose spectral components vary with time, hence Short Time Fourier Transform (STFT) method can be implemented to deduce the spectrum of the signal and the time of occurrence of spectral components to localize the frequency in time. When applying this technique, the signal is divided into small segments, and these segments are assumed to be stationary. The Fourier transform is then applied to the windowed signal segments advancing the window in time along the full length of the signal. Short Time Fourier Transform can be properly represented mathematically (Brook and Wynne, 1988)

$$X(\omega, t) = \int_{-\infty}^{\infty} x(t)\, g(t-k)e^{-i\omega t}dt \quad \textbf{(3.3)}$$

where g is the windowing function which is systematically moved along the length of the signal $x(t)$, and $\omega = 2\pi f$.

The result of the operation above is the time-frequency representation of the signal which shows the frequency components that are present in the signal and the corresponding time at which they occur. The narrower the window is, the better the time localization of the frequency spectrum, but giving a poorer frequency resolution. In a time frequency representation there is a trade-off between time localization and frequency resolution in the sense that good time-frequency resolution of the signal can be achieved by using a narrow window when looking for a high frequency and vice-versa. The disadvantage of this method is that once the window length has been chosen, that window will be the same for all frequencies, hence a technique with a window function that can be varied depending on whether high or low frequency spectral components are analysed is the best in order to obtain a better time-frequency resolution. With regard to the disadvantage mentioned above, the wavelet analysis method which will be discussed in the next chapter can be implemented.

3.5. Wavelet Analysis

Wavelet analysis has attracted attention for its ability to analyse rapidly changing transient signals. Any application using the Fourier Transform can be formulated using wavelets to provide more accurate localized temporal and frequency information. Wavelets are obtained from shifting and dilated or a scaled version of the mother wavelet and by construction. The advantage of wavelets is that they are much localized functions being able to resolve frequency transitions during short periods. There are different types of mother wavelets that can be used and these include among others, the Morlet, Paul, and Derivative of Gaussian (DOG) wavelets etc. (Torrence and Compo, 1998). In this study the Morlet wavelet function is used because the localization of signal characteristics in time and frequency domains can be accomplished with this wavelet function.

3.5.1 Wavelet Transform

Considering a real or complex-valued continuous time function ψ satisfying the following conditions**:**

$$\int_{-\infty}^{\infty}|\psi(t)|^2 dt < \infty \quad \textbf{(3.4)}$$

$$c_\psi = 2\pi \int_{-\infty}^{\infty} \frac{|\boldsymbol{\psi}(\omega)|^2}{|\omega|} d\omega < \infty \quad \textbf{(3.5)}$$

Where $\boldsymbol{\psi}$ is the Fourier Transform of ψ.The first condition implies that the function ψ has finite energy, and the second condition which is the admissibility condition, implies that if $\boldsymbol{\psi}(\omega)$ is smooth $\boldsymbol{\psi}(0)$=0, meaning the function integrates to zero. The function $\psi(t)$ is a mother wavelet if the two above mentioned conditions and admissibility properties are met and it can be presented by the following equation.

$$\psi_{ab}(t) = \frac{1}{\sqrt{a}}\psi\left(\frac{t-b}{a}\right) \quad \textbf{(3.6)}$$

Where a is the scale and b is the position of ψ. The complex $\frac{1}{\sqrt{a}}\psi\left(\frac{t-b}{a}\right)$ represents the wavelet basis function or the mother wavelet. The complex Morlet wavelet which was used in this study is given by the following equation;

$$\psi(t) = e^{-(t/c)^2} e^{i2\pi f_0 t} \quad \textbf{(3.7)}$$

where f_0 is the frequency parameter, t is the time and c is the damping parameter. This represents a time domain function that is a product of a Gaussian and complex exponential with center frequency f_0.

3.5.2 Continuous Wavelet Transform (CWT)

If ψ satisfies the conditions described above, then the wavelet transform of a real signal $s(t)$ with respect to the wavelet function $\psi(t)$is defined as

$$\mathrm{Ws(b,a)} = \frac{1}{\sqrt{a}} \int_{-\infty}^{\infty} \mathrm{S(t)}\, \psi^{*} \left(\frac{t-b}{a}\right) \mathrm{dt} \qquad \textbf{(3.8)}$$

Where * denotes the complex conjugate and this is defined on the open (b, a) half plane ($b \in \mathbf{R}$, $a > 0$). The parameter b corresponds to the time shift/translation and a, corresponds to the scale of the analyzing wavelet hence the scale and time parameters (a) and (b) are assumed to be continual values (Kumar, 1997).

3.5.3 Time-Frequency Localization

In this section time-frequency localization will be discussed considering time-frequency resolution. The above theory of Fourier Transform revealed its inability to present signals whose spectral components vary with time whilst wavelets has showed that the wavelet transforms have a good time-frequency resolution due to the fact that it uses a variable ‘window’ function by performing both the correlating and windowing process as illustrated in Figure 3.4. The wavelet transform technique can measure the time-frequency variations of spectral components like a windowed Fourier Transform, but it has a different time-frequency resolution (Mallat, 1998).

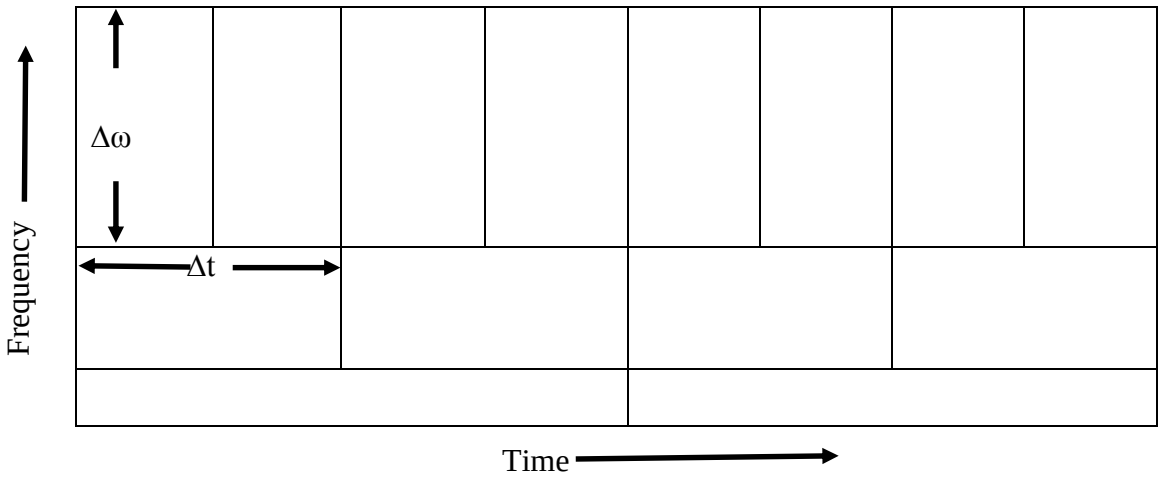

Figure 3.5: Time-frequency localization, the vertical and horizontal dimensions represent frequency and time respectively.

The frequency increase upward and time increases to the right. The change in time Δt represents the horizontal dimension of each cell while Δω is the vertical dimension of each cell, hence the area of each cell is given by Δt. Δω. Even if the dimensions of the cells changes, the area of each cell remains constant and it represents one value of the wavelet transform.

If the frequency is high, the horizontal dimensions of the cells are shorter which correspond to shorter window length. Therefore, the signal is better resolved in time and poorly resolved in frequency. In low frequencies the horizontal dimensions are longer and this corresponds to the longer window length, hence the signal is better resolved in frequency and poorly resolved in time. Wavelet analysis is designed to give good time resolution and poor frequency resolution at high frequencies, and vice versa (Kumar, 1997; Mthembu, 2006; Khanyile, 2011 and Mbatha, 2012).

3.5.4 Frequency Filtering

Frequency filtering refers to extracting the important part of any data while eliminating random contributions called "noise" or other unwanted features which obscure the ones that matter. Basically there are four common types of frequency filtering process which are low-pass, high-pass, band-pass and band-reject filters. The pass band refers to the frequencies that are allowed to pass, while the stop band contains those frequencies that are blocked and the division between the pass band and transition band is called the cutoff frequency. A low-pass filter allows low frequencies to pass unaltered whilst it attenuates high frequencies and high-pass filter is completely the opposite that is, it attenuates low frequencies passing high frequencies unaltered. A band-pass filter works to screen out frequencies that are too low or too high, giving easy passage only to frequencies within a certain range. Lastly a band-reject filter is the one that passes most frequencies unaltered, but attenuates those in a specific range to very low levels. It is the opposite of a band-pass filter, as illustrated in the Figure 3.6.

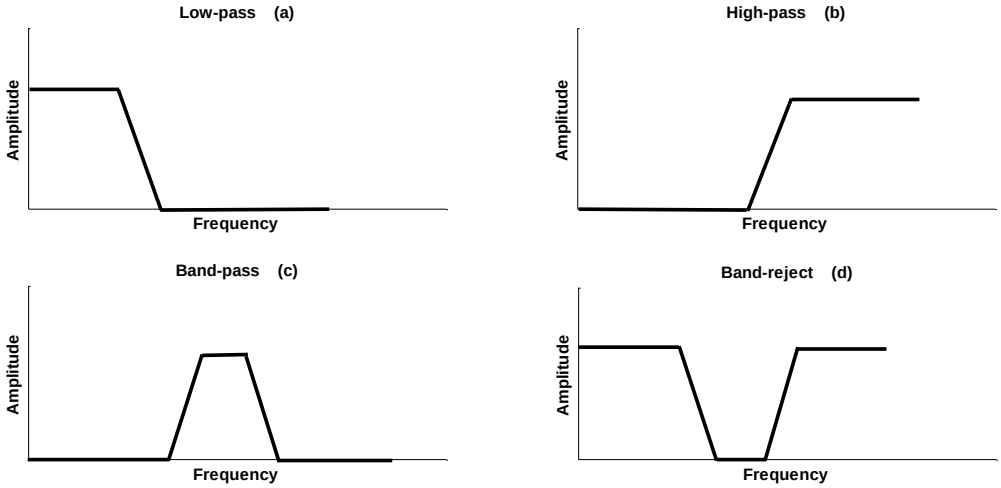

Figure 3.6: Four common frequency filter responses; low-pass (a), high-pass (b), band-pass (c), and band-reject (d), (Smith, 2003).

3.5.5 Complex Demodulation

Complex demodulation is a technique used to extract the local amplitude and phase of a periodic non-stationary signal. In general, it is implemented by multiplying a given time series by a complex sinusoid $\left(e^{-j\omega\, dt}\right)$ where $j = \sqrt{-1}$ and ωd is the demodulation frequency, and then pass the result through a low pass filter. Considering a non-stationary signal as explained by Priestly (1981) and noise in the mathematical form of;

$$x(t) = \sum_{j=1}^{m} X_j(t) exp(i\omega t) + Z(t) \qquad \textbf{(3.9)}$$

where $X_j(t)$ is the complex amplitude which shifts over the time showing the variation of the amplitude and phase of the j^{th} harmonic component. Complex demodulation helps in the detection of a particular component in a signal and also estimates its change in amplitude and phase (Priestley, 1981). The amplitude of the complex demodulation of the time series is a measure of the amplitude of the dominant frequency within the band pass around the demodulation frequency. The demodulated signal can be represented as;

$$x(t) = \frac{1}{2} X(t) exp[i\emptyset(t)] + \frac{1}{2} X(t) exp\left[-i\left(2\omega t + \emptyset(t)\right)\right] + Z(t) exp(i\omega t) \qquad \textbf{(3.10)}$$

On the right hand side the first term varies slowly with no power at or above the frequency ω, the second term varies at frequency 2ω and the third term varies at frequency ω. The component $Z(t)$ has no power at frequency ω hence the shifted third term has no power at zero frequency. A low pass filter is applied to remove frequencies at or above the frequency ω thus removing the second and third terms yielding;

$$x'(t) = \frac{1}{2} X'(t) exp(i\emptyset' t) \qquad \textbf{(3.11)}$$

Where the prime indicates smoothing and the type of smoothing used determines the output frequency band produced. The amplitude $X'$and phase $\emptyset'$ can then be extracted and presented as follows respectively;

$$X'^{(t)} = 2|x'| = 2[Re(x')^2 + Im(x')^2]^{\frac{1}{2}} \quad \textbf{(3.12)}$$

$$\emptyset'(t) = atan\left[\frac{Im(x\prime)}{Re(x\prime)}\right] \quad \textbf{(3.13)}$$

where Re and Im represents the real and imaginary parts respectively.

Chapter 4: Planetary Wave Activity and Tides using SANAE and Halley

4.1 Introduction

The middle atmosphere plays a crucial role as much as the understanding of the whole atmosphere is concerned, (Houghton, 1986). The dynamics of the middle atmosphere is reported to be controlled by vertically propagating planetary waves of significant amplitudes (e.g. Holton, 1979). As planetary waves propagate upwards through the middle atmosphere they attain large amplitudes as density decreases and they distribute momentum and energy from the lower to upper atmosphere (e.g. Clark et al., 1994; Fritts et al., 1999 and Mbatha et al., 2010b). Recent studies have revealed that wave-wave and mean flow wave interactions play a vital role in the dynamics of the middle atmosphere. During the process of planetary wave amplification a surf zone can be formed if the polar vortex is disturbed (e.g. Andrews et al., 1987 and Holton, 2004). As atmospheric waves interact with the mean flow processes such as wave filtering, wave breaking or mean wind reversal can be favoured (e.g. Dowdy, 2005; Mbatha et al., 2010b etc.). A study by Mayr et al., (2011), reported that as gravity waves propagates upwards they carry the accumulating imprints of non-linear interactions with the zonal mean flow, tides and planetary waves.

This chapter focuses on the middle atmosphere interaction of planetary waves of period ranging from 2 to 30 days and tides. This will pay attention to tidal wave activity at planetary wave scale focusing on diurnal and semidiurnal waves.Wave variability will be monitored from the stratosphere to the lower mesosphere. So many factors have been accredited to several wind and temperature variations which occur in the MLT region, to include Quasi Biennial Oscillation (QBO) (Namboothiri et al., 1994), Semi-Annual Oscillation (SAO) (Reed, 1966), solar variations and SSW. Earlier it has been outlined how SuperDARN radars were made to be useful in monitoring the dynamics of the MLT region.

4.2 Planetary Waves

The data used in this study was measured by two Southern Hemisphere high latitude HF radar stations, namely SANAE (72°S, 3°W) and Halley (76°S, 27°W). Using Torrence and Compo, (1998) wavelet analysis method, the wavelet spectra for the zonal wind and meridional wind variations for SANAE station were calculated and presented below. This method revealed the dominant wave activity of periods below 30 days which were noted for the years 2005 to 2007. Figure 4.1a, c, and e, the left column presents the zonal wind wavelet spectra and the right column (Figure 4.1b, d, and f) presents the meridional wavelet spectra. In general, the wave activity with a wave power of 500 $m^2.s^{-2}$ is observed around day 100 for the year 2005 and 2006.

In the year 2007 it was a different case because around day 100 there is no significant planetary wave activity compared to the previous years, but during winter around day 250 an intense wave activity was noted. The zonal wind component shows more wave activity compared to the meridional wind component. Figure 4.1a shows that during the year 2005 a quasi-10-day wave was observed around day 100 with a wave power of 500 $m^2.s^{-2}$. Around day 225, a quasi-7-day was observed and it had a maximum wave power of 1000 $m^2.s^{-2}$. A study by Wayne et al., (2011) on the long term behaviour of the MLT quasi-7-day wave at two radar sites at the Northern polar latitudes concluded that the wave activity is highly sporadic in nature. This was mainly because it had stronger wave activity during winter, moderate during the equinoxes and minimum during summer.

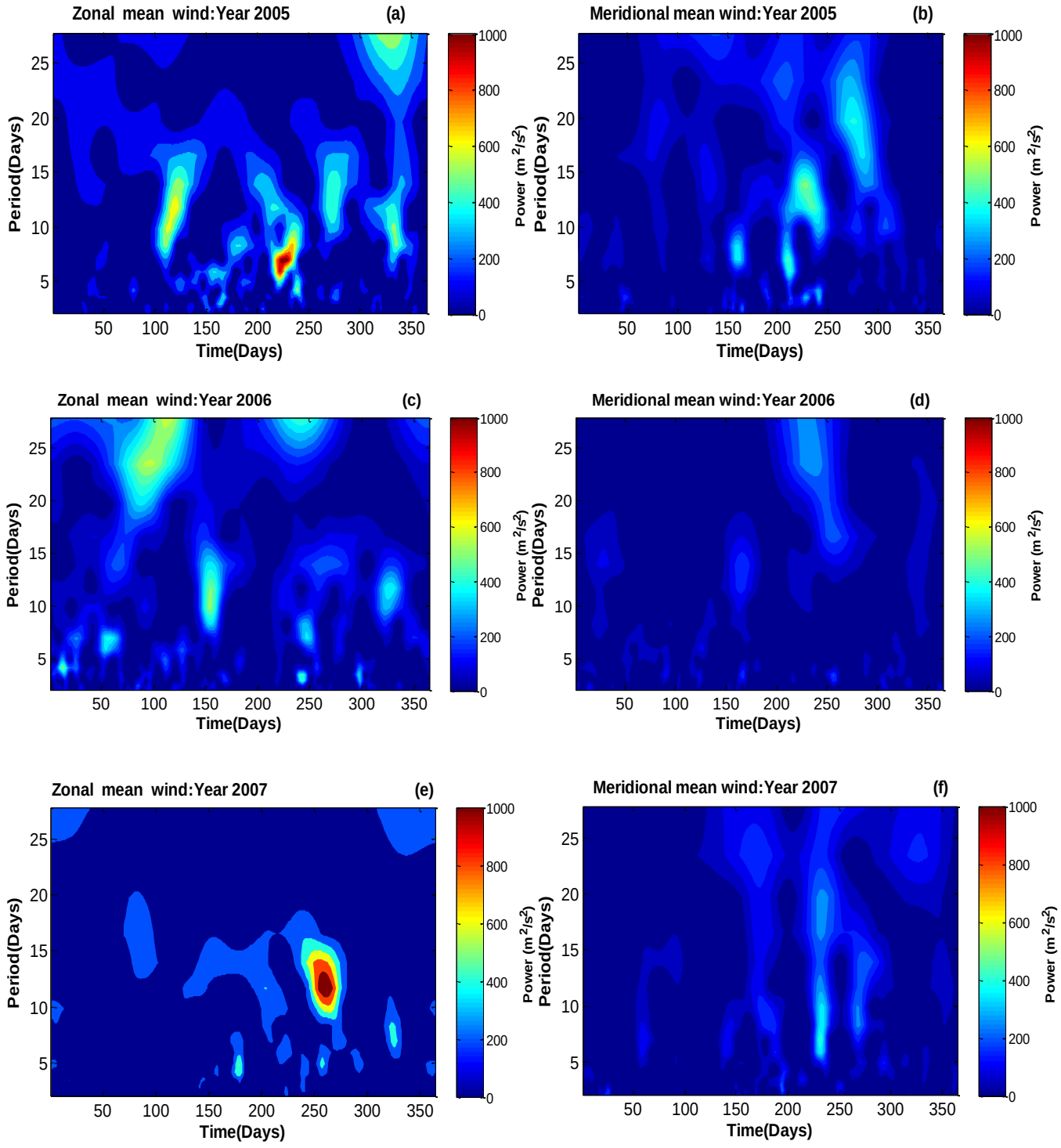

Figure 4.1: Wavelet power spectrum versus time (for the years 2005-2007) and period (less than 30 days) calculated for the zonal and meridional wind components for SANAE Super DARN HF radar wind at ~94km.

Compared to the years 2005 and 2007 the year 2006 (Figure 4.1c), shows a low maximum wave power of 600 $m^2.s^{-2}$. In Figure 4.1e the maximum zonal wind wave power of 1000 $m^2.s^{-2}$ and dominant periods between 8 and 14 days were noted during the winter season of the year 2007. In both zonal and meridional wind components, the winter months are observed to be characterised by bursts of wave activity with wave periods coinciding to quasi-10-day, quasi-14-day and quasi-16-day waves. The more dominant wave activity observed on approximately day 260 with a wave period centered at around 14 days with wavenumber s=0 and s=-1 is of greater importance to the dynamics of the MLT region. Less significantly, the wave activity of wave periods above 20 days with maximum wave power of 600 $m^2.s^{-2}$ and 400 $m^2.s^{-2}$ in the zonal and meridional winds respectively could have also contributed to the simulation of minor SSW.

It can be noted that in all the years from 2005 to 2007, the zonal wind component shows more planetary wave activity compared to the meridional wind component, but in all the cases there is an amplification of planetary waves during the winter season. In the year 2005 a strong wave activity of periods between 8 and 16 days was observed in zonal wind during winter season, but the strongest was observed around day 250 with dominant wave periods between 5 and 10 days. Of the three years (2005-2007), the strongest wave activity was observed in the year 2007 in the zonal wind component during winter season and it was dominated by wave periods between 10 and 16 days. A maximum wave power of about 1000 $m^2.s^{-2}$ was noted as mentioned above, hence this became the special year of interest for this study. A very strong planetary wave activity resembling traces of quasi-10-day and quasi-16-day waves centered at approximately 12 days was noted. Such a strong wave activity could be a result of wave-wave interaction. The zonal wave number, variation of tides amplitudes and investigation of minor SSW will be presented in the next chapter so that a complete analysis of the effects and possible strong wave activity can be classified.

During the spring and autumn seasons a strong wave activity with a planetary wave period of around 8 to16 days and 16 to 30 days in the zonal component was observed and most probably because this period is a transition time with strong trends in mean wind (e.g. Chshyolkova et al., 2006) and Mbatha, 2012). In this study, the year 2007 was chosen to be the year of interest to

investigate the interaction of planetary waves with tides during the period with strong wave activity.

A similar method of analysis was applied to the Halley station for the same period of (2005-2007) in both zonal and meridional wind components. Figure 4.2 shows the wavelet power spectra for Halley showing the wave activity of wave periods between 2 and 30 days. By merely looking, it can be noted that Halley is dominated by long period planetary waves compared to SANAE. In general, there is a good agreement between the two stations for example the zonal wind in each case shows more wave power activity compared to the meridional wind component. The interesting part with the Halley station is that the wave activity took place mostly during the winter season.

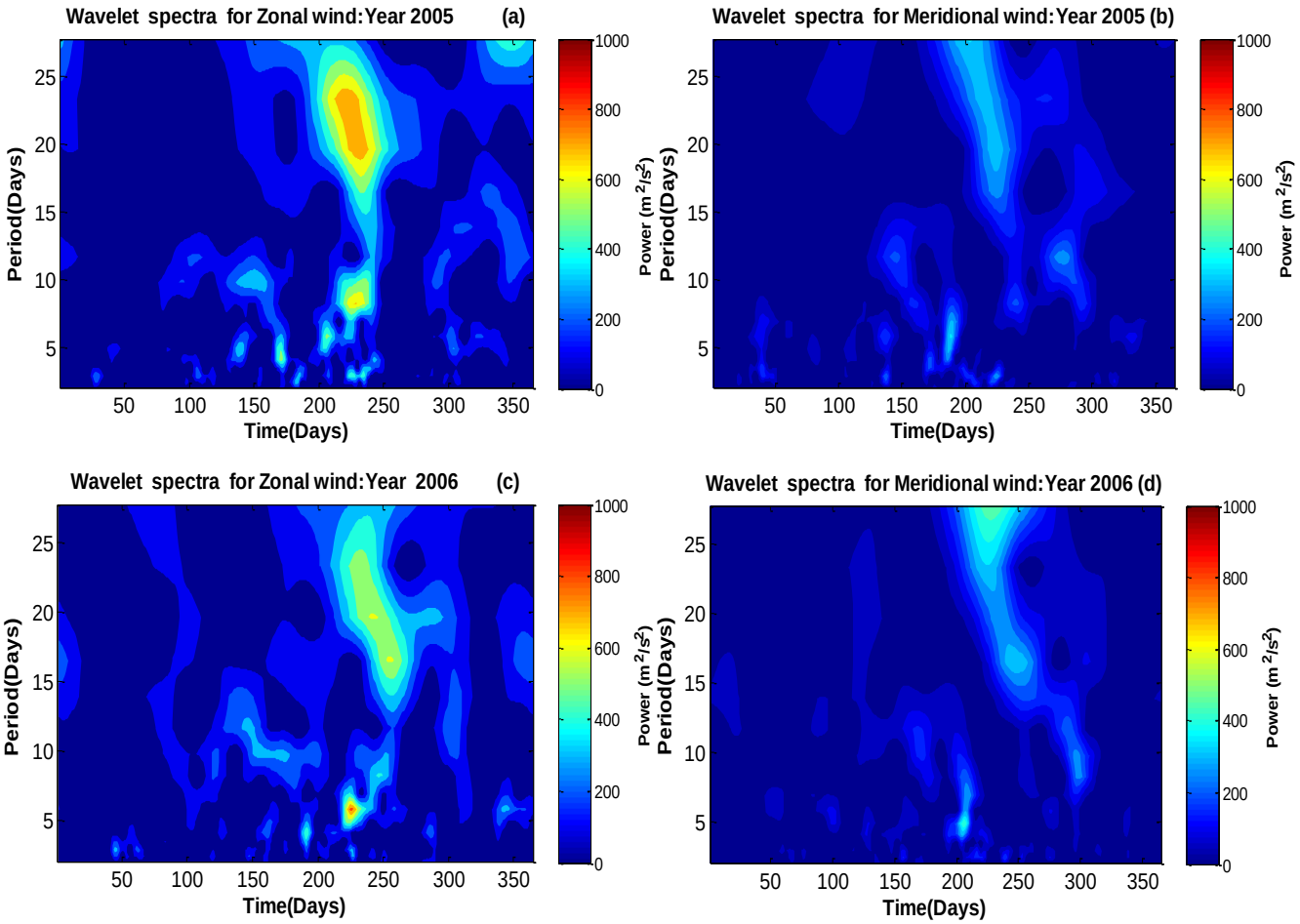

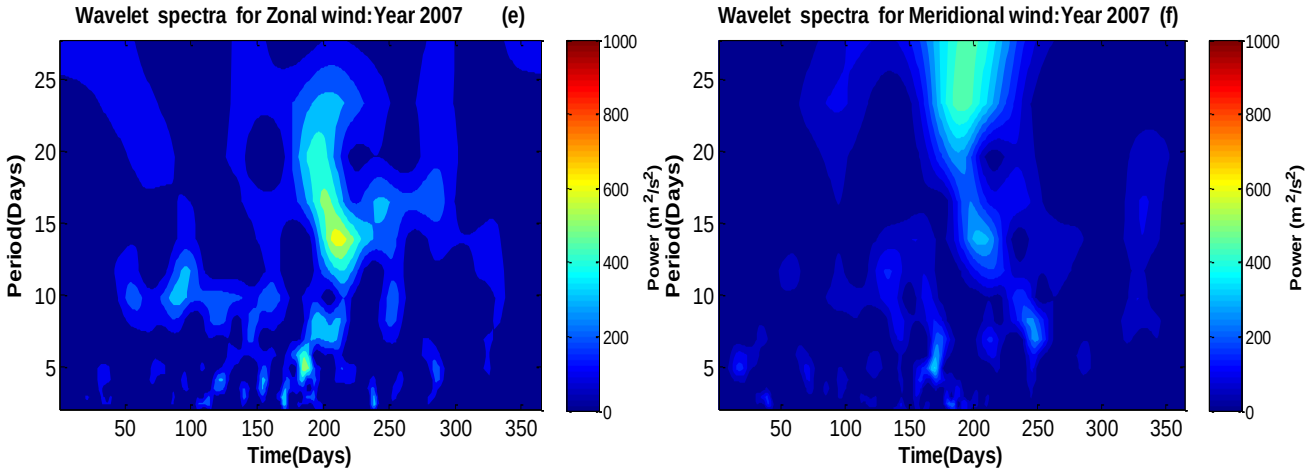

Figure 4.2: Wavelet power spectrum versus time (for years 2005-2007) and period (less than 30 days) calculated for the zonal and meridional wind components for Halley Super DARN HF radar wind at ~94 km.

Figure 4.2a, c, and e, presents the wavelet spectra of the zonal wind component. A trace of quasi-10-day wave and long period planetary waves whose wave periods stretches from 14 to 28 days were noted. The year 2005 (Figure 4.2a) shows a strong planetary wave activity of wave power of about 700 $m^2.s^{-2}$, and the quasi-10-day wave which is clearly defined compared to the other years. The same wave characteristics of the year 2005 were observed in the year 2006 (Figure 4.2c), but with less wave power. The planetary wave periods observed are a result of the amplification of 10-day, 14-day and 16-day planetary waves. The zonal component of the year 2007 (Figure 4.2e) shows the lowest wave power compared to the years 2005 and 2006, but there are similar wave characteristics though. This brings about a complete annual variance analysis that during the three year period, the maximum wave power was noted in the year 2005 and it started to decrease in the year 2006 and 2007 as well. Also, considering the time of long period planetary wave activity occurrence, it started around day 210 for the years 2005 and 2006 whilst for the year 2007 it commences earlier around day 180.

Figure 4.2b, d, and f, presents the wavelet spectra for the meridional wind component for the years 2005-2007. In all the years from 2005 to 2007 it can be noted that there is a presence of quasi-10-day, quasi-14-day and quasi-16-day wave amplification. The maximum wave power

observed in the meridional wind component of all the years was 500 $m^2.s^{-2}$ and it was noted during the year 2007. In all the years the meridional component shows the presence of long period waves of periods between 8 to 30 days. Unlike the case of the zonal wind component where there was an annual decrease of wave power. In the meridional wind component there was an annual increase in wave power from the year 2005 to 2007. The long period planetary wave activity started earlier in the year 2007 around day 155 while in the years 2005 and 2006 it started around day 180.

There is also a common trend showing internal wave amplification which goes along with the studies of Fedulina et al., (2004) and Chshyolkova et al., (2006), leading to longer period travelling waves in winter with periods ranging between 14 to 24 days in all the years but showing more wave power in zonal wind component. At low periods the wave activity is dominated by planetary waves of periods between 5 and 10 days and most significantly observed during the winter season of the year 2007 in zonal wind. The wave activity over the Halley station was more dominant during winter season, whilst at SANAE wave activity occurred in summer and winter and this could be a contribution of longitudinal difference of 24 degrees between the two stations.

4.3 Diurnal and Semidiurnal Tides

Since it was difficult to identify the shorter periods in the wavelet, the STFT was implemented. That was achieved by performing a dynamic Fourier spectrum using a 4 day data window that is shifted forward by 1 day at a time. The deduced power for a given data window was attributed to a central day given by day 2 of that particular 4 day data interval. This long data window result in the desired frequency resolution of 0.25 cycles per day. The four day average was considered to be significant if at least 55% of the hourly zonal or meridional wind values were captured.

Figure 4.3 to Figure 4.5 presents the contour plots showing the dynamic spectral analysis applied to the zonal and meridional wind components of SANAE HF radar wind data for the normalised power at ~94 km for the years 2005 to 2007. The power spectra has been normalised by δ^2/N where N is the number of data points and δ^2 is the variance of the time series. White noise would have an expectation value of one at all frequencies for such normalization (Torrence and Compo, 1998).

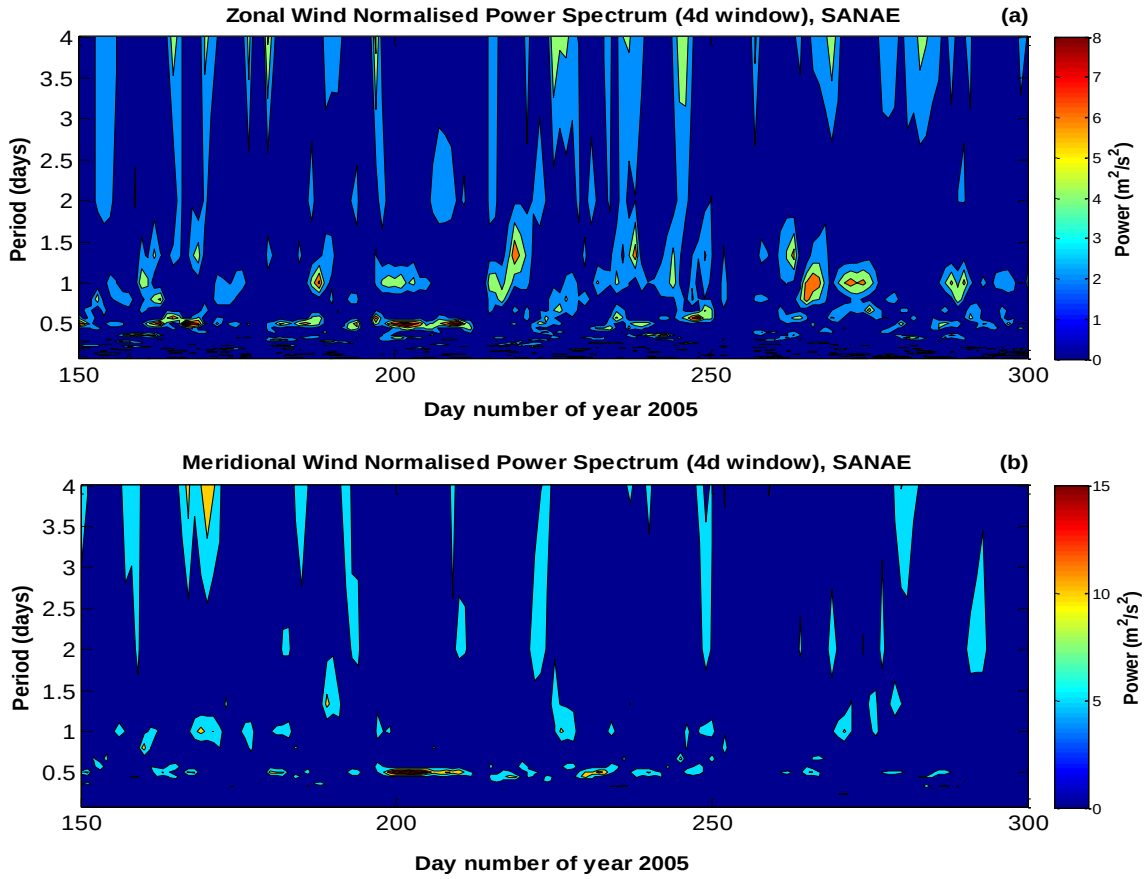

Figure 4.3: The normalised power spectra for the zonal (a) and meridional (b) wind component over SANAE station in 2005.

In all the figures from Figure 4.3 to Figure 4.5, it can be clearly seen that the zonal wind power spectra is characterised by dominant peaks near to periods of 0.5 day (semidiurnal tide) and 1 day (diurnal tide) waves in the midwinter. Considering Figure 4.3 to Figure 4.5, it is observed that the meridional wind power spectra is characterised by dominant peaks near periods of 0.5 day and 1 day waves, but the 0.5 day wave is more dominant showing a maximum wave power of approximately 7 $m^2.s^{-2}$. Of all the three years, the year 2007 shows a good and clear trace of diurnal and semidiurnal tides and these will be further investigated in detail later. More wave activity is observed in the zonal wind component compared to the meridional wind component in all the years from 2005 to 2007.

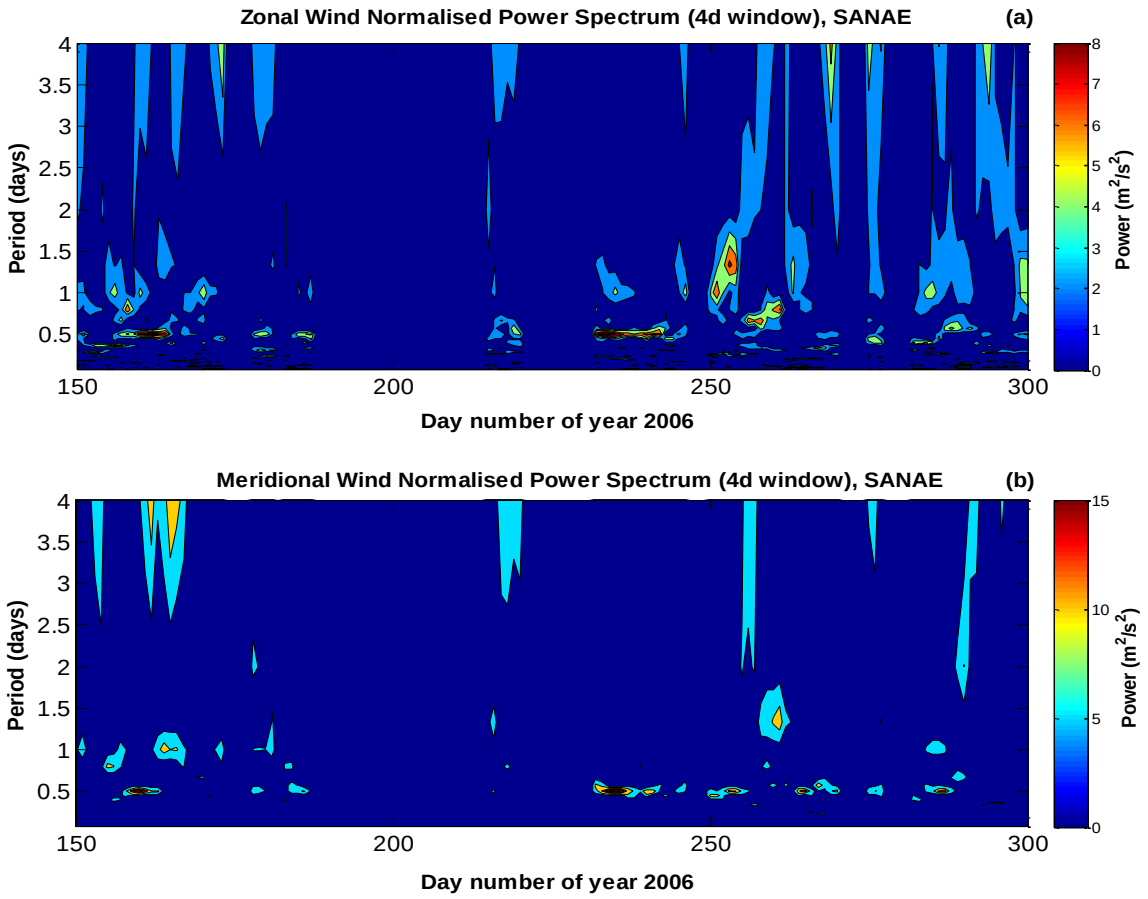

Figure 4.4: Same as Figure 4.3 but for the year 2006.

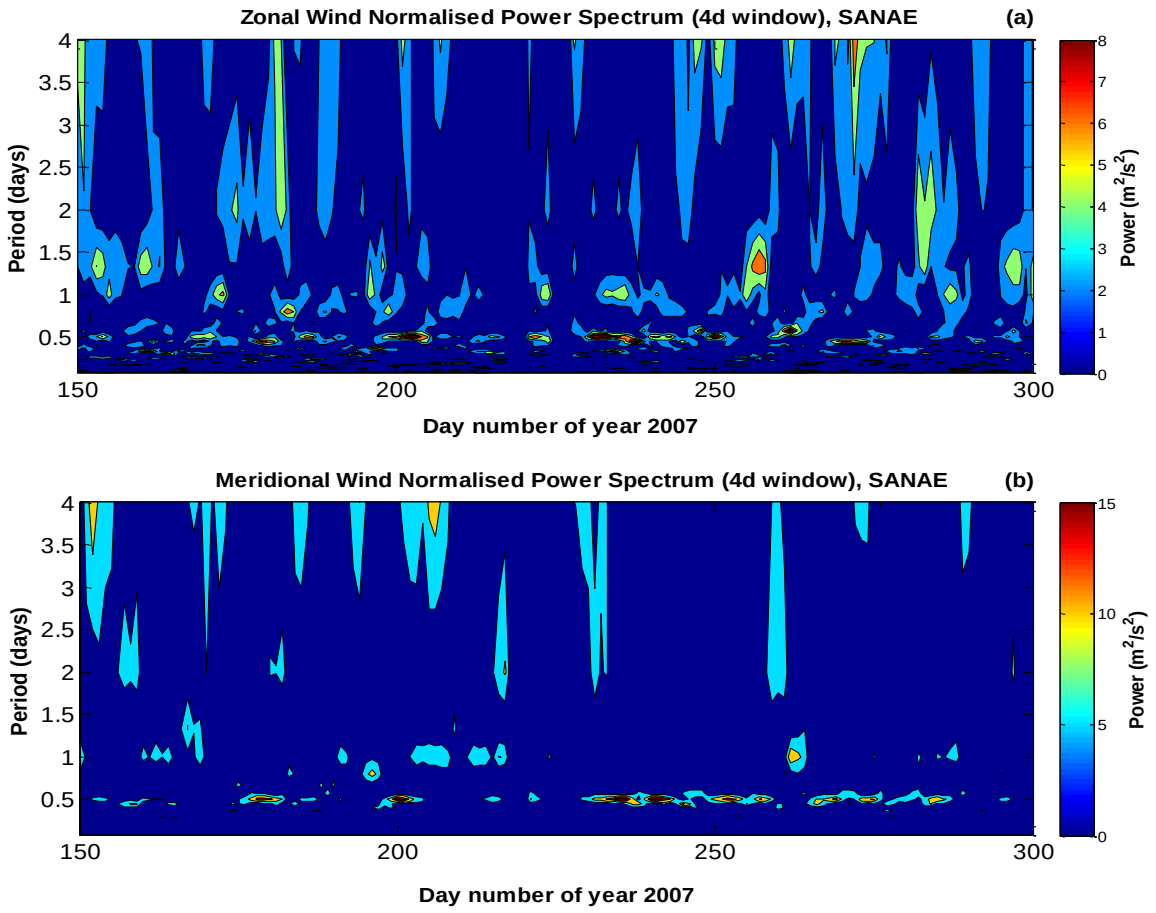

Figure 4.5: Same as Figure 4.3 but for the year 2007.

In Figure 4.6 to Figure 4.8 the horizontal grey thick line indicates the 90% confidence level using a chi-square test, assuming white noise as background spectrum (Torrence and Compo, 1998) while the dotted black line and the red line represents the DT and SDT normalised power spectra respectively. Figure 4.6 presents the normalised power spectra (top panels) and phase (bottom panels) for the 12 hour wave (SDT) and 24 hour wave (DT) for the year 2005 whilst Figure 4.7 and Figure 4.8 is for the years 2006 and 2007 respectively. For the three years 2005 to 2007 the normalised power of the SDT in the zonal and meridional wind components shows more power dominance thus more wave activity during winter and summer seasons.

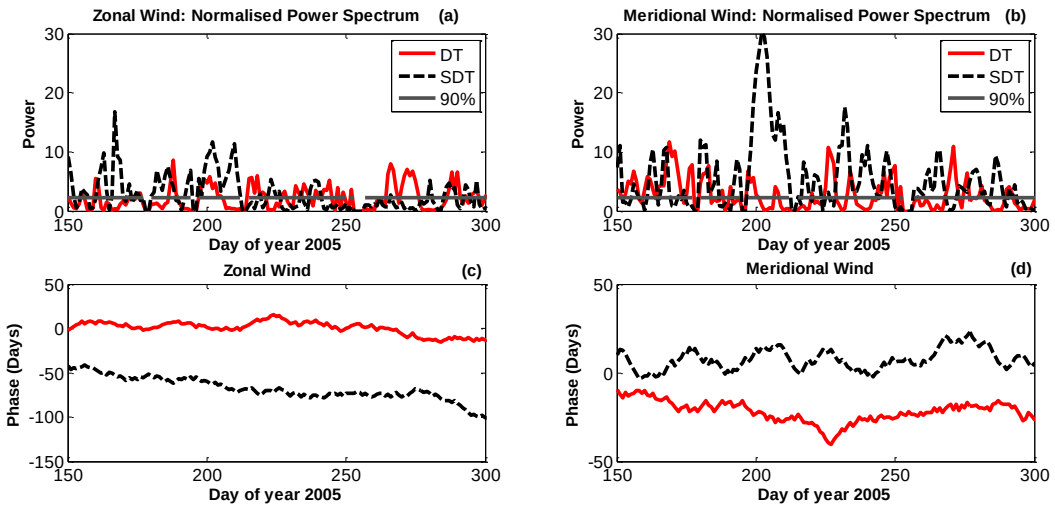

Figure 4.6: Normalised power spectra for the zonal (a) and meridional (b) wind components (top panels) and phase in zonal wind (c) and meridional wind (d) (bottom panels) over SANAE for the year 2005 obtained from complex demodulation. The horizontal gray line represents 90% confidence level.

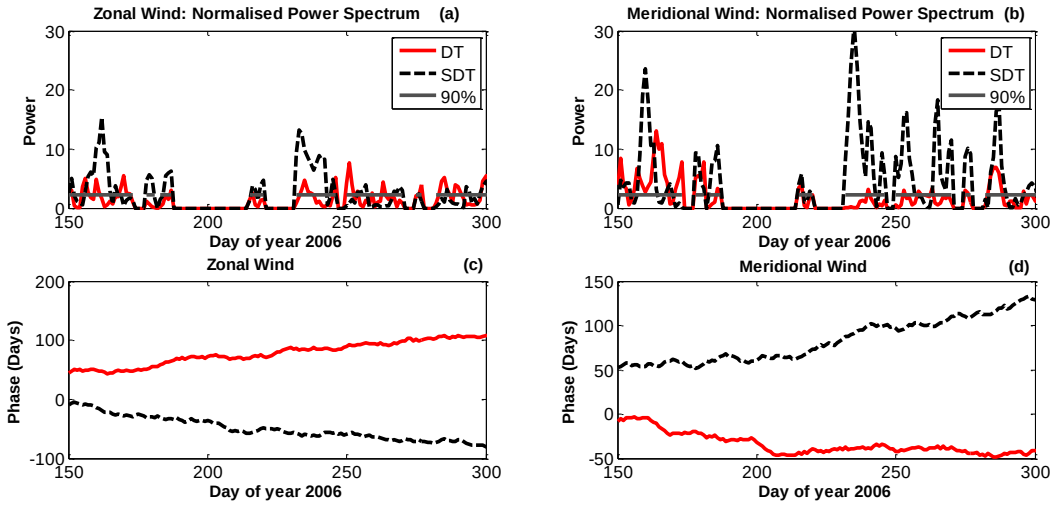

Figure 4.7: Same as Figure 4.6 but for the year 2006.

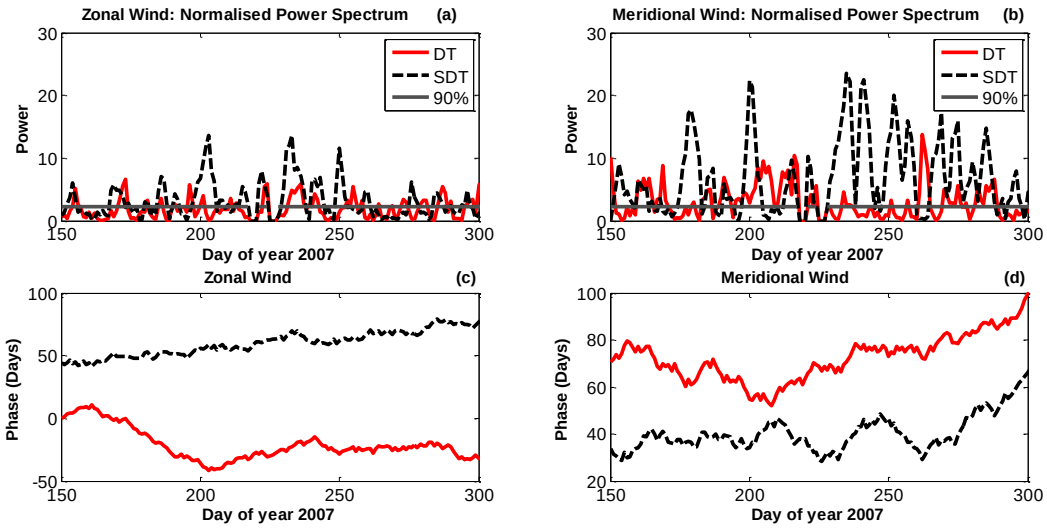

Figure 4.8: Same as Figure 4.6 but for the year 2007.

There is a common trend where by SDT is dominant most of the times, but DT in the zonal wind flow becomes slightly dominant during the winter season. During the year 2005 (Figure 4.6a), the SDT wave power dominates the DT except around day 220 and 270 when the DT becomes more dominant. In Figure 4.7a, the zonal wind DT for the year 2006 shows dominance around day 250 whilst during the year 2007 (Figure 4.8), it dominated around day 260. In general, it can be noted that the SDT wave activity dominated the DT wave by showing very large amplitudes especially in the meridional wind component. The years 2005 and 2006 were used as normal quiet years since no unusual SDT wave activity behavior was noted, unlike the year 2007 whose unique SDT wave characteristics considered being a specific year for this study. It is clear from Figure 4.6 to Figure 4.8 that the zonal wind component of the DT and SDT waves has a seasonal pattern characterised by enhanced wave activity in winter superimposed by short-term fluctuations. More wave activity is observed in winter where the wave power is above the 90% confidence level.

The phase variation of the year 2005 (Figure 4.6c, d), zonal wind component shows a general decrease in phase for both DT and SDT. The meridional wind shows noticeable phase

fluctuations for both DT and SDT. Around day 200 and day 230, the SDT phase increased and this coincided with an increase in amplitude. A sharp decrease in meridional DT phase is noted on approximately day number 225, exactly the same time when an increase in DT amplitude was taking place. Such an analysis goes well with a study by Clark et al., (2002) that, the phase decreases as the amplitude increases.

In Figure 4.7 the DT and SDT phase variation for the year 2006, shows that the two were out of phase since one increased as the other was decreasing. The zonal wind DT shows a general increase in phase whilst the SDT shows a general decrease in phase, (see Figure 4.7c). In the meridional component it can be noted that the DT shows a general decrease in phase whilst the SDT shows a general increase in phase, which shows that the two were out of phase as well, (see Figure 4.7d).

For the year 2007 more phase variations were noted in the meridional wind component compared to the zonal wind component (see Figure 4.8c, d). The zonal wind component shows a general decrease in phase for both DT and SDT. The meridional wind component was characterised by phase fluctuations and an interesting feature is observed around day 260 where a sharp decrease in DT phase was accompanied with an increase in DT amplitude. This again agrees well with a study by Clark et al., (2002) that, the phase decreases as the amplitude increases. The meridional component of the SDT shows different behavior because as the amplitude increased, the phase increased as well especially from approximately day number 240 to 260.

4.4 Zonal Wavenumber

This topic presents the calculation of wavenumbers of planetary waves which were presented above in chapter 4.1. Wavenumbers gives detail about the wave propagation direction and mainly small wavenumbers such as s=0, s=1 and s=2 are of greater importance since they contribute much to the atmospheric dynamics. The propagation speed of a wave can be approximated by the following equation (Pierre, 1961);

$$c = \overline{u} - \frac{\beta}{s^2} \qquad \textbf{(4.1)}$$

Where c is the wave propagation speed, $\bar{u}$ is the mean zonal, β is the planetary vorticity and $\boldsymbol{K}^2 = s^2 + l^2$ with s and l being the zonal wavenumber and meridional wavenumber respectively.

To analyse and understand the MLT atmospheric dynamics, important characteristics of waves such as the amplitude, propagation direction and zonal wavenumber must be calculated hence in this study complex demodulation method was implemented. The data from SANAE and Halley SuperDARN radar sites was used to estimate zonal wavenumbers mainly because their longitudinal separation of ~24 degrees is good enough to estimate reliable zonal wavenumbers. The zonal wavenumbers were calculated from the slope of the linear regression of the quasi-5-day, quasi-10-day and quasi-14-day wave phases as a function of longitude during winter months. This method is similar to the one used to study the quasi-2-day wave (QTDW) using the Northern Hemisphere SuperDARN HF radars by Malinga et al., (2007).
The wave number (s), derived from the phase as a function of longitude can be mathematically represented by the following equation, (Priestly, 1981 and Malinga et al., 2007);

$$s = \frac{\left(atan\left[\frac{Im(x')}{Re(x')}\right]_{Hal}(t) - atan\left[\frac{Im(y')}{Re(y')}\right]_{San}(t)\right)}{(Lon_{Hal} - Lon_{San})} \qquad \textbf{(4.2)}$$

Where Lon is the longitude and the phase is calculated from complex demodulation method presented earlier. The waves x and y corresponds to the wave obtained at Halley and SANAE stations respectively, propagating at common time (t).

The phase obtained in this analysis was from the 4 day Fourier spectral analysis method mainly because only phases that are well resolved in frequency were needed hence, a dynamic Fourier spectra method which uses a 4 day data window that is shifted forward by 1 day at a time was implemented. The phase deduced for a given data window was attributed to a central day given by day 2 of that particular 4 day data interval. This data window result in a frequency resolution of 0.025 cycles per day (cpd). The phases used are only those which correspond to the central days falling within the winter season, that is a time at which the spectral power tends to be above the 90% confidence level. For significance, the wavenumbers calculated were those at which

both sites (SANAE and Halley) had data, and the coefficient of determination was 55%. In the presentation of results the positive wavenumbers represent eastward propagating waves whilst negative wavenumbers represent the westward propagating waves.

Figure 4.9 to Figure 4.11 presents the zonal wavenumbers for 5-day, 10-day and 14-day waves which were extracted during the winter season of the years from 2005 to 2007. The left panel presents the zonal component while the right panel presents the meridional component showing the distribution of wavenumbers. The year 2005 shows a noticeable distribution of zonal wavenumbers in both zonal and meridional wind components (see Figure 4.9). The 5-day wave shows significant zonal wavenumbers of s=-1, s=5 and s=6 in the zonal and meridional wind components but the most dominant are s=5 and s=6. The 10-day wave shows significant zonal wavenumbers of s=$\pm$4, s=$\pm$3, s=$\pm$2, s=$\pm$1, and s=0 in the zonal and meridional wind components, but the most dominant are s=-2 and, s=-1 followed by s=-3 and s=0. The 14-day wave shows significant zonal wavenumbers of s=$\pm$6, s=-5, s=-2, s=$\pm$1, s=0 and s=3 in the zonal and meridional wind components, but the most dominant are s=-2 followed by s=0 then s=-1.

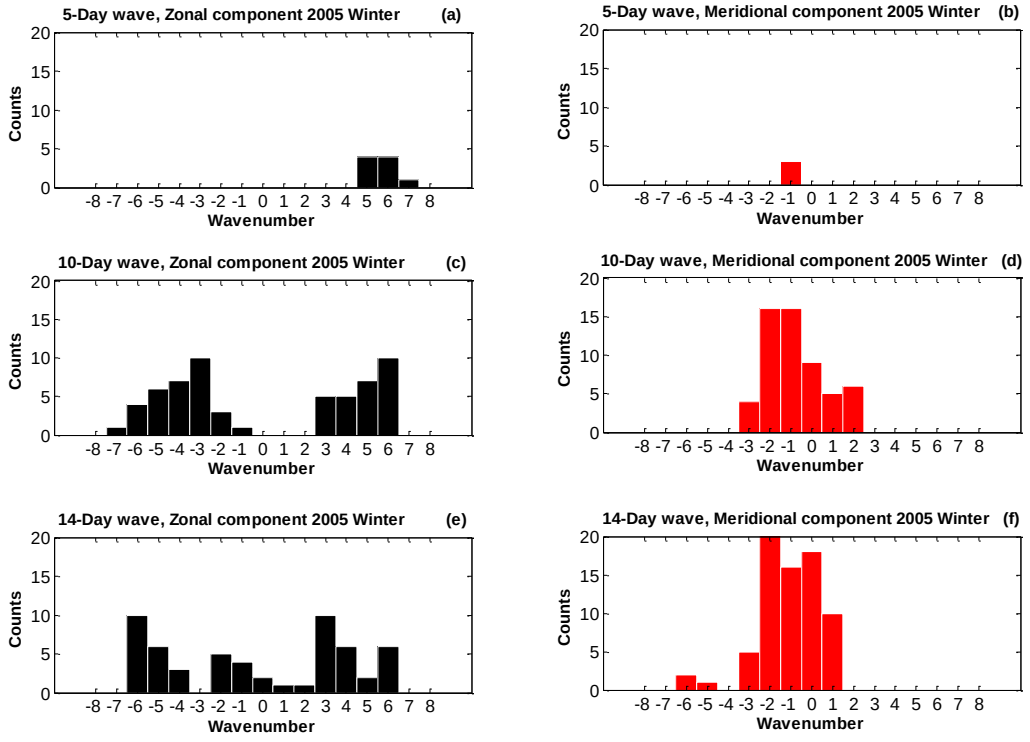

Figure 4.9: The distribution of the zonal wavenumber of the zonal wind component (left panel) and the meridional wind component (right panel) during the winter season of the year 2005. In the Figure, the negative wavenumbers represent the westward propagating wave.

For the year 2006 in the zonal and meridional wind components, the 5-day shows no significant zonal wavenumbers in both zonal and meridional components (see Figure 4.10). The 10-day wave shows significant zonal wavenumbers of s=±3, s=-1, s=2, s=4, s=5, s=6 in the zonal and meridional wind components, but the most dominant are s=3, s=4 and s=5 then followed by s=2. The 14-day wave shows significant zonal wavenumbers of s=±6, s=-4, s=-3, s=-2, s=-1 and s=0 in the zonal and meridional wind components, but the most dominant are s=-2 followed by s=-1 then s=-3.

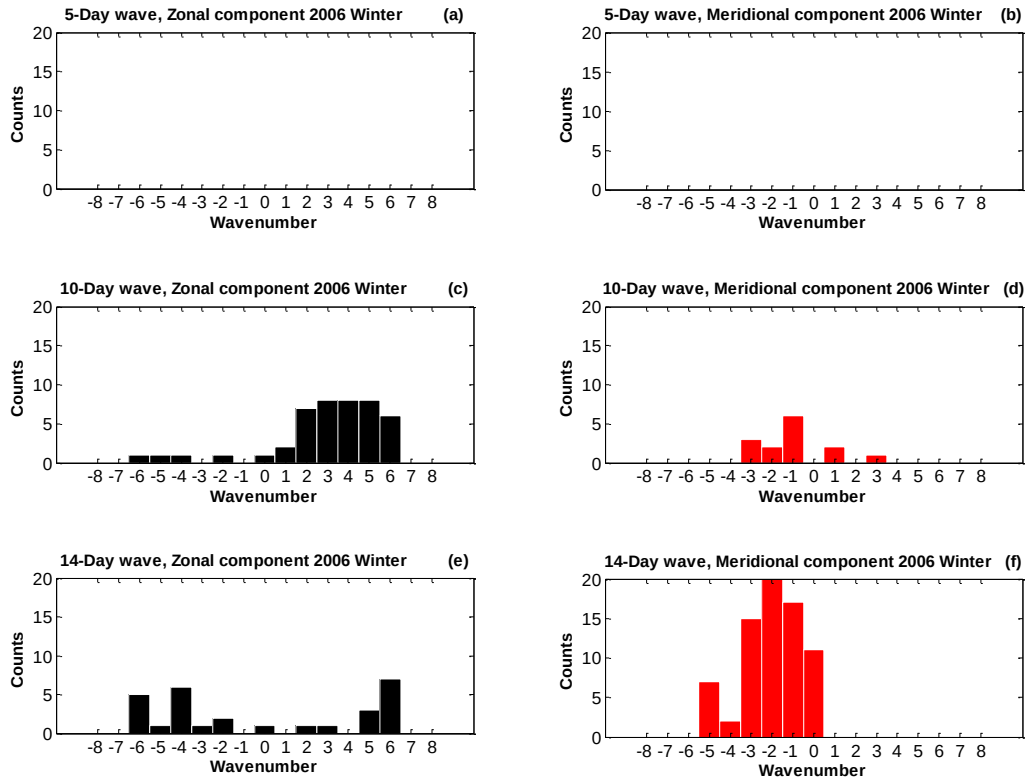

Figure 4.10: Same as Figure 4.9 but for the year 2006.

For the year 2007 in the zonal and meridional wind components the 5-day wave shows significant wavenumbers of s=-2, s=0 and s=7 and in this case they approximately have the same counts (see Figure 4.11) The 10-day wave shows significant zonal wavenumbers of s=±3, s=±1, s=1, s=2, s=3, s=4, s=5 and s=6 but the most dominant are s=2 followed by s=0 then s=3. The 14-day wave shows significant zonal wavenumbers of s=±6, s=-5, s=-2, s=±1 and s=0 in

the zonal and meridional wind components, but the most dominant are s=-1 followed by s=-2 then s=0.

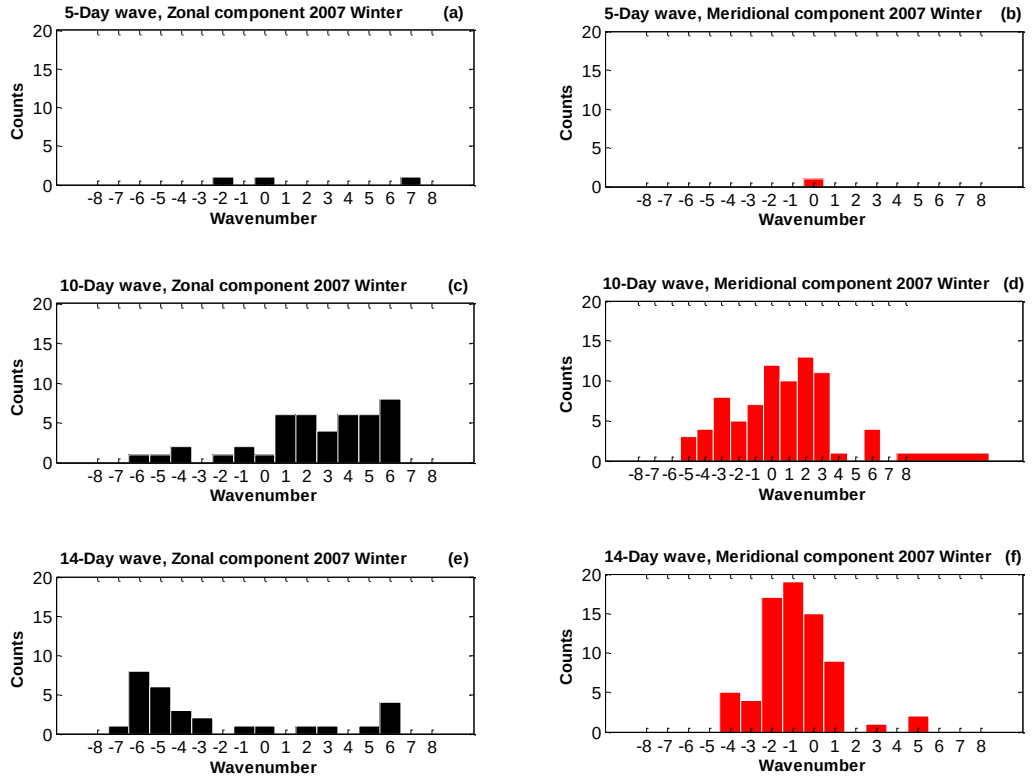

Figure 4.11: Same as Figure 4.9 but for the year 2007.

Generally, considering all the years from 2005 to 2007, it can be noted that the meridional wind component is dominated by short wavenumbers compared to the zonal wind component. There is an interesting trend in some years which shows dominance of a particular wavenumber for the same wave. The year 2005 wavenumber variation of the 14-day wave shows dominance of wavenumbers s=-2, s=-1 and s=0 which were observed in the other years except for s=0 which was not observed in the year 2006. The 10-day wave with wavenumbers s=2 and s=3 observed in the year 2006 were also noted in the year 2007. The presence of stationary waves (s=0), observed in the quasi-10-day and quasi-14-day is noted and such waves are known to propagate upward from the troposphere and are very strong but quite variable during winter (e.g. Pancheva et al., 2004).

4.5 Discussion and Summary

The zonal and meridional wind data components from the two radar stations, SANAE (72°S, 3°W) and Halley (76°S, 27°W) were used to study the MLT dynamics over the Southern Hemisphere at ~94 km for the years 1997 to 2007. The comparison of the wavelet spectra from the two stations SANAE and Halley revealed a good agreement between the two HF radar instruments. Wavelet analysis and STFT techniques were implemented and a 4 day moving window was used with 1 day overlap. The wave periods were studied by means of wavelet transform method. The wavelet amplitudes of the HF radar wind components were calculated for a period below 30 days at ~94 km altitude. The data from 2005 to 2007 was used for a better assessment of planetary wave activity in the Southern Hemisphere, and the year of interest was the year 2007. The normalised power spectra for both zonal and meridional wind components revealed dominant wave activity near periods of 0.5 day (semidiurnal tide) and 1 day waves (diurnal tide) which will be further analysed in this study.

The wave activity for the years 2005 to 2007 was observed to be dominant in winter and summer seasons in the zonal wind component whilst, the meridional wind wave activity was centered to the winter season. Dominant wave periods centered at 10-day, 14-day, 16-day and long planetary waves centered at approximately 22 days were observed in each case showing planetary wave amplification in winter. This is mainly because the winter months are known for their strong planetary wave activity over a wide period (Mbatha, 2012).

Chapter 5: Minor Sudden Stratospheric Warming for the Years 2007 and 2010

5.1 Introduction

This chapter presents the minor SSW events which occurred in the years 2007 and 2010. The interaction between planetary waves and tides during minor SSW will be investigated. The minor SSW event is investigated using NCEP re-analysis data, UKMO data assimilation and SANAE HF radar and Halley HF radar zonal wind. Much emphasis of this study is for the year 2007 since it is the one with all required data sets available. The first part presents year 2010 minor SSW but unfortunately, due to the unavailability of HF radar data during this year the interaction of planetary waves with the tides was not investigated. Minor SSW for the year 2007 is presented later in detail, paying attention to dominant wave periods noted, wave-wave interaction and the wavenumbers present during the occurrence of minor SSW events. The wave numbers presented were calculated from the two HF radar stations, namely SANAE and Halley with a longitudinal separation of ~24 degrees, reasonable enough to estimate significant wavenumbers.

5.2 Minor SSW Events during the Year 2010

In this study, the SSW events which took place during the year 2010 in the Southern Hemisphere were investigated using NECP reanalysis data. Figure 5.1 shows the mean and standard deviation of the zonal wind and temperature from NCEP reanalysis data for the years from (2002-2013) at 10 hPa. This Figure is going to be used as a measure of how the zonal wind at 60°S and the temperature at 80°S vary in any given year compared to the mean. Considering the general pattern obtained from the average of 11 years, it can be noted from Figure 5.1 that the standard deviation variations for both the zonal wind and temperature shows an increase from July to November. It is within this period of sudden increase of temperature accompanied by a decrease in zonal wind that we expect minor SSW events to take place. The figure clearly shows how the decrease in zonal wind as illustrated by the standard deviation, coincides with a significant increase in temperature for the months from July to November.

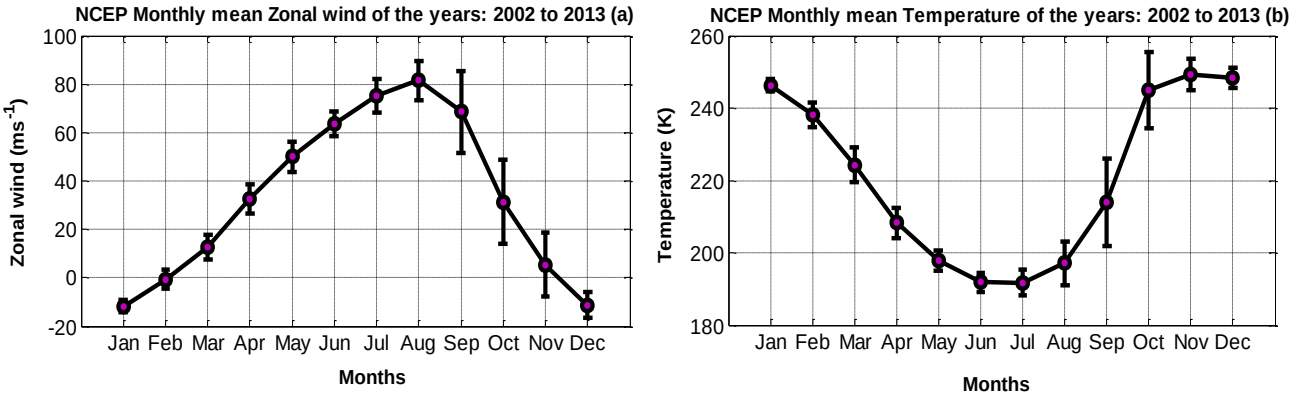

Figure 5.1: Mean and standard deviation of NCEP reanalysis zonal wind and temperature data for the years from 2002 to 2013.

Figure 5.2 presents the daily zonal mean wind at 60°S (green solid line) and temperature at 80°S (blue dotted line) from NCEP reanalysis data for the year 2010. The temperature was plotted together with the zonal wind so that their variation with time can be investigated for minor SSW events. A minor SSW event was recorded based on the definition which had been mentioned and explained earlier in section 2.2.4, which states that a SSW is classified as minor if at 10 hPa and 60° latitude there is a significant increase in temperature at any stratospheric level in any area of the winter time hemisphere, which leads to a slight decrease in the mean zonal wind which does not lead to the reversal of the wind direction.

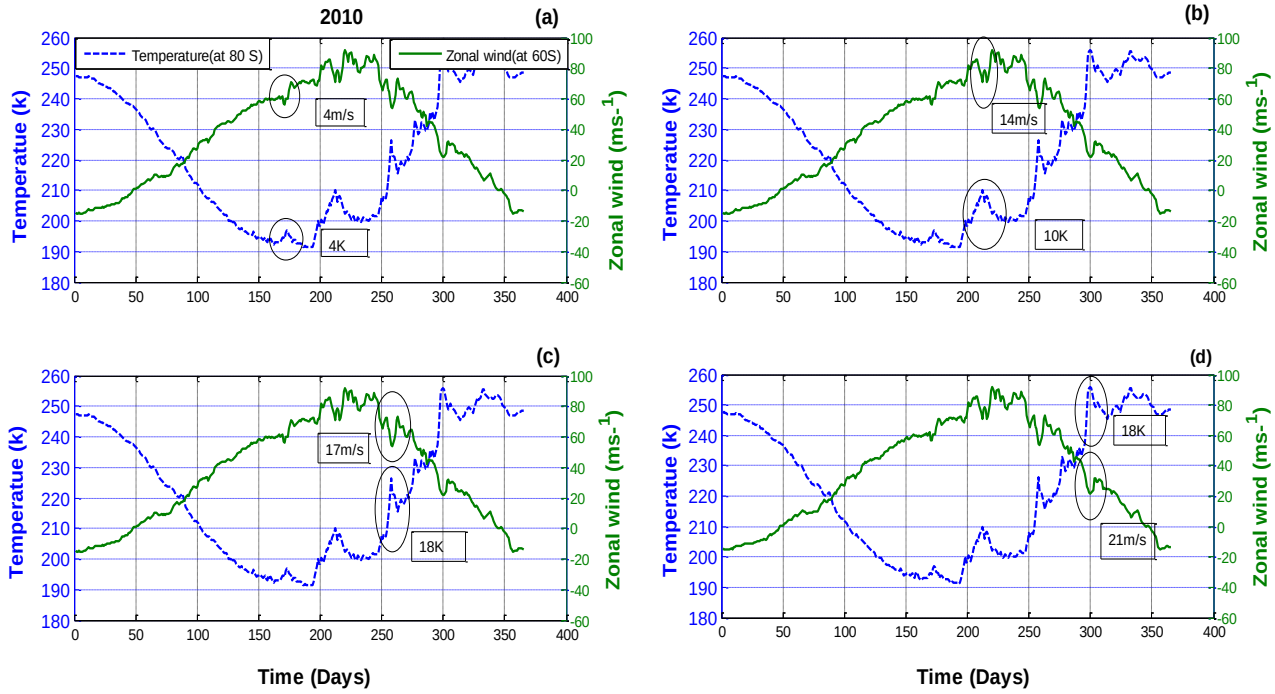

Figure 5.2: Daily zonal mean wind at 60°S (solid line) and temperature at 80°S (dotted line) from NCEP reanalysis for the year 2010. In the boxes are the magnitudes of the zonal mean wind and temperature differences from the mean.

In Figure 5.2a the first minor SSW event was noted at around day 173 and it took about 10 days, with zonal wind and temperature change of 4 $m.s^{-1}$ and 4 K in magnitude, respectively. The second minor SSW event (Figure 5.2b), is noted to have occurred on approximately day 215, and it took about 31 days with a change in magnitude of about 10 $m.s^{-1}$ and 18 K in zonal wind and temperature respectively. The third minor SSW event (Figure 5.2c), occurred on approximately day 258, taking about 10 days and there was a change in magnitude of 17 $m.s^{-1}$ and 18 K in zonal wind and temperature, respectively. The last SSW event (Figure 5.2d), is classified as a final warming because it took place in late winter on approximately day 300, lasting for about 31 days and there was a change in magnitude of 21 $m.s^{-1}$ and 18 K in zonal wind and temperature, respectively.

From the second minor SSW event (Figure 5.2b), to the last minor SSW event (Figure 5.2d), there is an interesting trend and pattern on the magnitude of change in temperature of (18 K), which is almost the same between successive minor SSW events. Moreover, all minor SSW events occurred after the same duration of time had elapsed hence an average common period of approximately 42 days was estimated. Such minor SSW events can simulate a SSW that is when it leads to the reversal of zonal wind. According to the World Meteorological Organisation (WMO) a stratospheric warming can be said to be major, if at 10 hPa or below the latitudinal mean temperature increases abruptly pole ward from 60° latitude with an associated wind circulation reversal. Such a scenario is rare in the Southern Hemisphere as it just happened once in 2002 and it was studied by few researchers (e.g. Baldwin et al., 2003; Dowdy et al., 2004 and Mbatha et al., 2010b). The summary of all minor SSW events which took place during the year 2010 are summarized in Table 5.1.

Table 5.1; The Minor Sudden Stratospheric Warming events for the year 2010 in the Southern Hemisphere using zonal wind and temperature data at 10 hPa. The corresponding day is mentioned in the form of Julian days.

Start Day	**End Day**	**Duration**	**Magnitude of ΔVelocity (m/s)**	**Magnitude of ΔTemperature (K)**
165	175	10	4	4
195	226	31	10	18
253	263	10	17	18
294	302	8	21	18*(Final Warming)

5.3 Planetary Wave Activity during 2010 Minor Sudden Stratospheric Warming

Theoretical studies (e.g. Charney and Drazin, 1961 and Andrews et al., 1987) and observational studies, (e.g. Liu et al., 2002; Dowdy et al., 2004; Mbatha et al., 2010b and Liu, 2005) have shown that the amplification of planetary waves in winter stratosphere are responsible for the occurrence of sudden stratospheric warming. Due to the importance of planetary waves during the stratospheric warming occurrences, the present research also investigated the activity of planetary waves for the year 2010.

Figure 5.3 presents the wavelet power spectra of the zonal mean wind and temperature for the NCEP reanalysis data of the year 2010. This was done to identify the periods which could have contributed to the formation of minor SSWs in the year 2010. It can be noted that, most of the wave activity was during the winter and spring months. The top panel shows that the zonal wind reached a maximum wave power of 460 $m^2.s^{-2}$ around day 220 while the temperature (bottom panel), acquires a maximum wave power of approximately 300 $m^2.s^{-2}$ around day 280. The wave activity was characterised with commonly known planetary wave periods in the middle atmosphere which are; quasi-10-day, quasi-14-day and quasi-16-day waves. Long period planetary waves of wave periods ranging from 14 to 30 days and centered at approximately 20

days show dominance and could have played a major role in the MLT dynamics during the occurrence of minor SSW events.

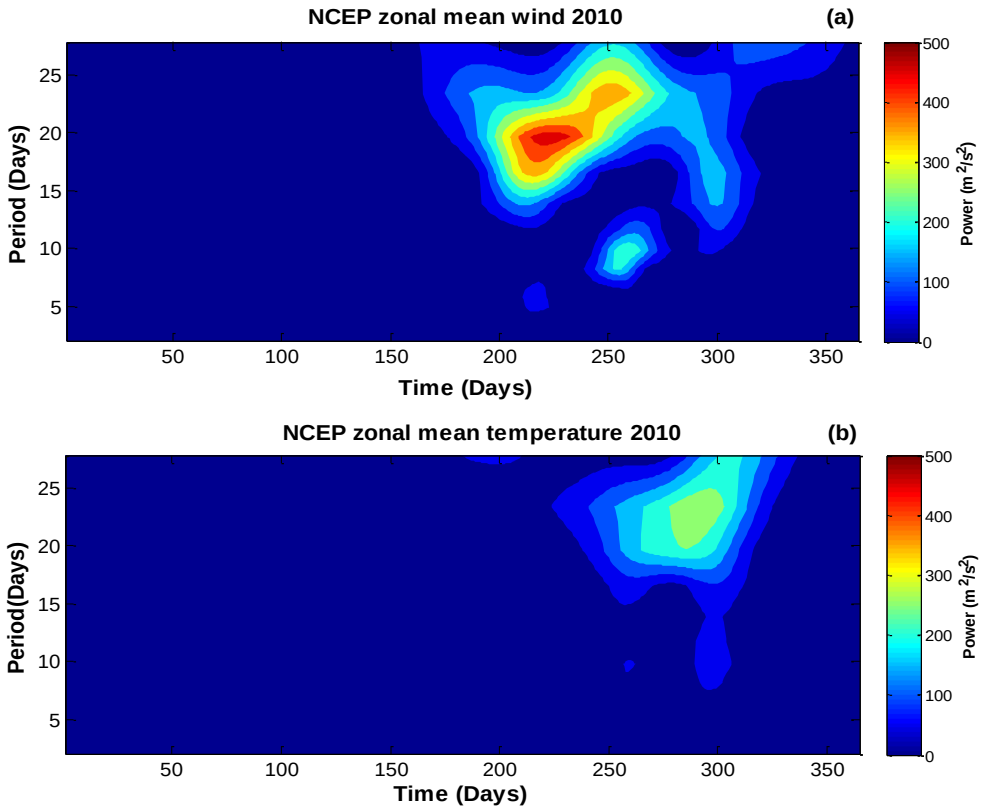

Figure 5.3: Wavelet spectra for zonal mean wind at 60°S and temperature at 80°S at 10 hPa using NCEP reanalysis data for the year 2010.

Considering Figure 5.3a, it is clear that the zonal wind wave activity started on approximately day 120 before any wave activity was noted in the temperature variations (see Figure 5.3b). In the zonal mean temperature, the wave activity commenced on approximately day 225 which was well after the zonal wind had started to show fluctuations. It can be deduced that the change in zonal wind triggers the slowing down of mean flow and the increase in temperature. Also, the wave periods between 16 and 24 days with a wave power of about 400 $m^2.s^{-2}$ were more dominant, showing the amplification of quasi-16-day planetary wave. Overall, it is observed that the stratosphere was characterised by long period planetary waves with periods between 10 and 25 days. The quasi-20-day wave observed during winter period seems to have contributed to the

change in dynamics of the stratosphere during winter months of 2010 due to its strength (see Figure 5.3a).

The stratosphere background wind and stability fields have an important impact on the planetary wave vertical propagation in the stratosphere because at times critical level filtering can prevent waves from propagating through to deposit momentum and energy to higher altitudes (Espy et al., 2004 and Jacobi et al., 2005). This disturbs MLT dynamics in parameters such as density and stability (Holton and Alexander, 2000). Wave interactions in the MLT are important in maintaining equilibrium of propagating waves and dissipating waves (Pancheva et al., 2008).

Figure 5.4 shows the variation of the UKMO zonal mean zonal wind at 60 degrees south for the year 2010 at 10, 3, 1, and 0.3 hPa pressure levels. In general an eastward zonal wind mean flow is observed to reach its maximum value of about 90 $m.s^{-1}$ during winter months. Figure 5.5 presents the UKMO meridional wind at 10 hPa, 3 hPa, 1 hPa and 0.3 hPa pressure levels (similar to Figure 5.4). In this figure it is observed that the strongest peaks of wind velocity are found in late winter month. However, there is overall evidence of weak wind strength in the meridional wind component compared to the zonal wind component. This is consistent with observations reported by Mbatha et al., (2012). At 0.3 hPa (Figure 5.5d) two sharp peaks can be identified, the first one at around day 210 reached maximum amplitude of approximately 9 $m.s^{-1}$ and the second peak at around day 260 reached maximum amplitude of approximately 7 $m.s^{-1}$. In general maximum amplitude is observed during the winter period and this could be due to wave-wave interactions.

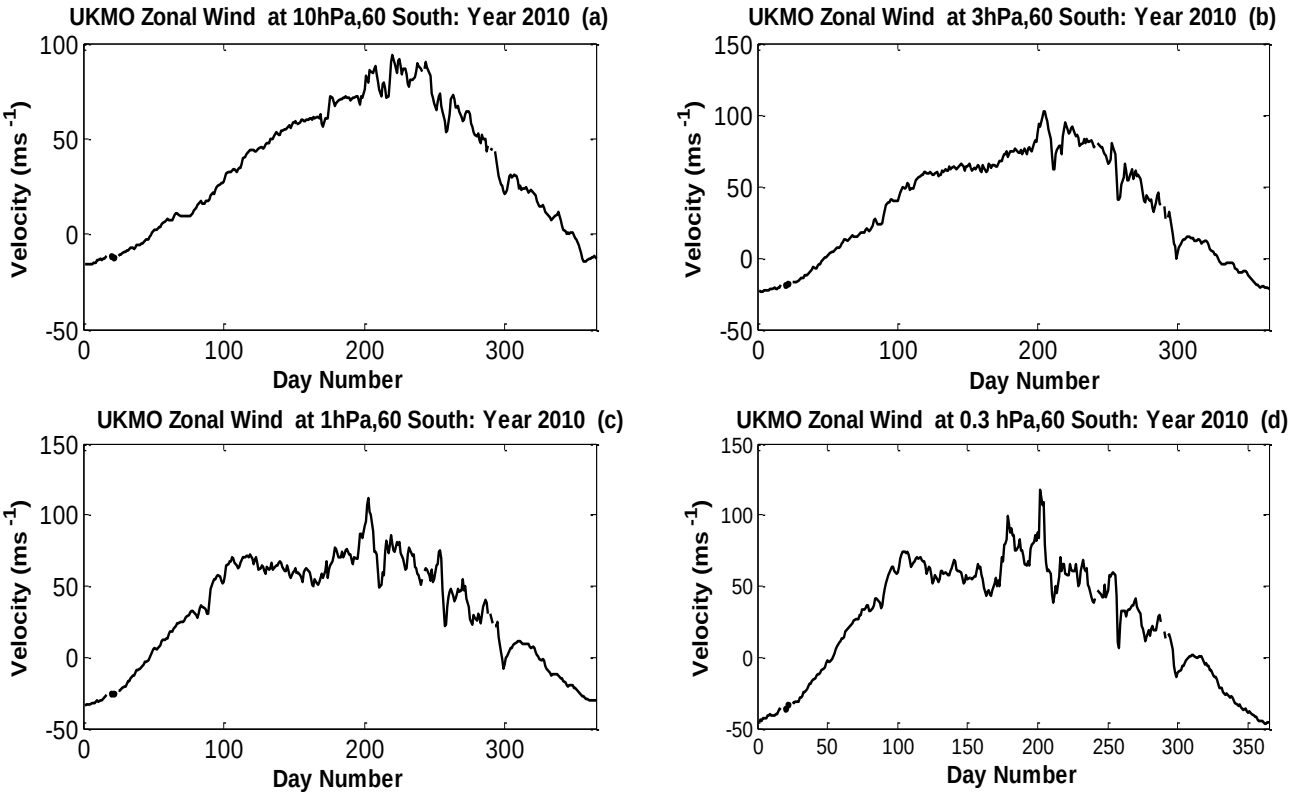

Figure 5.4: UKMO zonal mean zonal wind at 60°S and at different pressure levels (10 hPa, 3 hPa, 1 hPa, and 0.3 hPa) for the year 2010.

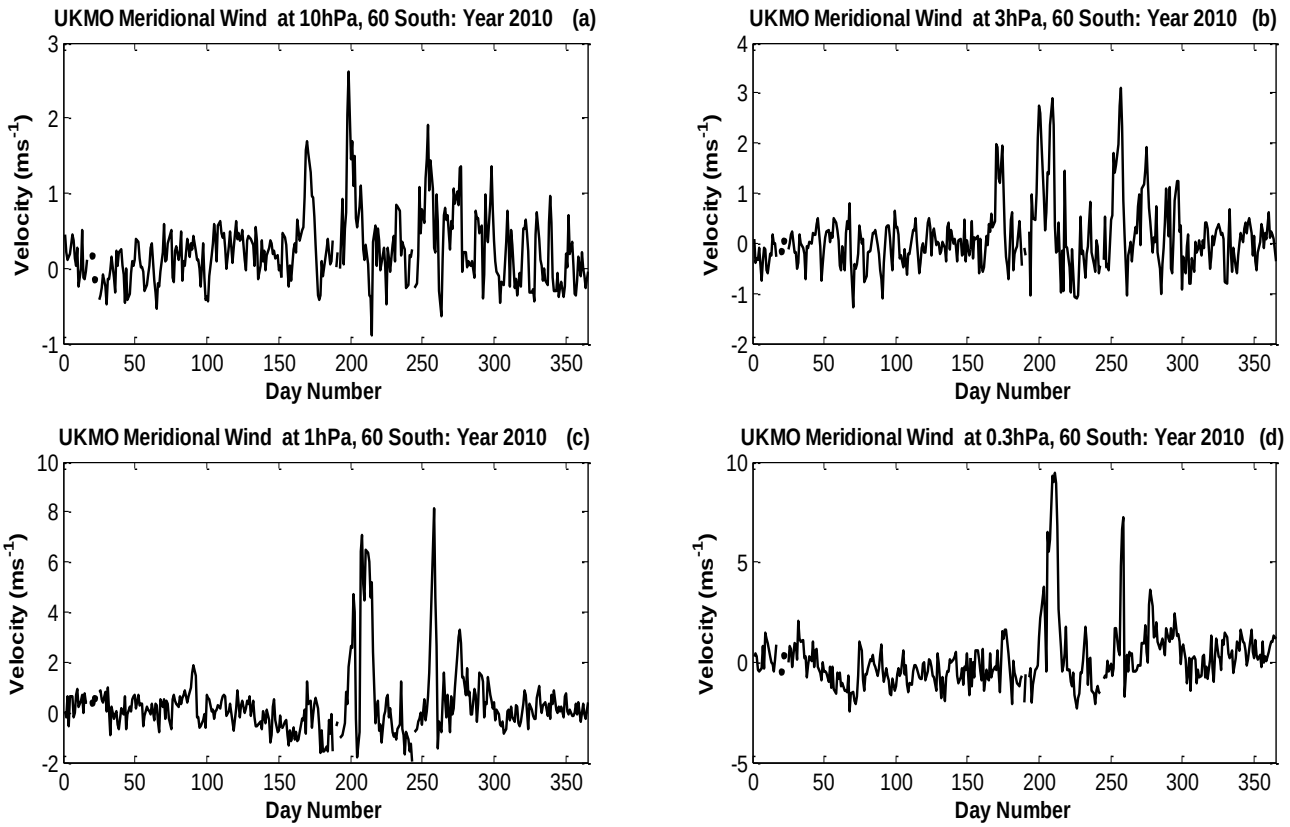

Figure 5.5: UKMO meridional mean wind at 80°S and at different pressure levels (10 hPa, 3 hPa, 1 hPa, and 0.3 hPa) for the year 2010.

It has been shown in several studies that planetary waves that originate from the lower atmosphere and propagate upwards are the main contributor to the formation of stratospheric warming events (e.g. Palo et al., 2005; Mbatha et al., 2010b and Chandran et al., 2013). Major stratospheric warming is an unusual phenomenon in the Southern Hemisphere hence minor sudden stratospheric warming is usually observed. In the year 2010, stronger minor SSW events were observed at approximated Julian day number 220, 270 and 300. A series of minor sudden stratospheric warming events took place during the Southern Hemisphere winter months of 2010. To examine the presence and temporal evolution of long period waves in the stratosphere before, during and after the onset of the stratospheric warming event, the wavelet power spectra of the UKMO zonal mean zonal wind for 10, 3, 1, and 0.3 hPa pressure levels were calculated for the

planetary wave periods between 2 and 28 days and the time interval from the 1st of January 2010 to 31 December 2010. The contour plots of the wavelet power spectra obtained are presented in Figure 5.6. It is clearly observed that there is a strong presence of planetary waves of periods between 5 and 25 days during winter months. This planetary wave activity seems to dissipate in late winter. An interesting feature is what seems to be the amplification of this wave activity with increase in altitude (decrease in pressure).

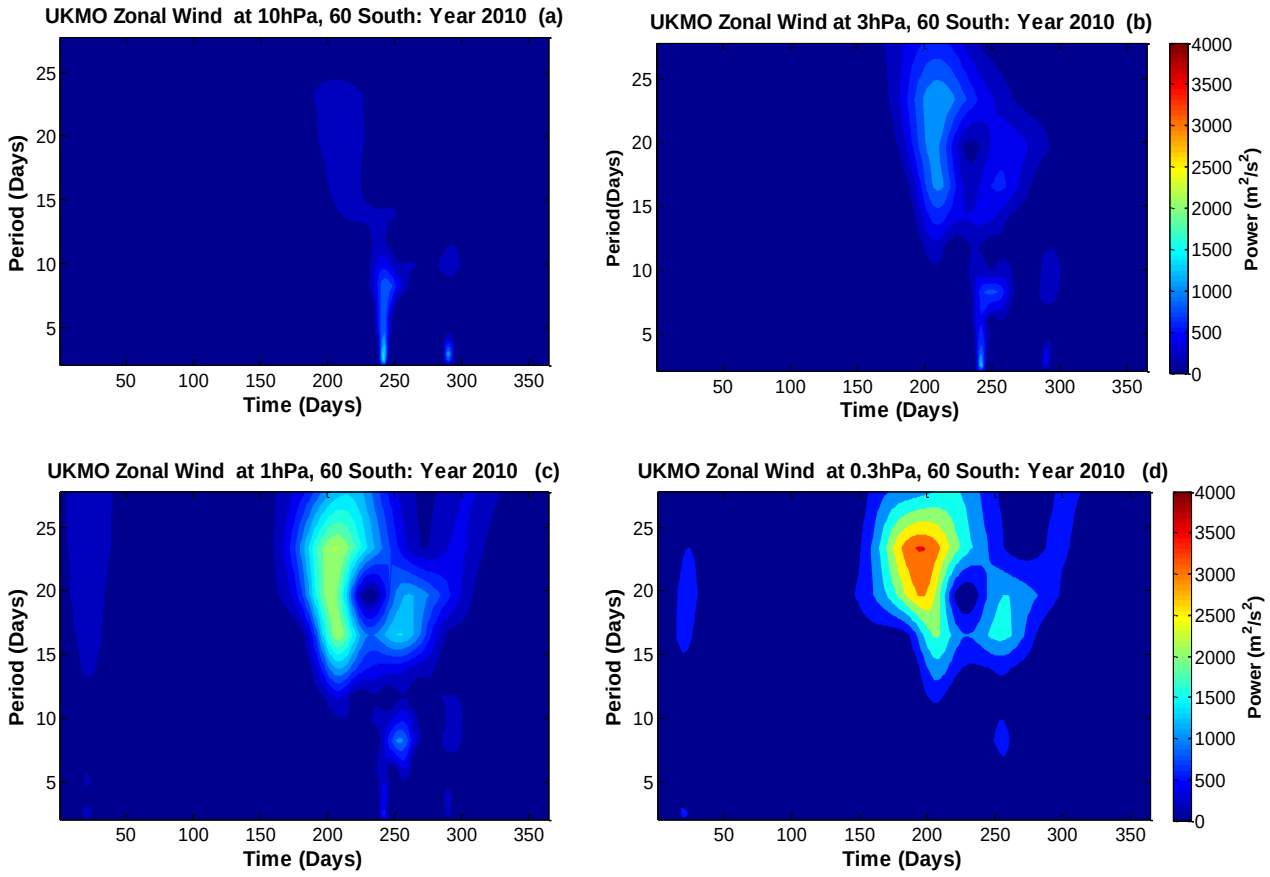

Figure 5.6: Wavelet spectra for UKMO zonal mean zonal wind at 60°S for the year 2010.

A follow up study will be to investigate a possible coupling between stratosphere and mesosphere during this event. Considering part (d) of Figure 5.6, it can be noted that a dominant wave activity around day 200 with wave period centered around 20 days and a maximum wave power of approximately 3500 $m^2.s^{-2}$. The minor SSW events started at roughly Julian day number 165 to 302 which is the same period during which strong quasi-20-day was noted, hence

this wave could have contributed to the deceleration of zonal mean wind or the formation of minor SSW events during this period. A study by Kishore et al., (2012) on the planetary waves in the upper stratosphere and lower mesosphere during 2009 arctic major stratospheric warming discovered the presence of an upward propagating 20–30 day planetary wave during the SSW period. This shows that a quasi-20-day wave can enhance the formation of a minor SSW.

Another interesting feature observed in Figure 5.6a is that, at low altitude there is clear evidence of waves with wave periods below 5 days observed at around day 240. As these waves propagate upwards, their wave activity decreases until they diminish whilst long period waves become more active (see Figure 5.6d). This is consistent with a previous study by Pancheva et al, (2000a, b) in which they discovered that the interactions between different members of the ensemble of planetary waves at MLT heights resulted in significant modulation of the amplitude of one planetary wave at the period of another planetary wave. In this study, the non-linear interaction and modulation of planetary waves could have caused the deceleration of the zonal mean wind, thereby leading to the formation of minor SSW.

5.4 Minor SSW Events during the Year 2007

For the year 2007 detailed information about the comparison of the variation of zonal wind and temperature with the mean obtained for a period of 9 years (2002-2013) was presented. The mean was obtained in order to realize the general pattern expected in a quiet or normal year (year without SSW). Even though this period of time comprises of some years with minor SSW events taking the mean will represent a normal expected trend since the years with minor SSW events will be compensated with quiet years.

Figure 5.7 presents the zonal wind for the year 2007 (solid black line) and mean zonal wind for nine years from 2002 to 2013 (red dotted line) at 10 hPa and 60°S (latitude). The figure clearly shows how the zonal wind for the year 2007 from January to December varies with time compared to the mean zonal wind. It can be noted that the two agrees well from day number 1 to approximately day 190. The zonal wind for the year 2007 shows strong wind variations during the winter period, thus when a significant difference compared to the mean is noted and this could be due to strong planetary wave activity during winter months. The major driver of the

winter stratospheric dynamics is centered on the interaction of planetary waves and the zonal mean flow (Andrews et al., 1987).

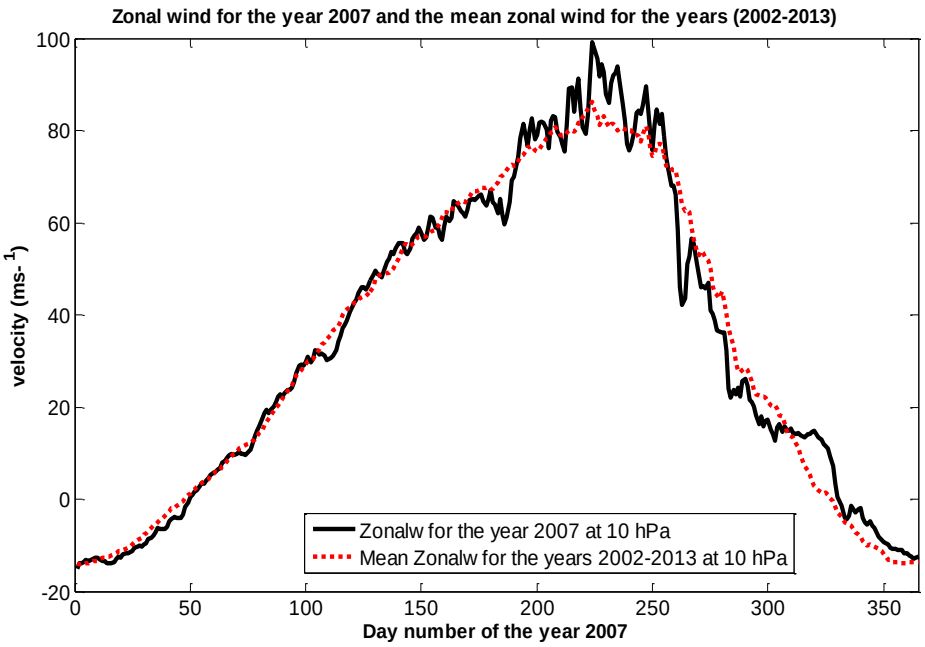

Figure 5.7: Zonal wind for the year 2007 (solid black line) and mean zonal wind for nine years from 2002 to 2013 (red dotted line) at 10hPa and 60°S.

Figure 5.8 presents temperature for the year 2007 (solid black line) and the mean temperature for nine years from 2002 to 2013 (red dotted line) at 10 hPa and 80°S. The temperature variation for the year 2007 and the mean shows good agreement from Julian day number 1 to day number 120. A noticeable difference was observed from day number 200 when the temperature for the year 2007 started to show more variation during the winter months. This is primarily due to wave-wave interaction and wave-mean flow interaction in the MLT which leads to an abrupt increase in planetary waves and tides amplitudes until wave breaking occurs, that is if the amplitudes exceeds the instability thresholds (Lindzen, 1981 and Huang et al., 2013). A furthered analysis was done to verify the magnitude by which the zonal wind decreases as the temperature increased during the same period of zonal wind and temperature variations.

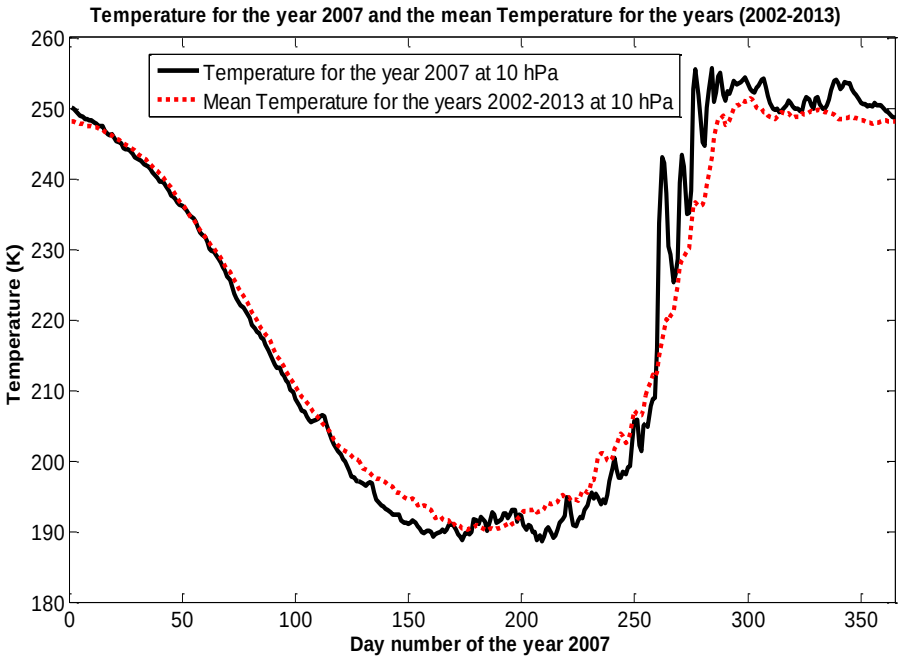

Figure 5.8: Temperature for the year 2007 (solid black line) and the mean temperature for nine years from 2002 to 2013 (red dotted line) at 10 hPa and 80°S.

During the year 2007 stronger minor SSW events were observed on approximated Julian day numbers 220, 240, 250 and 265 (see Figure 5.9 and Table 5.2). As explained above, in the case of investigating minor SSW events which took place during the year 2010, the same method was applied for the year 2007. From Table 5.2 it can be noted that there is approximately the same duration of about 10 days between two successive minor SSW events. The minor SSW event of greater magnitude was noted on approximately day number 263. This is indicated by zonal wind deceleration of 34 $m.s^{-1}$ and an increase in temperature of about 25 K.

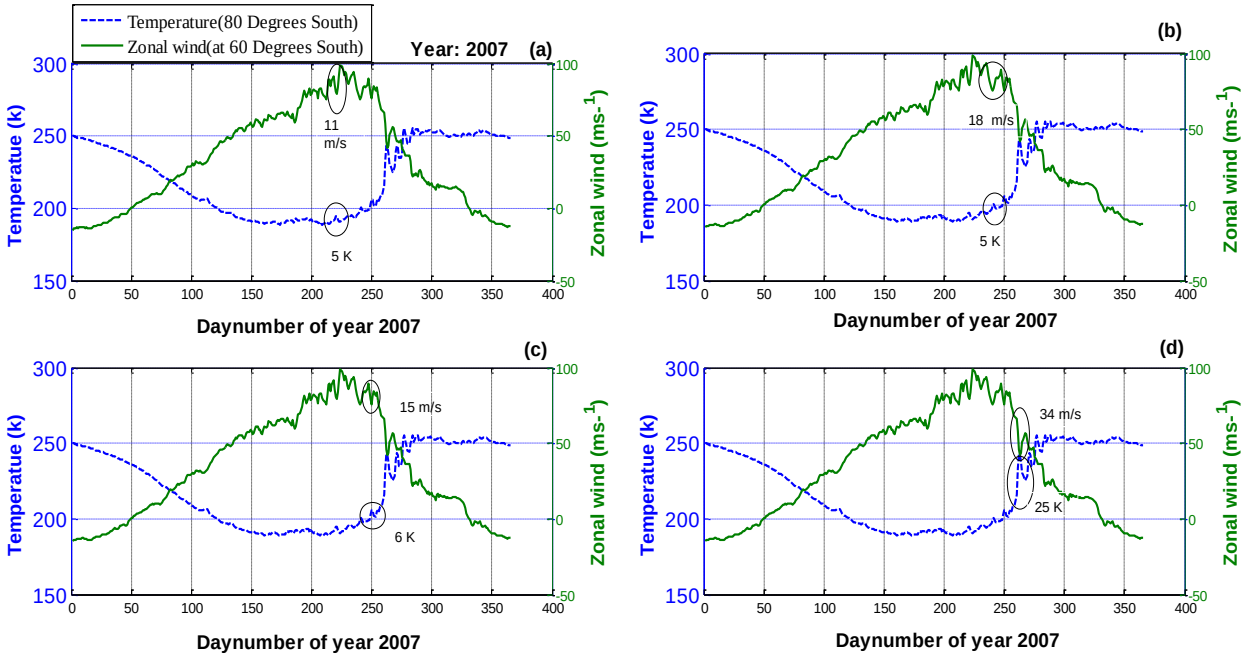

Figure 5.9: Daily zonal mean wind at 60°S (solid line) and temperature at 80°S (dotted line) from NCEP reanalysis for the year 2007. The values on the circled minor SSW incidents are the magnitudes of the zonal mean wind and temperature differences from the mean.

Table 5.2; The analysis of Minor Sudden Stratospheric Warming events for the year 2007 in the Southern Hemisphere using zonal wind and temperature data at 10 hPa.

Start Day	**End Day**	**Duration**	**Magnitude of ΔVelocity (m/s)**	**Magnitude of ΔTemperature (K)**
215	223	8	11	5
235	244	9	18	5
247	253	6	15	6
260	267	7	34	25

5.5 Minor SSW Events during the Year 2007 using UKMO and SANAE HF Radar

To examine the presence and temporal evolution of long period waves in the stratosphere before, during and after the onset of the stratospheric warming event, the wavelet power spectra of the UKMO zonal mean zonal wind component for 10 hPa, 3 hPa, 1 hPa, and 0.3 hPa pressure levels were calculated for the period range from 2 to 28 days and the time interval from 1 January 2007 to 31 December 2007. Unlike the task which was performed above for the year 2010, since the year 2007 is a specific year of interest for this study and have all the required data, the DT and SDT during the occurrence of minor SSW events will be investigated in detail.

This will involve taking note of tidal wave amplitude variations and the wave periods which were dominant during minor SSW events. Figure 5.10 (top panel) presents the DT and SDT instantaneous amplitude from SANAE HF radar at ~94 km while the bottom panel presents SANAE daily mean (dotted line), UKMO zonal mean wind and Temperature at 10 and 3 hPa pressure levels for the year 2007. Concentrating on the approximate Julian day numbers 220, 240, 250 and 265 when successive minor SSW were noted, DT and SDT wave variations were investigated. From Figure 5.10 (top panel) it can be noted that there was an increase in amplitude during the days corresponding to the occurrence of minor SSW events.

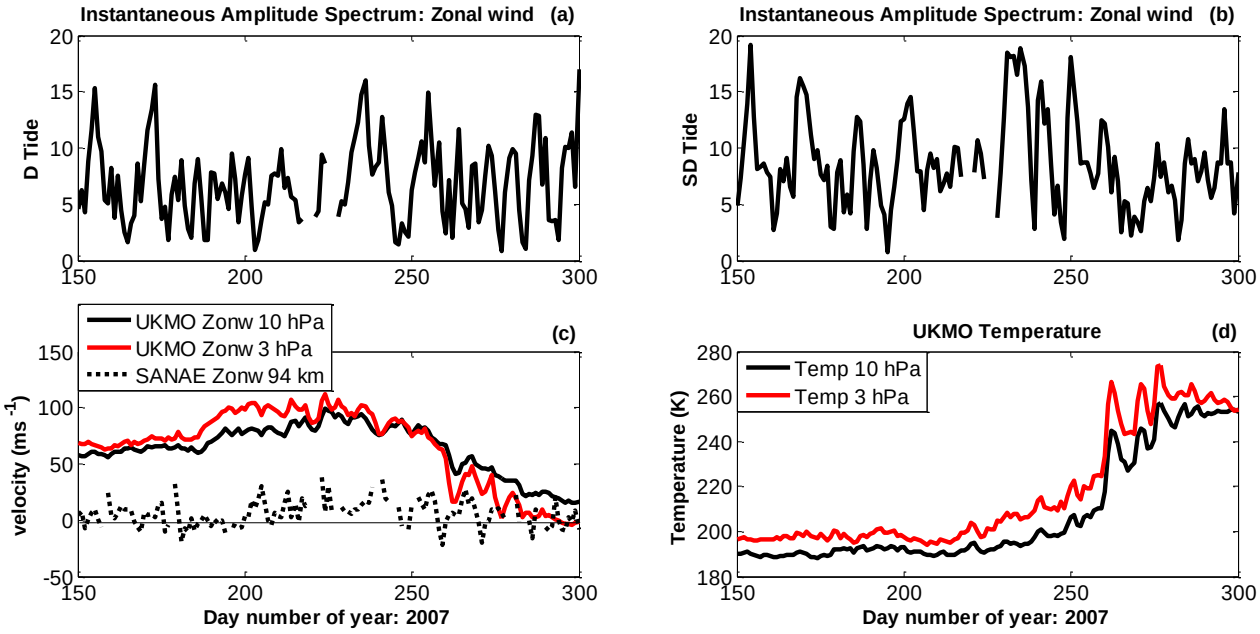

Figure 5.10: DT and SDT instantaneous amplitude from SANAE HF radar at ~94 km (top panel). SANAE daily mean (dotted line) and UKMO zonal mean wind and temperature at (10 and 3) hPa pressure levels (bottom panel), for the year 2007.

The bottom panel (c) shows the variation of SANAE daily mean zonal wind showing variations during minor SSW events illustrated with UKMO zonal mean wind at 10 and 3 hPa. Of the three last peaks observed from approximately day number 260 to 280 in the bottom panel (d) representing the UKMO temperature variations and similar peaks for the zonal wind variations in the bottom panel (c), only the first spike was classified as a significant minor SSW event in this study. This is mainly because the increase in temperature at 10 hPa (d) does not correspond to a noticeable zonal wind deceleration at the same pressure level (see Figure 5.10c), black solid line. It will be clearer if temperature variations at 3 hPa have been considered but that will not obey the World Meteorological Organisation classification of a SSW that, it has to be at 10 hPa pressure level.

Figure 5.11 presents the contour plots of the wavelet power spectra obtained from UKMO zonal mean zonal wind at 60°S for the year 2007 from Julian day number 54 to 365 at 10, 3 and 1 hPa pressure levels. It can be observed that there is a very strong wave activity with long wave

periods ranging between 5 and 28 days during winter. There is evidence of wave activity amplification as the wave propagates upwards. Such wave amplification could be a result of wave-wave interaction and it may lead to the formation of minor SSW. At 10 hPa pressure level (Figure 5.11a), a maximum wave power of about 600 $m^2.s^{-2}$ is noted. As the wave propagates vertically upwards traces of wave amplification are noted at 3 hPa and 1 hPa pressure levels. At 1 hPa pressure level (Figure 5.11c), a significant wave amplification is noted in the wave power which seems to have intensified to about 1500 $m^2.s^{-2}$.

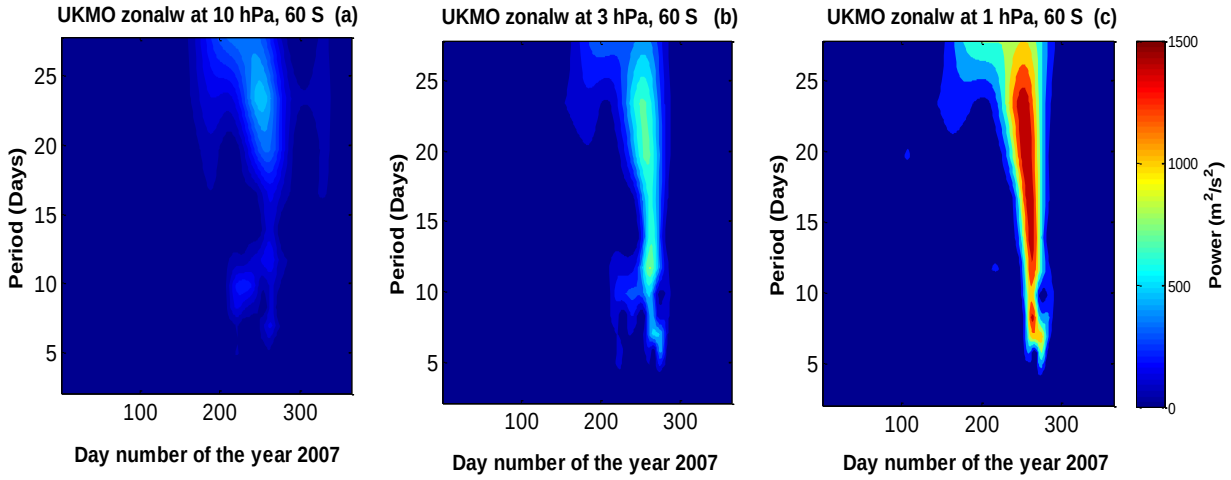

Figure 5.11: Wavelet spectra for UKMO zonal mean zonal wind at 60°S for the year 2007 at (10 hPa, 3 hPa, 1 hPa, and 0.3 hPa) pressure levels.

All the increase in wave activity or the maximum peaks of the spectra are identified during the winter months and this could have simulated the formation of minor SSW. When there is a non-linear interaction of the upward propagating planetary waves and tides, the modulation of tides which results in very high amplitudes occurs. This will effect more MLT wave-wave interactions causing the deceleration of the zonal mean wind until the wave breaking occurs (e.g. Liu et al., 2014). There will be a downward circulation which initiates adiabatic heating in the stratosphere resulting from the deceleration of the eastward flow by planetary waves (Liu and Roble, 2002).

5.6 Diurnal and Semidiurnal Tides in the Middle Atmosphere and their Interaction with Planetary Waves during Minor SSW

MLT dynamics is characterised by planetary waves and tidal waves interaction with the mean flow. In this study the zonal and meridional wind for SANAE for the year 2007 was used to analyse diurnal and semidiurnal tides interaction with planetary waves. Figure 5.12 shows tidal variations or the instantaneous amplitude spectrum derived from band-pass filter for diurnal tide (with high and low cutoff frequencies of 0.8 and 1.2 Hz respectively) and semidiurnal tide (with high and low cutoff frequencies of 0.3 and 0.8 Hz respectively). The DT amplitude variations in both zonal and meridional wind components show a general increase in amplitude between day number 100 to 200 and 250 to 320 (see Figure 5.12a, c). Although amplitude variations are similar, the meridional wind shows smaller amplitudes compared to the zonal wind component.

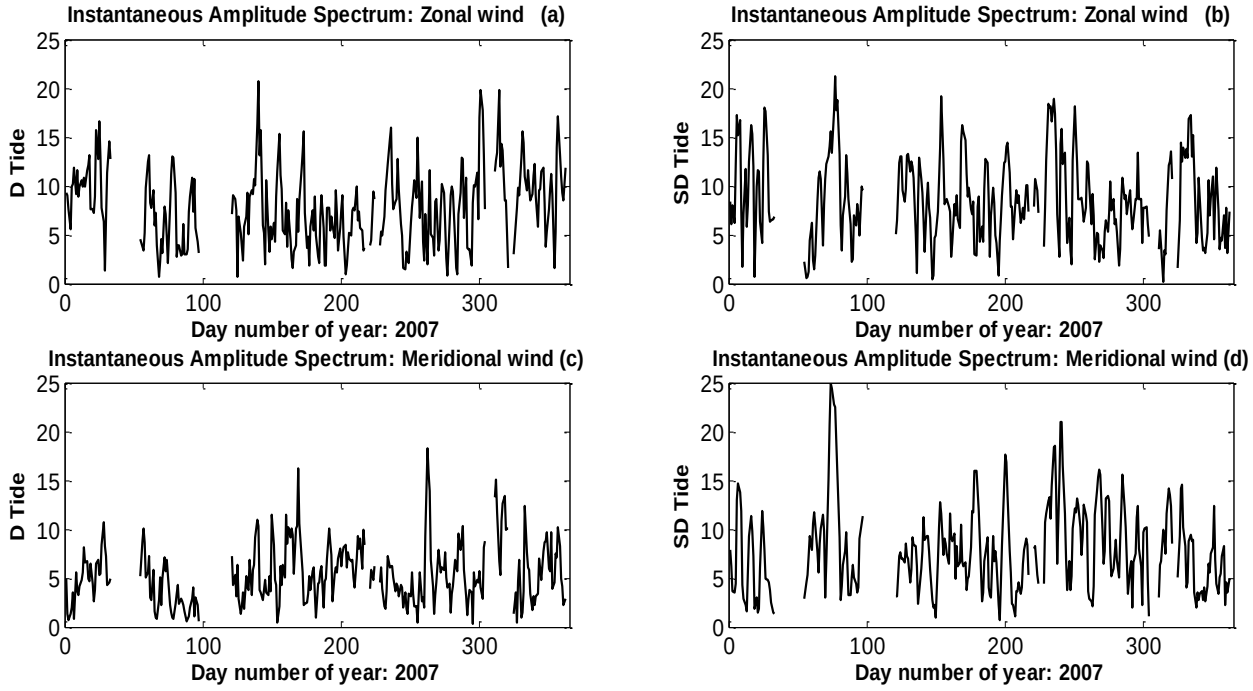

Figure 5.12: Diurnal and semidiurnal tides instantaneous amplitude spectrum using SANAE HF radar.

The DT amplitude variation attained maximum amplitude of approximately 21 $m.s^{-1}$ in the zonal wind component and about 19 $m.s^{-1}$ in the meridional wind component. There is a common feature noted in Figure 5.12b, d, that the SDT amplitude increased from approximately day 50 to day 100 reaching a maximum of approximately 22 $m.s^{-1}$ in the zonal component and about 24 $m.s^{-1}$ in the meridional component. In general, the zonal wind component shows greater amplitude compared to the meridional wind component. There are instances where sharp peaks are observed and this could be a period during which modulation of tides by planetary wave is taking place.

The instantaneous amplitude was subjected to wavelet analysis to study the tidal variability at planetary wave scale. Wavelet analysis (Torrence and Compo, 1998), for the zonal wind and meridional wind DT and SDT variations for SANAE are presented in Figure 5.13. This is to investigate the interaction and amplification of tides with quasi-10-day wave and quasi-16-day wave from dominant wave periods below 30 days for the year 2007. In this figure it can be noted that tidal amplitudes show variability at different planetary wave scales showing evidence of wave-wave interaction in the MLT.

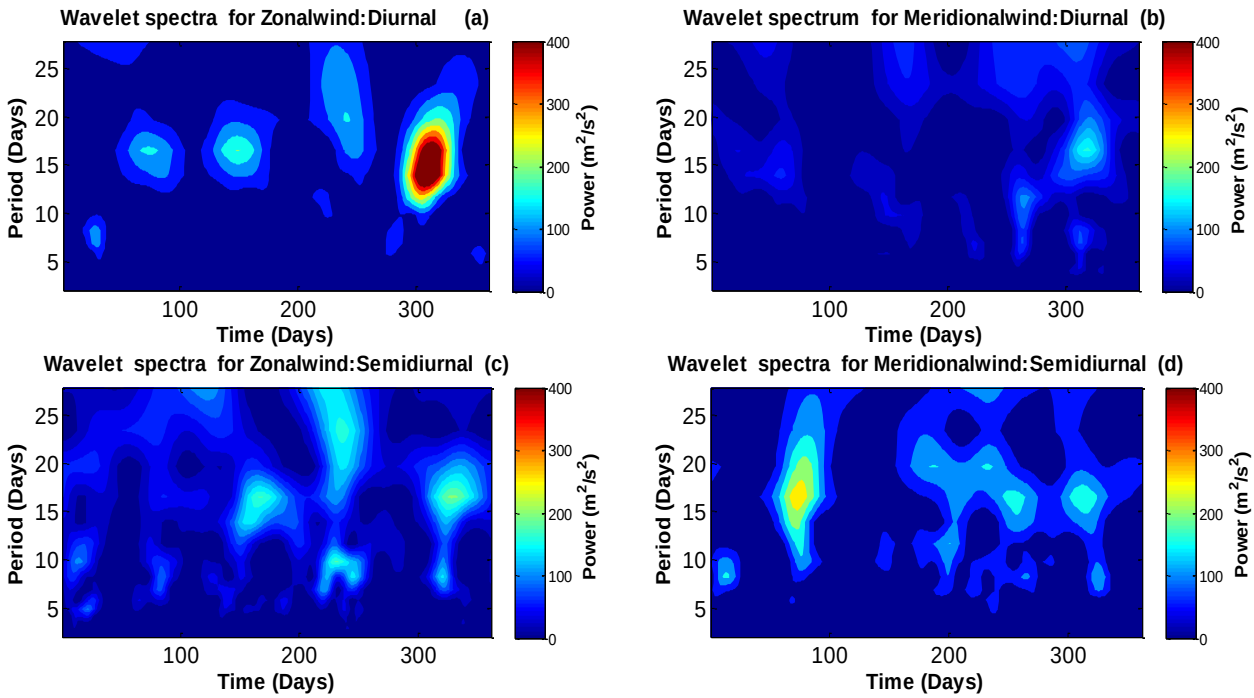

Figure 5.13: Wavelet power spectrum versus time for the year 2007 for zonal wind (left panel) and meridional wind (right panel) for SANAE HF radar at ~94 km. DT is shown on the top panel whilst SDT is on the bottom panel.

The zonal wind diurnal tide (Figure 5.13a) shows dominance of wave oscillations with periods ranging from 14-18 days centered at around day 16. This reveals the presence of quasi-16-day wave at planetary wave scale (Kumar et al., 2006), and it was more dominant on approximately day 310 with a maximum wave power of 400 $m^2.s^{-2}$. Such an observation of tidal variability at quasi-16-day periodicity provides evidence of the modulation of tides by planetary waves. This goes along with a study by Kumar et al., (2006) in which they used meteor radar observations of solar tides and planetary wave interaction in the MLT region at ~94 km over Trivandrum (8.5°N, 77°E). Using the wavelet analysis technique, they discovered that the zonal and meridional tides were modulated by the quasi-16-day planetary wave. In this study, the westward propagation quasi-16-day wave of zonal wavenumbers s=-1 and s=-2 observed at around day 310 interacted with the DT and may have contributed much to the change in dynamics of the MLT and occurrence of minor SSW.

The meridional DT spectra (Figure 5.13b) show the presence of quasi-10-day and quasi-16-day waves which look similar to the waves observed in the zonal wind component though it is weaker. This is represented by the wave activity stretching from day 5 to day 14 wave period centered at 10 days (quasi-10-day) with a maximum wave power of 140 $m^2.s^{-2}$ and the other stretching from day 14 to day 18 wave period centered at day 16 (quasi-16-day wave) mostly around day number 270 to 310. The SDT variation in zonal and meridional wind components (Figure 5.13c, d) shows common wave periods of 8-12 days centered at 10 days wave period (quasi-10-day) with a maximum wave power of 150 $m^2.s^{-2}$. In general, the SDT is dominated by quasi-16-day wave at planetary wave scale with a maximum wave power of 250 $m^2.s^{-2}$ observed around day 70. This reveals that there is a wave-wave interaction of tidal waves by planetary waves. There is also another wave activity observed around day 15 in Figure 5.13a, c, which happens to be a weak quasi-5-day wave in the zonal wind. In general, the modulation of tides by quasi-10-day, quasi-14-day and quasi-16-day planetary waves was noted and this wave-wave interaction in the MLT could have contributed much to the simulation of minor SSW. A study by Pancheva, (2000a) and Pancheva et al., (2003) concluded that there was a significant modulation of SDT amplitudes at periods of planetary waves, corresponding to quasi-10-day and quasi-16-day periods. They revealed that the non-linear interaction between the SDT and the

quasi-16-day wave was much stronger than those between the DT and the 16-day wave. In this study the same analysis is observed although the DT modulation shows more wave power around day 310 (see Figure 5.13).

Considering the DT at Halley (Figure 5.14, top panel) a maximum wave power of 250 $m^2.s^{-2}$ was noted at around day 120 in zonal wind and in the meridional wind a maximum wave power of 180 $m^2.s^{-2}$ was noted around day 310. In both cases, the DT revealed the presence of quasi-10-day and quasi-16-day waves with more wave activity observed during the winter similar to what was observed for SANAE. The zonal wind DT shows long period planetary waves stretching from 8 to 30 days wave periods. At around day 210 the presence of a weak quasi-14-day wave is noted with a low wave power of 90 $m^2.s^{-2}$. In Figure 5.14d the presence of quasi-5-day wave is noted though it is very weak. Similarly, the presence of quasi-5-day wave was observed in the MLT region over the Northern Hemisphere, (Day et al., 2012).

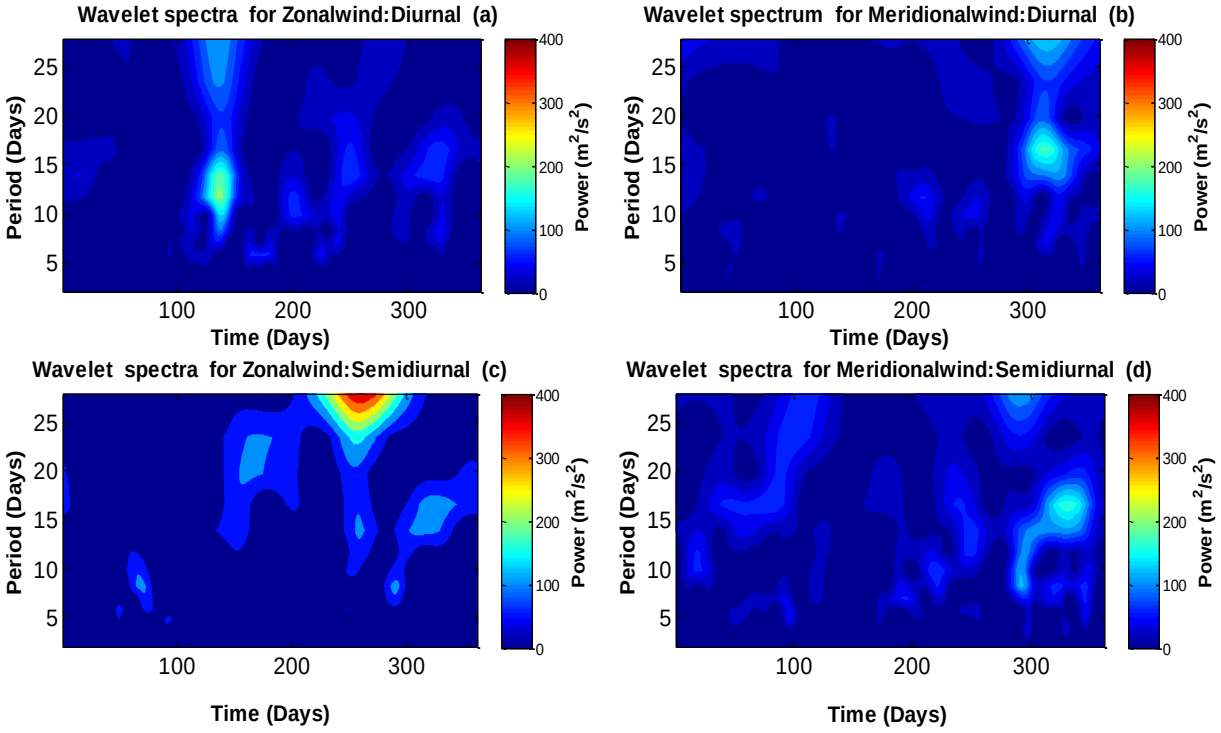

Figure 5.14: Wavelet power spectrum versus time for the year 2007 for zonal wind (left panel) and meridional wind (right panel) for Halley HF radar at ~94 km. DT is shown on the top panel whilst SDT is on the bottom panel.

Considering the SDT in zonal and meridional wind for Halley Figure 5.14 bottom panel the maximum wave power of 350 $m^2.s^{-2}$ is observed around day 250 where there is evidence of long period planetary wave activity with wave periods ranging from 10 to 30 days. In Figure 5.13 (SANAE) and Figure 5.14 (Halley), there is a clear similarity and consistence of the results showing a good agreement between the SANAE and Halley HF radar instruments. The results from both stations revealed the dominance of quasi-10-day and quasi-16-day waves with the latter being the most dominant. The current study has revealed that dominant waves (quasi-10-day and quasi-16-day) tidal amplitudes show variability at several scales less than a season and this could have played a major role in the formation of minor SSW events.

5.7 Zonal Wavenumbers

The data from SANAE and Halley SuperDARN radar sites was used to calculate zonal wavenumbers because the longitudinal difference between the radar sites of ~24 is good enough to obtain reliable zonal wavenumbers. The zonal wavenumbers during winter months which were calculated from the slope of linear regression of 5-day, 10-day and 16-day wave phases for DT and SDT as a function of longitude were presented in Figure 5.15. As explained earlier in chapter 4.3, the phase obtained in this analysis is from the 4 day Fourier spectral analysis method mainly because only phases that are well resolved in frequency were needed hence, a dynamic Fourier spectra method which uses a 4 day data window that is shifted forward by 1 day at a time was implemented. For significance, the wavenumbers calculated were those at which both sites (SANAE and Halley) had data, and the coefficient of determination was 55%. The positive wavenumbers represent eastward propagating waves whilst negative wavenumbers represent the westward propagating waves.

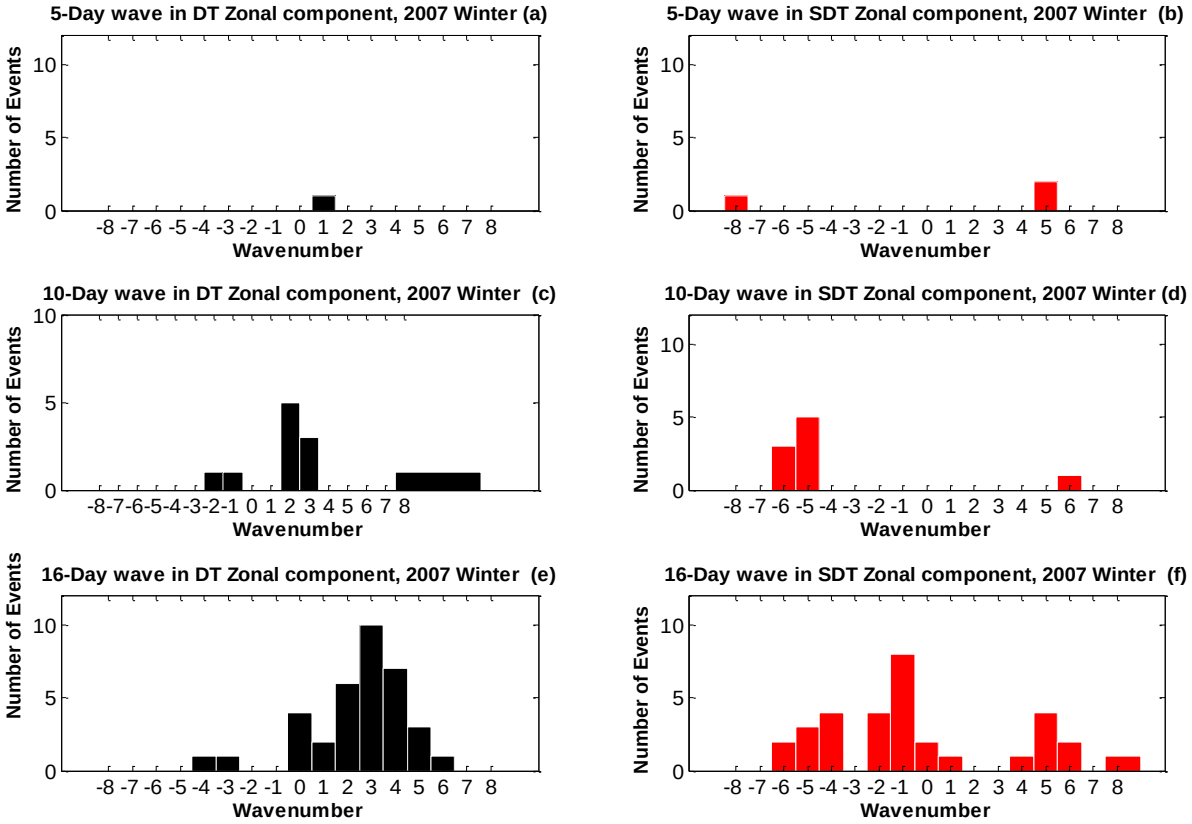

Figure 5.15: The distribution of the zonal wavenumber for the DT (left panel) and SDT (right panel) zonal wind component during the winter season of the year 2007. In the Figure, the negative wavenumbers represent the westward propagating wave.

For the 5-day waves (Figure 5.15a, b), zonal wavenumbers of s=1, s=5 and s=8 are noted. An eastward quasi-5-day wave propagation in DT is significant since smaller wavenumbers are the ones contributing much to the MLT dynamics. The 10-day wave (Figure 5.15c, d) shows significant zonal wavenumbers of s=-1, s=-2, s=5, s=$\pm$6 and s=8 but the most dominant are s=2 and s=5. Eastward propagation small wavenumbers s=2 and s=3 in the quasi-10-day wave in DT are of greater importance and could have contributed much to the formation of minor SSW events. Figure 5.15d, e shows the 16-day significant zonal wavenumbers of s=0, s=$\pm$1, s=$\pm$2, s=$\pm$3, s=$\pm$4 and s=5 but the most dominant are s=3 followed by s=1 then s=4. The stationary planetary wave and eastward propagating quasi-16-day in DT with zonal wavenumbers s=1, s=2, s=3 and s=4 could have contributed greatly on the wave interaction which resulted in the

formation of minor SSW. The quasi-16-day in SDT with an eastward propagation and zonal wavenumbers s=1 and s=4 and westward propagation with zonal wavenumbers s=-4, s=-2 and s=-1 were vital to the causes of minor SSW events as well. The stationary wave was present in both DT and SDT quasi-16-day wave and this wavenumber could have played a big role for the occurrence of minor SSW.

Based on Wavelet power spectra on Figure 5.13 it can be observed that DT and SDT shows wave activity with wave period below 25. This analysis is in agreement with a study by (Pancheva et al., 2000a, b) in which they discovered amplitude variations by a significant nonlinear interaction between tides and planetary waves with periods between 2 and 20 days. Some previous studies have shown that planetary waves of smaller wavenumbers (e.g. s=0, s=$\pm$1 and s=$\pm$2) are the contributing factor for the deceleration of the mean flow and the mesospheric cooling in the MLT region during the major SSW in the Southern Hemisphere (e.g. Cho et al., 2004 and Mbatha et al., 2010b). In this study eastward zonal wavenumbers of s=1 and s=2 have been found in the Southern Hemisphere which agrees with a study by Macdonald et al., (2011), which reveals that the eastward propagating wavenumber s=1 is generally the largest amplitude mode in the Southern Hemisphere winter, followed by the eastward propagating s =2 mode.

Considering the days on which minor SSW events took place as illustrated in Table 5.2 above, it can be noted that the quasi-10-day and quasi-16-day waves had more wave activity compared to the 5-day wave in both the DT and SDT. This means that the 5-day wave had a lesser contribution to the onset of minor SSW events. The nonlinear interaction of DT with quasi-10-day wave with wavenumbers s=2 and s=3, eastward propagation could have imposed a significant contribution to the deceleration of the mean flow for the enhancement of minor SSW events. The modulation of DT by quasi-16-day wave with wavenumbers s=0, s=2 and s=3 could have contributed to the deceleration of the mean flow as well. The SDT interacted with westward propagation quasi-16-day wave with wavenumbers s=-1 and s=-2 and this might have enhanced the formation of minor SSW events. A study by Laskar et al., (2014) revealed that for those major SSW events in which the quasi-16-day amplitudes are high, the broad variations in the amplitudes of semidiurnal tide and the quasi-16-day amplitudes were quite similar.

A similarity of the significant wave numbers of s=-1, s=±5 and s=3 noted in the zonal wind for the quasi-10-day wave discussed earlier in chapter 4.3 (Figure 4.11) and the zonal wavenumbers for DT in Figure 5.15, was noted. This gives evidence of wave-wave interaction during the modulation of DT by quasi-10-day wave in the MLT. Such an analysis is similar to a convincing conclusion that stationary and traveling waves with the same zonal wave number when present together would interfere and this interference will result in transient fluctuations of the wave amplitude with time (e.g. Smith, 1985). Such non-linear interactions will decelerate the mean flow and leads to wave breaking, which will in turn form minor SSW.

5.8 Summary and Discussion

In this chapter, the NCEP reanalysis data and the UKMO data assimilation were used to analyse the planetary wave activity during the years 2007 and 2010 minor SSW by investigating the variation of zonal mean wind at 60°S and temperature at 80°S with time. Four minor SSW events were noted in each case and the last SSW event for the year 2010 was classified as a final warming.

To examine the presence and temporal evolution of long period waves in the stratosphere before, during and after the onset of the minor stratospheric warming events, the wavelet power spectra of the UKMO zonal mean zonal wind component for 10 hPa, 3 hPa, 1 hPa, and 0.3 hPa pressure levels were calculated for the period range from 2 to 28 days. A very strong presence of planetary waves of periods between 5 and 28 days during winter months was noted and it seemed to dissipate in late winter. The presence of quasi-10-day and quasi-16-day waves during minor SSW events was also noted. The amplification of the wave activity was concluded from the fact that the wave activity gets stronger and stronger as it propagate upwards. For the year 2007 the presence of quasi-10-day, quasi-16-day wave and quasi-14-day waves of zonal wavenumbers s=0 and s=-1 was noted.

The diurnal tide and semidiurnal tide interaction with planetary waves was analysed. The zonal and meridional wind components for the year 2007, showed the amplification of the DT and SDT by quasi-10-day and quasi-16-day waves. The maximum wave activity was observed during the winter months. In general, the DT revealed traces of more planetary wave activity compared to the SDT.

Chapter 6

6.1 Summary and Conclusion

In this study, the dynamics of the Southern Hemisphere middle atmosphere was investigated using SANAE and Halley HF radars with the focus on waves with periods less than 30 days. UKMO data assimilation and NCEP reanalysis data were used to investigate minor Sudden Stratospheric Warming for the years 2007 and 2010. Chapter 3 presented all the instruments and data analysis techniques that were used in this study. This includes the Short-Time Fourier Transform, wavelet analysis and complex-demodulation techniques which were implemented for data processing.

Planetary and tidal waves were investigated since they play an important role in the middle atmosphere dynamics. In Chapter 4 the zonal and meridional wind components of meteor wind data measured by the SANAE and Halley SuperDARN HF radars were used to investigate the variation of the daily mean wind, planetary and tidal waves of periods below 30 days in the MLT of the Southern Hemisphere for the years 2005 to 2007. There was a good agreement between the two instruments used and this coincides well with the expected, since the two instruments are separated by a longitudinal difference of ~24 degrees, good enough to estimate or measure the same variable in the common time mode of operation. The interaction of planetary waves with tides for the year 2007 was studied using zonal wind data from SANAE and Halley stations and there was good agreement between these two data sets as well. The DT and SDT showed the presence of quasi-10-day, quasi-14-day, quasi-16-day wave and some long period planetary waves. These waves could have interfered with the DT and SDT leading to the deceleration of the zonal mean flow, hence leading to the formation of minor SSW events. The wave activity was more dominant during the winter season though some traces of wave activity were noted in summer and spring.

Significant short zonal wavenumbers were investigated for the years 2005 to 2007 from the linear regression of phase as a function of longitude. The specific year of interest for this study, the year 2007 revealed that the zonal and meridional wind components of the 5-day wave

showed significant wavenumbers of s=-2, s=0 and s=7 with approximately the same number of counts.

The 10-day wave showed significant zonal wavenumbers of s=±3, s=±1, s=1, s=2, s=3, s=4, s=5 and s=6 but the most dominant were s=2 followed by s=0 then s=3. The 14-day wave showed significant zonal wavenumbers of s=±6, s=-5, s=-2, s=±1 and s=0 in the zonal and meridional wind components, but the most dominant were s=-1 followed by s=-2 then s=0. The wave numbers s=0 and s=1 were the contributing factors for the deceleration of the mean flow and the mesospheric cooling in the MLT region during the year 2002, which is a major SSW in the Southern Hemisphere, similar to studies by Mbatha et al., (2010b) and Chou et al., (2004). It can be concluded that short zonal wave in the quasi-10-day, quasi-14-day and quasi-16-day waves contributed to the enhancement of the year 2007 minor SSW events. In chapter 5 the NCEP reanalysis data was used to analyse the planetary wave activity during the minor SSW for the years 2007 and 2010. The tides and planetary wave interaction during the minor SSW for the year 2007 was investigated using the UKMO data assimilation and both the DT and SDT showed the presence of quasi-10-day and quasi-16-day waves.

The minor Sudden Stratospheric Warming over the Southern Hemisphere for the year 2010 was studied and four minor SSW events including the final warming were observed during the winter season. All events managed to decelerate the mean flow associated with an increase in temperature, but did not manage to reverse wind propagation direction to cause a major sudden stratospheric warming which was the same case for the year 2007. Minor SSW events are responsible for the preconditioning of the stratosphere for a major sudden stratospheric warming to occur. The Major SSW phenomenon is common in the Northern Hemisphere unlike in the Southern Hemisphere, where it was once noted in the year 2002 and was reported by (e.g. Baldwin et al., 2003; Dowdy et al., 2004; Mbatha et al., 2010b and Dowdy, 2005). In the year 2010 the reversal of zonal mean flow from eastward direction to a westward direction only took place from approximately day 300 which is a general change of season and no warming usually takes place until the next reason.

The NCEP and UKMO data sets proved to be consistent and reliable in estimating minor SSW events since they displayed similar results when a similar year of interest was investigated. The two data sets showed exactly the same wave variation with time in both magnitude and time. The

UKMO data was used to investigate the planetary waves during minor SSW and it was found that there was wave amplification as the wave propagates vertically upwards.

6.2 Future work

In the climatology of planetary waves and tides coupling the mesosphere, the analysis can be done using more instruments (e.g. in situ instruments, satellite data and HF Radar data in order for the instruments to complement each other for best results). The variation of planetary waves and tides can be investigated at different latitudes to find their origin and how they propagate upwards. This involves investigating the coupling between stratosphere and mesosphere and interaction of planetary waves with tides during minor SSW events. Such an analysis will be useful in circumstances where by a wave propagates from the Northern Hemisphere causing effect on the Southern Hemisphere. This will give information of the origin and propagation of such waves which emanate from one Hemisphere to another and the comparison of events which occurs in different Hemispheres at the same time frame. An inter-annual comparative study over a long period of years can be used to find the trend of minor SSW patterns. This will be a stepping stone based on the minor SSW events observed during the pre-conditioning of the stratosphere prior to the occurrence of the once ever observed major Southern Hemisphere stratospheric warming in the year 2002 (e.g. Baldwin et al., 2003; Mbatha et al., 2010b; Dowdy et al., 2004 and Dowdy, 2005). Predictions of the next probable intense minor SSW or a major SSW can possibly be achieved.

References

Andrews, D. G., Holton, J. R, and Leovy, C. B.: Middle Atmospheric Dynamics, vol. 40, 489 pp, Elsevier, New York, 1987.

Andrews, D. G.: An introduction to atmospheric physics, Cambridge Univ Pr, 2000.

Andrew, J.D., Robert A.V., Masaki, T., Kiyoshi, I., Yasuhiro, M., Werner, S., and Damian J.M.: Polar mesosphere and lower thermosphere dynamics: 1.Mean wind and gravity wave climatologies, journal of geophysical research, vol. 112, d17104, doi: 10.1029-2006jd008126, 2007.

Alexander, M. J. and Pfister, L.: Gravity wave momentum flux in the lower stratosphere over convection, geophysical research letters, vol. 22, 15, 2029-2032, 1995.

Alexander, M. J. and Dunkerton, T. J.: A spectral parameterization of mean-flow forcing due to breaking gravity waves, Journal of the Atmospheric Sciences, vol. 56, 4167-4182, 1999.

Anne K.S.: Global Dynamics of the MLT, Surv Geophys vol. 33, 1177–123, 2012.

Baldwin, M.P, and Dunkerton, T.J.: Propagation of the Arctic Oscillation from the stratosphere to the troposphere. Journal of geophysical research, vol. 104, no. d24, pages 30,937-30,946, 1999.

Baldwin, M., Hirooka, T., OSNeill, A., Yoden, S., Charlton, A. J., Hio, Y., Lahoz, W. A.,and Mori, A.: Major stratospheric warming in the Southern Hemisphere in 2002: Dynamical aspects of the ozone hole split, SPARC newsletter, 20, 24-26, 2003.

Banks,P.M., Kockarts, G.; Aeronomy, doi:10.1016/B978-0-12-077802-7.50002-6, academic press, 1973.

Batista, P., Clemesha, B., Tokumoto, A., and Lima, L.: Structure of the mean winds and tides in the meteor region over Cachoeira Paulista, Brazil (22.7) and its comparison with models, Journal of Atmospheric and Solar-Terrestrial Physics 66, 623 - 636, 2004.

Baumgaertner, A. J. G., McDonald, A. J., Fraser, G. J., and Plank, G. E.: Long-term observations of mean winds and tides in the upper mesosphere and lower thermosphere above Scott Base, Antarctica, Journal of Atmospheric and Solar-Terrestrial Physics, 67, 1480-1496, 2005.

Baumgaertner, A. J. G.: Observations of Middle Atmosphere Dynamics over Antarctica, PhD thesis, 2007.

Bencherif, H., Amraoui, L. E., Semane, N., Massart, S., Charyulu, D. V., Hauchecorne, A., and Peuch, V. H.: Examination of the 2002 major warming in the Southern Hemisphere using ground based and Odin/SMR assimilated data: stratospheric ozone distributions and tropic/mid-latitude exchange, Canadian Journal of Physics, 85, 1287-1300, 2007.

Bracewell, R. N.: The Fourier transform and its applications, ed 3, New York, Marcgrwa-Hill 2000.

Bremer, J., Schminder, R., Greisiger, K.M., Hoffmann, P., Kurschner, D., and Singer, W.: Solar cycle dependence and long-term trends in the wind field of the mesosphere/lower thermosphere, Journal of Atmospheric and Solar-Terrestrial Physics Vol 59, 5, 497–509, 1997.

Bristow, W. A., Yee, J. H., Zhu, X., and Greenwald, R. A.: Simultaneous observations of the July 1996 2-day wave event using the Super Dual Auroral Radar Network and the High Resolution Doppler Imager, Journal of Geophysical Research, 104, 12 715, 1999.

Brook, D. and Wynne, R. J.: Signal processing: Principles and applications, Edward Arnold London, 1988.

Butler, A.B., Seidel, D.J., Hardiman, S.C., Butchart, N., Birner, T., and Matc, A.: defining sudden stratospheric warmings, DOI:10.1175/BAMS,D,13,00173.2, 2015.

Chanin, M. L. and Hauchecorne, A.: Lidar observation of gravity and tidal waves in the stratosphere and mesosphere, Journal of Geophysical Research, 86, 9715-9721, 1981.

Chandran, A., Garcia, R.R., Collins, R.L., Chang, L.C.: Secondary planetary waves in the middle and upper atmosphere following the stratospheric sudden warming event of January 2012, geophysical research letters, vol. 40, 1861–1867, doi:10.1002/grl.50373, 2013.

Charney, J. G. and Drazin, P. G.: Propagation of planetary-scale disturbances from the lower into the upper atmosphere, Journal of Geophysical Research, 66, 83-109, 1961.

Cho, Y. M., Shepherd, G. G., Won, Y. I., Sargoytchev, S., Brown, S., and Solheim, B.: MLT cooling during stratospheric warming events, Geophysical Research Letters, 31, L10 104, 2004.

Chshyolkova, T., Manson, A. H., Meek, C. E., Avery, S. K., Thorsen, D., MacDougall, J. W., Hocking, W., Murayama, Y., and Igarashi, K.: Planetary wave coupling processes in the middle atmosphere (30-90 km): A study involving MetO and MFR data, Journal of Atmospheric and Solar-Terrestrial Physics, 68, 353-368, 2006.

Clark, R. R., Current, A. C., and Manson, A. H., et al.: Global properties of the 2-day wave from mesosphere lower-thermosphere radar observations, J. Atmos. Terr. Phys, 56, 1279, 1994.

Clark, R. R., Burrage, M. D., Franke, S. J., Manson, A. H., Meek, C. E., Mitchell, N. J., and Muller, H. G.: Observations of 7-d planetary waves with MLT radars and the UARS-HRDI instrument, Journal of Atmospheric and Solar-Terrestrial Physics, 64, 1217-1228, 2002.

Day, K.A.: Mean winds, Temperatures and the 16-day and 5-day Planetary waves in the Mesosphere and lower Thermosphere over Bear Lake Observatory, 12, 1571-1585, 2012.

Detrick, D. L., and Rosenberg, T. J.: A phased-array radio wave imager for studies of cosmic noise absorption, Radio, Sci, 25, 325-338, 1990.

Donelan, M. A., Longuet-Higgins, M. S., and Turner, J. S.: Non-stationary analysis of the directional properties of propagating waves, Journal of Physical Oceanography, 26, 1901-1914, 1996.

Dowdy, A. J., Vincent, R. A., Murphy, D. J., Tsutsumi, M., Riggin, D. M., and Jarvis, M. J.: The large-scale dynamics of the mesosphere-lower thermosphere during the Southern Hemisphere stratospheric warming of 2002, Geophysical Research Letters, 31, L14 102, 2004.

Dowdy, A. J.: Polar Middle Atmosphere Dynamics, Ph.D. thesis, University of Adelaide, 2005.

Espy, P., Jones, G., Swenson, G., Tang, J., and Taylor, M.: Tidal modulation of the gravity-wave momentum flux in the Antarctic mesosphere. Geophysical research letters, geophysical research letters, vol. 31, L11111, doi:10.1029/2004 GL019624, 2004.

Espy, P. J., and Hibbins, R. E.: Mesospheric planetary waves over Antarctica during 2002, Geophys. Res. Lett, 32, L21804, doi: 10.1029/2005GL023886, 2005.

Farge, M.: Wavelet transforms and their applications to turbulence, Annual Review of Fluid Mechanics, 24, 395-458, 1992.

Fazlul, L., Duggirala, P., and Bhaskara, V.: Vertical coupling of atmospheres: dependence on strength of sudden stratospheric warming and solar activity, Earth, Planets and Space, 66-94, 2014.

Fedulina, I. N., Pogoreltsev, A. I., and Vaughan, G.: Seasonal, inter annual and short-term variability of planetary waves in Met Office stratospheric assimilated fields, Quarterly Journal of the Royal Meteorological Society, 130, 2445-2458, 2004.

Forbes, J. M.: Tidal and planetary waves, The upper mesosphere and lower thermosphere: a review of experiment and theory. Geophysical Union, Washington, D.C, doi: 10.1029/ GM087p0067, 1995.

Forbes, J. M., Russell, J., Miyahara, S., Zhang, X., Palo, S., Mlynczak, M., Mertens, C. J., and Hagan, M. E.: Troposphere-thermosphere tidal coupling as measured by the SABER instrument on TIMED during July–September 2002, doi: 10.1029/2005JA011492, 2006.

Fritts, D. C.: Shear Excitation of Atmospheric Gravity Waves. Journal of atmospheric sciences, 39, 1936-1952, 1982.

Fritts, D. C., Isler, J. R., Lieberman, R. S., Burrage, M. D., Marsh, D. R., Nakamura,T., Tsuda, T., Vincent, R. A., and Reid, I. M.: Two-day wave structure and mean flow interactions observed by radar and High Resolution Doppler Imager, Journal of Geophysical Research, 104, 3953-3969, 1999.

Gavrilov, N.M., Kshevetskii, S.P.: Three-dimensional numerical simulation of nonlinear acoustic-gravity wave propagation from the troposphere to the thermosphere, Earth, Planets and Space 66-88, 2014.

Greenwald, R. A., Baker, K. B., Dudeney, J. R., Pinnock, M., Jones, T. B., Thomas, E. C., Villain, J. -P., Cerisier, J. -C., Senior, C., Hanuise, C., Hunsucker, R. D., Sofko, G., Koehler, Nielsen, J.E., Pellinen, R., Walker, A. D., Sato, N, and Yamagishi, H.: DARN/SuperDARN: A global view of the dynamics of high latitude convections, Space Sci. Rev, 71, 761-796, 1995.

Hall, G. E., MacDougall, J. W., Moorcroft, D. R, and J.P. St.-Maurice.: Super Dual Auroral Radar Network observations of meteor echoes, J. Geophys. Res, 102, 14, 603-14,614, 1997.

Hernandez, G.: Climatology of the upper mesosphere temperature above South Pole (90°S): Mesospheric cooling during 2002, Geophysical Research Letters, 30, 1535, 2003.

Hibbins, R. E. and Jarvis, M. J.: A long-term comparison of wind and tide measurements in the upper mesosphere recorded with an imaging Doppler interferometer and Super-DARN radar at Halley, Antarctica, Atmospheric Chemistry and Physics Discussions, 7, 6573-6601, 2007.

Hibbins, R. E. and Jarvis, M. J.: A long-term comparison of wind and tide measurements in the upper mesosphere recorded with an imaging Doppler interferometer and SuperDARN radar at Halley, Antarctica, Atmos. Chem. Phys., 8, 1367–1376, 2008.

Hibbins, R. E., Marsh, O. J., McDonald, A. J., and Jarvis, M. J.: Inter annual variability of the s=1 and s=2 components of the semidiurnal tide in the Antarctic MLT, Journal of Atmospheric and Solar-Terrestrial Physics, 72, 794-800, 2010.

Hines, C. O.: A modelling of atmospheric gravity waves and wave drag generated by isotropic and anisotropic terrain, journal of atmospheric sciences, 45, 309-322, 1988.

Holton, J. R.: The dynamic meteorology of the stratosphere and mesosphere, in: Research supported by the National Science Foundation Boston, American Meteorological Society. Meteorological Monograph, No. 37, 224 p, vol. 15, 1975.

Holton, J. R.: A semi-spectral numerical model for wave-mean flow interactions in the stratosphere: Application to sudden stratospheric warming, J. Atmos. Sci., 33, 1639-1649, 1976.

Holton, J. R.: Equatorial wave-mean flow interaction: A numerical study of the role of latitudinal shear. Journal of atmospheric sciences 1030, volume 36, 1979.

Holton, J. R. and Alexander, M. J.: The role of waves in the transport circulation of the middle atmosphere, Atmospheric science across the stratopause, pp. 21-35, 2000.

Holton, J. R.: An introduction to dynamic meteorology, 4th Edition, Academic press, 2004.

Houghton, J.T.: The physics of atmospheres, Cambridge University Press, 271 pp., Great Britain, 1986.

Huang, K. M., Liu, A. Z., Zhang, S. D., Yi, F., Huang C. M., Gan Q., Gong ,Y., and Zhang, Y. H.: A nonlinear interaction event between a 16-day wave and a diurnal tide from meteor radar observations, Ann. Geophys, 31, 2039–2048, 2013.

Hussey, G. C., Meek, C. E., André, A. H., Manson, A. H., Sofko, G. J, and Hall, C. M.: A comparison of Northern Hemisphere wind using SuperDARN meteor trail and MF radar wind measurements, J. Geophys. Res, 105, 18,053-18066, 2000.

Jacobi, C.: On the solar cycle dependence of winds and planetary waves as seen from mid-latitude D1 LF mesopause region wind measurements, in: Annales Geophysicae, vol. 16, pp. 1534-1543, Springer, 1998.

Jacobi, C., Portnyagin, Y. I., Merzlyakov, E. G., Solovjova, T. V., Makarov, N. A., and K "urschner, D.: A long-term comparison of mesopause region wind measurements over Eastern and Central Europe, Journal of Atmospheric and Solar-Terrestrial Physics, 67, 229-240, 2005.

Kalnay, E. C., Kanamitsu, M., Kistler, R., Collins, W., Deaven, D., Gandin, L., Iredell, M., Saha, S., White, G., Woollen, J., et al.: The NCEP/NCAR 40-year reanalysis project, Bulletin of the American Meteorological Society, 77, 437-471, 1996.

Khanyile, B.S.: An investigation of the atmospheric wave dynamics in the polar region using ground based instruments, MSc thesis, University of Fort Hare, 2011.

Kishore, P., Velicogna, I., Venkat Ratnam, M., Jiang, J. H., and Madhavi. G. N.: Planetary waves in the upper stratosphere and lower mesosphere during 2009 Arctic major stratospheric warming. Ann. Geophys., 30, 1529–1538, 2012.

Kleinknecht, N.: Planetary Wave Oscillations Observed in Ozone from Troll Station Antarctica, Master thesis, Norwegian University, 2010.

Kruger, K., Naujokat, B., and Labitzke, K.: The unusual midwinter warming in the Southern Hemisphere stratosphere 2002: A comparison to Northern Hemisphere phenomena, Journal of the Atmospheric Sciences, 62, 603-613, 2005.

Kshevetskii, S.P., and Gavrilov, N.M.: Three-dimensional numerical simulation of nonlinear acoustic-gravity wave propagation from the troposphere to the thermosphere, Earth, Planets and Space, 66-88, 2014.

Kshudiram S.: The earth's atmosphere. Its physics and dynamics, Doi 10.1007/978, 3, 540, 78427, 2, 2008.

Kumar, P., and Foutoula, G.E.: Wavelet analysis for geophysical applications. American geophysical union, reviews of geophysics, 1997.

Kumar, K. K., Deepa, V., Antonita, T. M., and Ram Kumar, G.: Meteor radar observations of solar tides and planetary wave interaction in the MLT region, ILWS workshop GOA, 2006.

Kuttippurath, J., and Nikulin, G.: A comparative study of the major sudden stratospheric warming in the Arctic winters 2003/2004–2009/2010, 12, 8115–8129, 2012.

Labitzke, K. and Naujokat, B.: The lower Arctic stratosphere in winter since 1952, SPARC Newsletter, 15, 11-14, 2000.

Laskar, F., Pallamraju, D., and Veenadhari, B.: Vertical coupling of atmospheres: dependence on strength of sudden stratospheric warming and solar activity, Planets and Space 66-94, 2014.

Lester, M.: The Super Dual Auroral Radar Network (SuperDARN): An overview of its development and science, doi: 10.3724/SP.J.1085.2013.0000, Vol. 24 No. 1: 1-11, 2013.

Lima, L.M., Alves, E.O., Batista, P.P., Clemesha, B.R., Medeiros, A.F., Buriti, R.A.: Sudden stratospheric warming effects on the mesospheric tides and 2-day wave dynamics at 7 °S, Journal of Atmospheric and Solar-Terrestrial Physics 78–79, 99–107, 2012.

Limpasuvan, V., Hartmann, D. L., Thompson, D. W. J., Jeev, K., and Yung, Y. L.: The Life Cycle of the Northern Hemisphere Sudden Stratospheric Warming, journal of climate volume 17, 2584, 2004.

Lindzen, R. S.: Turbulence and Stress Owing to Gravity Wave and Tidal Breakdown, journal of geophysical research, vol. 86, no. ci0, pages 9707-9714, 1981.

Liu, H.L., and Roble, R. G.: A study of a self-generated stratospheric sudden warming and its mesospheric–lower thermosphere impacts using the coupled TIME-GCM/CCM3, 2002.

Liu, H. L. and Roble, R. G.: Dynamical coupling of the stratosphere and mesosphere in the 2002 Southern Hemisphere major stratospheric sudden warming, Geophysical Research Letters, 32, L13 804, doi: 10.1029/2005GL022 939, 2005.

Liu1, X., Xu, J., Liu, H.L., Yue, J., and Yuan, W.: Simulations of large winds and wind shears induced by gravity wave breaking in the mesosphere and lower thermosphere (MLT) region, Ann. Geophys., 32, 543–552, 2014.

Lorenc, A.C., Bell, R.S., and Macpherson, B.: The Meteorological Office Analysis Correction data assimilation scheme. Q. J. R. Meteorol. Soc., 117: 59–90, 1991.

Macdonald, A, J., Hibbins, R.E., Jarvis, and M.J.: Properties of the quasi-16-day wave derived from EOS MLS observations, journal of geophysical research atmospheres, 2011.

Malinga, S. B.: A comparative study of atmosphere dynamics in the mesosphere and lower thermosphere (MLT) near Grahamstown (South Africa) and Adelaide (Australia), PHD thesis, Rhodes University, 2001.

Malinga, S. and Poole, L. M. G.: The 16-day variation in the mean flow at Grahamstown (33.3°S, 26.5°E), Annales geophysicae, 20, 2027-2032, 2002.

Malinga, S. B., Poole, L. M. G., and Vincent, R. A.: Long term variations in the mesospheric mean flow observed at Grahamstown (South Africa) and Adelaide (Australia), Journal of Atmospheric and Solar-Terrestrial Physics, 66, 1745-1754, 2004.

Malinga, S. B. and Ruohoniemi, J. M.: The quasi-2-day wave studied using the Northern Hemisphere SuperDARN HF radars, Annales Geophysicae, vol. 25, pp. 1767-1778, 2007.

Mallat, S.: A Wavelet Tour of Signal Processing, ISBN 13: 978-0-12-374370-1, 1998.

Manney, G. L., Swinbank R., Massie S. T. M., Gelman E., Miller A. J.R., Nagatan A., O'Neill and Zurek R. W.: Comparison of U.K. Meteorological Office and U.S. National Meteorological Center stratospheric analyses during Northern and Southern winter, journal of geophysical research, vol. 101, no. d6, pages 10, 311-10, 334, 1996.

Matsuno, T.: A dynamic model of the stratospheric sudden warming, J. Atmos. Sci, 28, 1479-1494, 1971.

Mayr, H.G., Mengel, J.G., Chan, K.L., Huang, and F.T.: Middle atmosphere dynamics with gravity wave interactions in the numerical spectral model: Tides and planetary waves, journal of atmospheric and solar-terrestrial physics 73, 711–730, 2011.

Mbatha, N., Sivakumar, V., Bencherif, H., Malinga, S. B., R., P. S., Moorgawa, A., and Michaelis, M. M.: Durban rayleigh lidar measurements of the Stratosphere-Mesosphere temperature structure, in: 25th International Laser Radar Conference, 2010a.

Mbatha, N., Sivakumar, V., Malinga, S. B., Bencherif, H., and Pillay, S. R.: Study on the impact of sudden stratosphere warming in the upper mesosphere-lower thermosphere regions using satellite and HF radar, Atmospheric Chemistry and Physics, 10, 1-8, 2010b.

Mbatha, N.B: Study on 2002 Sudden Stratospheric Warming, Mesosphere-Lower Thermosphere wind structure and dynamics and middle atmospheric temperature structure, based on SuperDARN HF RADAR, LIDAR, Riometer, Satellites and Models, PHD thesis, University of KwaZulu-Natal, 2012.

Mthembu, S.: An investigation of ultra-low frequency pulsations using radar data and solar wind data, University of KwaZulu-Natal, 2006.

Nakamura, T., Tsuda, T., Maekawa, R., Tsutsumi, M., Shiokawa, K., and Ogawa, T. Seasonal variation of gravity waves with various temporal and horizontal scales in the MLT region observed with radar and airglow imaging. Advances in Space Research, 1737-1742, 2001.

Namboothiri, S. P., Meek, C. E., and Manson, A. H.: Variations of mean winds and solar tides in the mesosphere and lower thermosphere over time scales ranging from 6 months to 11years: Saskatoon, 52° N, 107° W, Journal of Atmospheric and Solar-Terrestrial Physics,56, 1313-1325, 1994.

Oleynikov, A., Jacobi, C., and Sosnovchik, D.: Parameters of internal gravity waves in the Mesosphere-lower thermosphere region derived from meteor radar wind measurements. Annales Geophysicae, 23, 3431–3437, 2005.

Palo, S. E., Forbes, J. M., Zhang, X., Russell III, J. M., Mertens, C. J., and Mlynczak, M. G.: Planetary wave coupling from the stratosphere to the thermosphere during the year 2002 Southern Hemisphere pre-stratwarm period. Geophysical research letters, vol. 32, l23809, doi: 10.1029-2005gl024298, 2005.

Pancheva, D., Mukhtarov, P.: Wavelet analysis on transient behaviour of tidal amplitude fluctuations observed by meteor radar in the lower thermosphere above Bulgaria, Ann. Geophysicae 18, 316-331, EGS Springer-Verlag, 2000a.

Pancheva, D., Beard, A. G., Mitchell, N.J., and Muller, H. G.: Nonlinear interactions between planetary waves in the mesosphere/lower-thermosphere region. Journal of geophysical research, 157-170, 2000b.

Pancheva, D., Mukhtarov, P., Mitchell, N.J., Beard, A.G., Muller, H.G.: A comparative study on winds and tidal variability in the mesosphere/lower-thermosphere region over Bulgaria and the UK. Ann. Geophysicae 18, 1304-1315, EGS-Springer-verlag, 2000c.

Pancheva, D., Haldoupis, C., Meek, C. E., Manson, A. H., and Mitchell, N. J.: Evidence of a role for modulated atmospheric tides in the dependence of sporadic E layers on planetary waves, journal of geophysical research, vol. 108, no. a5, 1176, doi:10.1029/2002ja009788, 2003.

Pancheva, D., Mitchell, N. J., Manson, A. H., Meek, C. E., Jacobi, C., Portnyagin, Y., Merzlyakov, E., Hocking, W. K., MacDougall, J., Singer, W., et al.: Variability of the quasi-2-day wave observed in the MLT region during the PSMOS campaign of June-August 1999, Journal of atmospheric and solar-terrestrial physics, 66, 539-565, 2004.

Pancheva, D., Mukhtarov, P., Mitchell, N., Merzlyakov, E., Smith, A., Andonov, B., et al.: Planetary waves in coupling the stratosphere and mesosphere during the major stratospheric warming in 2003/2004, journal of geophysical research, vol. 113, d12105, doi:10.1029-2007jd009011, 2008.

Pancheva, D., Mukhtarov, P., Andonov, B., and Forbes, J.: Global distribution and climatological features of the 5-6-day planetary waves seen in the SABER/TIMED temperatures (2002-2007). Journal of Atmospheric and Solar-Terrestrial Physics, Journal of Atmospheric and Solar-Terrestrial Physics 72, 26–37, 2010.

Pierre, W.: Theory of very long waves in a zonal atmosphere flow, 1961.

Portnyagin, Y. I., Forbes, J. M., Fraser, G. J., Vincent, R. A., Avery, S. K., Lysenko, I. A., and Makarov, N. A.: Dynamics of the Antarctic and Arctic mesosphere and lower thermosphere regions. The prevailing wind, journal of atmospheric and terrestrial physics, 55, 827-841, 1993.

Priestley, M. B.: Spectral analysis and time series. Volume 2: Multivariate series, prediction and control, Academic Press, 1981.

Reed, R. J.: Zonal wind behavior in the equatorial stratosphere and lower mesosphere, J. Geophys Res, 71, 4223–4233, 1966.

Riggin, D., Liu, H., Lieberman, R., Roble, R., Russell, J., and Mertens, C.: Observations of the 5-day wave in the mesosphere and lower thermosphere. Journal of Atmospheric and Solar-terrestrial Physics, 2005.

Salby, M., and Callaghan, P. Seasonal amplification of the 2 day wave relationship between normal mode and instability. Journal of the Atmospheric Sciences, 2000.

Shepherd, T. G.: The Middle atmosphere, J. Atms. Sol. Terr. Phys, 62, 1587-1601, 2000.

Shepherd, M.G., Wub, D.L., Fedulinac, I.N., Gurubarand, S., Russelle, J.M., Mlynczakf, M.G and Shepher, G.G.: Stratospheric warming effects on the tropical mesospheric temperature field, 69, 2309–2337, 2007.

Shiotani, M., Shimoda, N., and Hirota, I.: Inter-annual variability of the stratospheric circulation in the Southern Hemisphere, quarterly journal of the royal meteorological society, 119, 531-546, 1993.

Sivakumar, V., Rao, P. B., and Krishnaiah, M.: Lidar measurements of stratosphere-mesosphere thermal structure at low latitude: Comparison with satellite data and models, Journal of Geophysical Research, 108, 4342, 2003.

Smith, A.S.: Wave transience and wave-mean flow interaction caused by the interference of stationary and travelling waves. Journal of the Atmospheric Sciences 42, 6, 529–535, 1985.

Smith, S.W.: The Scientists and Engineer's Guide to digital Processing, Califonia technical publishing, 2003.

Swinbank, R. and O'Neill, A.: A stratosphere-troposphere data assimilation system, Monthly Weather Review, 122, 686, 702, 1994.

Thompson, D., Baldwin, M., and Solomon, S.: Stratosphere-Troposphere coupling in the Southern Hemisphere. Journal of the atmospheric sciences volume 62, 708, 2004.

Torrence, C., and Compo, G. P.: A practical guide to wavelet analysis, Bulletin of the American Meteorological Society, 79, 61-78, 1998.

Torrence, C., and Webster, P. J.: Inter decadal changes in the ENSO monsoon system, Journal of Climate, 12, 2679-2690, 1999.

Tunbridge, V., and Mitchell, N.: The two-day wave in the Antarctic and Arctic mesosphere and lower thermosphere. Atmos. Chem. Phys, 6377-6388, 2009.

Varavut, L., Dennis, L.H., David, W.J.T., Kumar, J., and Yuk L.Y.: Stratosphere-troposphere evolution during polar vortex intensification, Journal of Geo-physical Research, 110, D24 101, doi: 10.1029/2005JD006 302, 2005.

Vincent, A.R., Alexander M.J.: Gravity waves in the tropical lower stratosphere: An observational study of seasonal and inter-annual variability. Journal of geophysical research, vol. 105, NO. D14, 17,971-17,982, 2000.

Volland, H.: Atmospheric tidal and planetary waves, Springer, 1988.

Von Zahn1, U., Baumgarten1, G., Berger, U., Fiedler, J., and Hartogh. P.: Noctilucent clouds and the mesospheric water vapour, Atmos. Chem. Phys., 4, 2449, 2464, and 2004.

Walterscheid, R. L., Sivjee, G.G., and Roble, R. G.: Mesospheric and lower thermosphere manifestations of a stratospheric warming event over Eureka, Canada (80°N), Geophysical Research Letters, 27, 2897-2900, 2000.

Wayne, K., Hocking, G., Kishore, K.: Long term behavior of the MLT quasi-7-day wave at two radar-sites at northern polar latitudes, journal of atmospheric and solar-terrestrial physics 73, 1616–1628, 2011.

WMO; Assessment of our understanding of the processes controlling its present distribution and change, World Meteorological Organization, Global Ozone Research and Monitoring Project-Report, 1985.

Yamashita, C., Liu, H. L., and Chu, X.: Responses of mesosphere and lower thermosphere temperatures to gravity wave forcing during stratospheric sudden warming, Geophysical Research Letters, 37, L09803, doi: 10.1029/2009GL042351, 2010.

Zhang, X., and J.M. Forbes: Longitudinal Variation of Tides in the MLT Region: Part 1, Tides Driven by Tropospheric Net Radiative Heating, doi 10.1029/2010.